

**ANALYSIS OF SHORT AND LONG TERM DEFORMATIONS IN A
CONTINUOUS PRECAST PRESTRESSED CONCRETE GIRDER**

A Thesis

by

TRISTAN MARTIN SARREMEJANE

Submitted to the Office of Graduate and Professional Studies of
Texas A&M University
in partial fulfillment of the requirements for the degree of

MASTER OF SCIENCE

Chair of Committee,	John B Mander
Committee Members,	Mary Beth Hueste
	James Caverlee
Head of Department,	Robin Autenrieth

December 2014

Major Subject: Civil Engineering

Copyright 2014 Tristan M Sarremejane

ABSTRACT

A precast prestressed concrete girder using in-span splices to extend the span length is constructed to investigate performance under service and ultimate load conditions. Continuity is provided through the splices by a combination of mild steel reinforcement plus post-tensioned prestress. The thesis focuses on the study of short and long term deformations in the test specimen between the time the pretensioned prestressed segments were first cast, through splicing, deck construction and curing, and then initial testing. To support these observations, three creep frames are set up and shrinkage readings are taken.

Previous research is reviewed to determine what models should be used for the analysis of the experimental results. A time-dependent Matlab program based on AAASHTO recommendations is developed to predict the prestress losses due to the short and long-term deformations. Experimental observations from the test specimen are compared to those predictions. The predictions by most models available for assessing long-term deformations due to creep and shrinkage are overestimated when compared to the experimental observations. Unreliable predictions of prestress losses due to long-term deformations may have significant repercussions on a long-span structure; an over-estimation may lead to a design being too conservative, while an under-estimation may lead to cracking and thereby excessive deflections under service loading.

It appears that the over-estimation is, in part, due to the girder units being constructed with self-consolidating concrete (SCC). It is concluded that improved estimates of deformations for such structures composed of SCC girders can be achieved if a correction factor of 0.6 is applied to the AASHTO recommendations.

ACKNOWLEDGEMENTS

I would like to thank my committee chair, Dr. John Mander, as well as my committee member, Dr. Mary-Beth Hueste for giving me the opportunity to work on such a large scale research project. I would also like to thank them for their guidance and support. I also thank Dr. James Caverlee for being part of my committee.

I would like to dedicate this thesis to my mother, Christine Lienard, father, Philippe Sarremejane and my grandparents for their support through the years and their help to make my journey in the USA a reality.

This project was a team effort. Reza Baie, Michelle Prouty and I were part of the team. I have been responsible for the following tasks: help with the construction of the girder, help with the main testing, my primary responsibility was to characterize creep and shrinkage deformations from time of initial casting of segments through construction until the time of the main testing of the girder

TABLE OF CONTENTS

	Page
ABSTRACT	ii
ACKNOWLEDGEMENTS	iii
TABLE OF CONTENTS	iv
LIST OF FIGURES	vii
LIST OF TABLES	x
1. INTRODUCTION.....	1
1.1. Research Objectives	1
1.2. Methodology	2
1.2.1. Task 1 : Literature Review	2
1.2.2. Task 2 : Experimental Work	2
1.2.3. Task 3 : Analyzing Data	2
1.2.4. Task 4 : Results and Discussion	3
1.2.5. Task 5 : Summary and Conclusion	3
1.3. Organization of Thesis	3
2. LITERATURE REVIEW	5
2.1. Spliced Girder.....	5
2.1.1. Scope	5
2.1.2. Past Practice in On-Pier Splicing Of Girders	5
2.1.3. Past Practice in In-Span Splicing	6
2.1.4. Discussions with Industry Stakeholders.....	9
2.1.5. NCHRP Report 517.....	10
2.1.6. Recent AASHTO (6 th Edition) Code Revisions.....	13
2.1.7. Sylvan Avenue Bridge	16
2.2. Prestress Losses.....	20
2.2.1. Short Term Losses.....	20
2.2.2. Long Term Losses.....	21
2.3. Methods Used To Determine Prestress Lossses.....	21
2.3.1. Lump Sum Mass.....	22
2.3.2. Approximate Method	22
2.3.3. Time Dependent Method.....	22
2.4. Background History	23
2.4.1. Huo, et al. (2001).....	23

2.4.2.	NCHRP 496 Tadros, et al. (2003)	23
2.4.3.	Waldron (2004)	24
2.4.4.	Hale, et al. (2006)	24
2.4.5.	Trejo, et al. (2008)	25
2.4.6.	Al-Omaishi, et al. (2009)	25
2.4.7.	NCHRP 628 Khayat, et al. (2009)	26
2.4.8.	Pan, et al. (2013)	26
2.4.9.	Summary	27
2.5.	Models	28
2.5.1.	AASHTO LRFD (2004)	28
2.5.2.	AASHTO LRFD (2006)	30
2.5.3.	CEB-FIP (1993)	36
3.	EXPERIMENTAL WORK	38
3.1.	Spliced Girder Construction	38
3.1.1.	Introduction	38
3.1.2.	Test Specimen Properties	39
3.1.3.	Instrumentation	46
3.1.4.	Construction Process	49
3.2.	Creep Frames	61
3.2.1.	Sulfur Capping	63
3.2.2.	Gaging Cylinders and Steel Plates	65
3.2.3.	Half Cylinders	67
3.2.4.	Wiring and DAQ	68
3.2.5.	Assembling Creep Frames	68
3.2.6.	Loading the Creep Frames and Recording Data	69
3.3.	Shrinkage Readings	71
4.	RESULTS AND DISCUSSION	72
4.1.	Predictions From AASHTO LRFD 2006	72
4.2.	Data from the Girder	77
4.3.	Data from Shinkage Readings	90
4.4.	Data from the Creep Frames	93
5.	SUMMARY, CONCLUSION AND RECOMMENDATIONS	103
5.1.	Summary	103
5.2.	Conclusion	103
5.3.	Recommendations	105

REFERENCES.....107

LIST OF FIGURES

	Page
Figure 2.1. Design Examples from NCHRP Report 517 (2004).....	12
Figure 2.2. Clause 5.2 AASHTO	13
Figure 2.3. Clause 5.9.5.2.3c AASHTO.....	13
Figure 2.4. Clause 5.14.1.3.1 AASHTO	14
Figure 2.5. Clause 4.14.1.3.2d AASHTO	15
Figure 2.6. Clause C5.14.1.3.2b AASHTO.....	15
Figure 2.7. Clause C5.14.1.3.4 AASHTO.....	16
Figure 2.8. Use of Spliced Girders for the Sylvan Avenue Bridge.....	17
Figure 2.9. Different Sections of the Sylvan Avenue Bridge.....	18
Figure 2.10. Pictures of the Construction Process (Webber 2013).	19
Figure 3.1. Prototype Bridge and the Test Specimen (Hueste et al, 2014).	39
Figure 3.2. Test Specimen (Hueste et al. 2014).	40
Figure 3.3. Cross Section of Modified Tx70 Girder (Hueste et al. 2014).....	40
Figure 3.4. Detailing of the Splice (Hueste et al. 2014).	41
Figure 3.5. Post-Tensioning Layout (Hueste et al. 2014).	45
Figure 3.6. Surface Strain Gages (Hueste et al. 2014).	47
Figure 3.7. Embedded Concrete Gages (Hueste et al, 2014).	47
Figure 3.8. String Potentiometers Locations (Hueste et al. 2014).	48
Figure 3.9. Positiones of LVDTs (Hueste et al. 2014).	48
Figure 3.10. Alignment of Girder Segments.	50
Figure 3.11. Placing Ducts between Segments.	51
Figure 3.12. Splice Details.	52
Figure 3.13. Splice Formwork.....	53
Figure 3.14. Deck Formwork.	54
Figure 3.15. Casting the Splices and making Cylinder and Beam Samples.	55
Figure 3.16. Deck Preparation and Casting.....	56

Figure 3.17. External Instrumentation.....	58
Figure 3.18. Post-Tensioning Operation.	59
Figure 3.19. Grouting Operation.	60
Figure 3.20. Creep Frame Test Setup.....	62
Figure 3.21. Capping Cylinders.	64
Figure 3.22. One Gaged Steel Plate.	66
Figure 3.23. Concrete Cylinder Ready for Gaging.	66
Figure 3.24. Cylinders and Plates, Gaged and Coated.	68
Figure 3.25. Bridge Circuit.	69
Figure 3.26. Loading of the Creep Frames.....	70
Figure 3.27. Shrinkage Measurement Device.	71
Figure 4.1. Prestress Losses in Pretensioning.	73
Figure 4.2. Stress Profiles from $t=1$ day to $t=209$ days.....	75
Figure 4.3. Strain Profiles from $t=1$ day to $t=209$ days.....	76
Figure 4.4. Post-Tensioning Load.	77
Figure 4.5. Effect of Post-Tensioning with Time.....	79
Figure 4.6. Test Specimen (Hueste et al. 2014).	80
Figure 4.7. Effect of Post-Tensioning on the Splices.....	81
Figure 4.8. Strain Profile for Splice 2.	83
Figure 4.9. Strain Profile Average of Section D & F.....	84
Figure 4.10. Strain Profile for Section D.	85
Figure 4.11. Strain Profile for Section F.	86
Figure 4.12. Strain Profile Summary.	87
Figure 4.13. Final Stress and Strain Profiles Including Predictions from 4.1.....	87
Figure 4.14. Failure in Compression.....	89
Figure 4.15. Shrinkage Readings Compared to Shrinkage Models.	91
Figure 4.16. Comparison of Shrinkage Models with Experimental Data.	92
Figure 4.17. Data from the Creep Frames.	95
Figure 4.18. Cracked Top Half Cylinder of the Third Frame.	95

Figure 4.19. Creep Frames Data Compared to Creep Models.	96
Figure 4.20. Creep Frames Data Compared to ASSHTO LRFD 2006 Model.....	97
Figure 4.21. Creep Frames Data Compared to AASHTO 2004 & CEB-FIP Models.....	98
Figure 4.22. Overestimation of Creep Strain	100
Figure 4.23. Modified AASHTO LRFD 2006 Compared to Creep Data	102

LIST OF TABLES

	Page
Table 2.1. Local Post-Tensioned Splicing (Hueste et al, 2012).	7
Table 2.2. Continuity PT Load-Balancing Prestress (Hueste et al, 2012).	8
Table 3.1. Section Properties of the Modified Tx70 Girder (Hueste et al. 2014).	41
Table 3.2. Compressive Strength of SCC used for Girder Segments.	42
Table 3.3. Modulus of Elasticity of SCC used for Girder Segments.	42
Table 3.4. Properties of Concrete used for Splices.	43
Table 3.5. Properties of Concrete used for Deck.	43
Table 3.6. Pretensioning Details.	44
Table 3.7. Post-Tensioning Details.	44
Table 3.8. Steel Properties.....	44
Table 3.9. Batches used for the Creep Frames.....	62
Table 3.10. Loading applied to each Creep Frame.	62
Table 3.11. Compressive Strength of the Half Cylinders.	67
Table 4.1. Chronology of Girder’s Life.	72
Table 4.2. Description of Losses.....	74
Table 4.3. Percentage of Losses.....	74
Table 4.4. Post-Tensioning Force	78
Table 4.5. Limits in Compression and Tension.	88
Table 4.6. Compression and Tension Available before Limit	88
Table 4.7. Overestimation of Shrinkage Readings by Shrinkage Models.	90
Table 4.8. Force Applied on the Creep Frames.....	93
Table 4.9. Overestimation of the Creep Strain by Creep Models	99

1. INTRODUCTION

1.1. RESEARCH OBJECTIVES

The motivation of this thesis is to investigate the behavior of a precast prestressed spliced girder test specimen. Increasing the span length of precast prestressed girders is of high importance as precast use in Texas is widespread due to the standardization of precast elements. Studying the behavior of the splices under loading will help create recommendations in order to design connections that will provide structural continuity between precast segments.

This thesis will focus on short and long-term deformations produced by loading. The construction of a precast prestressed spliced girder imply several steps in the construction process:

- Prestensioning of the precast segments
- Casting the splices
- Casting the deck
- Post-tensioning the overall specimen

The above events happen at different time and between each of these, structural deformations evolve. The concrete undergoes shrinking and creep effects; steel reinforcement and strands also relax.

A key idea of prestressed concrete design is to balance a proportion of dead weight (objectively near unity) in order to avoid cracking at service when live load is applied on the structure. That is why it becomes crucial to carefully predict how a structure will behave between the events mentioned above in order to provide an appropriate design leading to an optimal and serviceable constructed facility.

Unfortunately, models predicting long-term deformations have often shown to over-predict deformations especially when high strength concrete is used which has become the norm nowadays. The uniqueness of this project makes it really interesting and challenging to explore how a contemporary structure will behave compared to what the theory predicts.

This research intends to investigate a test specimen and use currently available models to compare observed experimental behavior to predictions.

1.2. METHODOLOGY

1.2.1. Task 1 : Literature Review

The literature review is the logical first step investigating past and current practice. It allows one to define the actual state-of-the-art. It is important to read and document what has been done towards spliced precast prestressed girders and long-term deformations. Numerous studies have investigated spliced girders, coming up with different design ideas. It was necessary to investigate all the methods that have been used to spliced girders in past research projects in order to determine the most adequate path to follow for our project.

Long-term deformations have been addressed by many researchers, comparing available models to experimental data and modifying those models when needed. The present project is unique as it is a continuous precast prestressed concrete girder using Self Consolidating Concrete (SCC). The main objective of the literature review is to determine what models are applicable to provide the best predictions of the prestress losses due to short and long-term deformations.

1.2.2. Task 2 : Experimental Work

The experimental work was divided into two principal activities: the construction of a precast prestressed spliced concrete girder; and the set up of three creep frames to investigate related creep effects. The experimental work consisted of constructing the test specimen and testing it under different load conditions to investigate overall service and ultimate load behavior.

In order to study the long-term creep and shrinkage losses in the continuous precast prestressed concrete girder. Three creep frames were set up and shrinkage readings were taken from prismatic specimens.

1.2.3. Task 3 : Analyzing Data

Data were taken during the post-tensioning of the girder as well as during each test. The first step was to compare all the data available to determine the main trend and

also select what instrumentation gave the most reliable data for future analysis by excluding the data that did not seem reliable. Data from the creep frames and shrinkage prisms were also investigated and analyzed.

1.2.4. Task 4 : Results and Discussion

Once all the data was organized, it was necessary to compare the data with models available within design codes or past research. The major goal herein was to investigate the response of the specimen during and after the post-tensioning to determine the prestress losses caused by short and long-term deformations. The goal is to compare the data from the girder with available models as well as with the data coming from the creep frames and the shrinkage readings.

In order to predict the deformations over time, a Matlab program was developed to follow the timeline of the events, specifically: releasing of the prestressing strands; casting of splices; deck placement; post-tensioning and then further ongoing post-construction losses. It is well known that design codes tend to overestimate losses; Therefore, it is essential to use a time-stepping analysis to validate predictions against test outcomes.

1.2.5. Task 5 : Summary and Conclusion

After conducting a thorough analysis of experimental data, it should be possible to correlate the predictions with the observations so a designer can assess the degree of conservatism in the estimates, if any. This helps one to better understand the behavior of the prestress losses when precast prestressed segments are connected together using splices. The understanding of the losses in the prestress is imperative as it will influence the state of stress in the structure during its life time.

1.3. ORGANIZATION OF THESIS

This first chapter has presented an introduction as well as the motivation of this research project. The second chapter provides a comprehensive literature review investigating past research in the field of spliced girders as well as prestress losses caused by short and long-term deformations. It also present current code equations used to determine prestress losses. The third chapter presents the work performed in the High

Bay Laboratory (HBL) which includes the construction of the precast prestressed spliced girder as well as the preparation of the creep frames including pictures and explanations. Chapter four presents the results obtained followed by a discussion of the results in Chapter 5. Finally, Chapter 6 discusses new knowledge this project has brought and recommendations for present practice.

2. LITERATURE REVIEW

2.1. SPLICED GIRDER

2.1.1. Scope

In the phase one TTI/TxDOT Report 0-6651-1 (Hueste et al, 2012) of this project, a detailed literature review gathering relevant past research dealing with spliced girders was presented. This chapter summarizes key points from that work and goes on to include new information. In particular, the NCHRP 517 Report (Castrodale and White, 2004), which is the most recent body of work on the subject and essentially represents the state-of-the-art, is discussed. Recent modifications to the AASHTO LRFD third edition of the specifications that arise from the NCHRP work are also described. During the course of the present 4-year investigation, the design and construction of the Sylvan Avenue Bridge crossing the Trinity River near Dallas Texas was conducted. The recent modifications to the AASHTO LRFD Specifications along with the Sylvan Avenue Bridge represent the current state-of-the-practice where girders are spliced in-span to extend the overall span length of concrete slab on prestressed concrete girder bridges.

2.1.2. Past Practice in On-Pier Splicing Of Girders

On-pier splicing of girders is mostly used to provide span-to-span continuity and thereby extend span length for the design load carrying requirements. Precast-prestressed girder units generally do not exceed 160 ft. While this limitation is mostly governed by the prestressed girder weight, often girder unit lengths in Texas are limited to 140 ft due to transportation roadway restrictions between the casting plant and bridge site. Past research dealing with on-pier splicing may be divided in two main categories: splice designs including post-tensioning options; and reinforced concrete options that do not require field post-tensioning operations.

Full details may be found in the 6651-1 report (Hueste et al, 2012). Also refer to Kaar et al. (1960), Mattock and Kaar (1960), Bishop (1962), Dimmerling et al. (2005), Miller et al. (2004), Mirmiran et al. (2001b), Koch (2008), Newhouse et al. (2005),

Tadros and Sun (2003), Sun (2004), and Tadros (2007), Castrodale and White (2004), Lounis et al. (1997), and Abdel-Karim and Tadros (1992 and 1995).

While certain on-pier splicing methods may be quite economical and include straightforward fabrication and erection details, the major disadvantage limiting the span length to 160 feet remains. For longer spans, the designer inevitably needs to consider using in-span splicing, which is the major subject of this research.

2.1.3. Past Practice in In-Span Splicing

In-span splicing provides the possibility to significantly increase the span length through providing continuity, potentially doubling the interior span limit to approximately 300 feet. Different types of in-span splice designs have been described in the 6651-1 report. Those designs can be divided into two broad categories:

2.1.3.1. Locally Post-Tensioned Splices

This method does not aim to provide overall load balancing prestress, rather it aims to limit field operations that use post-tensioning. While this approach is perhaps the most straight forward from a construction standpoint, there is a general lack of continuity and the advantageous load balancing. Refer to Table 2.1.

2.1.3.2. General Post-Tensioning of Girder Segments to Provide Continuity

As outlined in Table 2.2, post-tensioned prestress is applied over several girders to provide continuity. Generally the tendons are placed in grouted ducts which are stressed and later grouted. If the ducts are draped through the girder segments, load balancing of gravity effects may be applied. This negates deflections within each spans, while the bridge deck section is subject to an almost constant state of axial compressive stress. By providing continuity load-balancing post-tensioning, span lengths may be substantially increased to some 300 ft. For more information, refer to Caroland et al. (1992), (Castrodale and White 2004), Janssen and Spaans (1994), Fitzgerald and Stelmack (1996), Endicott (1996), Ronald (2001), Tadros and Sun (2003), Nikzad et al. (2006), and Endicott (2005). This previous body of work was considered in developing prototype designs for the present investigation.

Table 2.1. Local Post-Tensioned Splicing (Hueste et al, 2012).

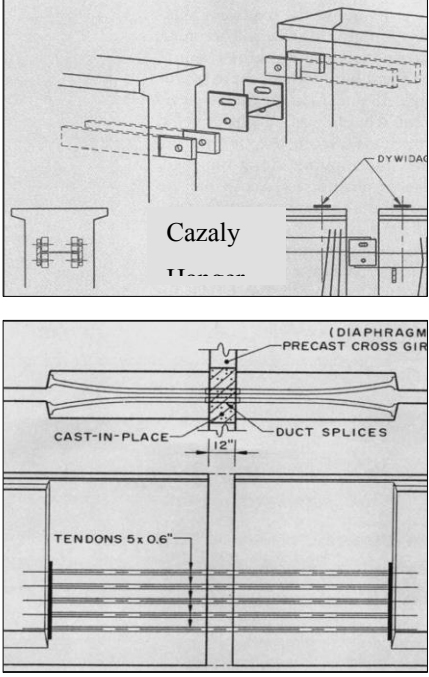
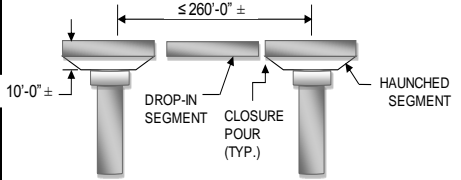
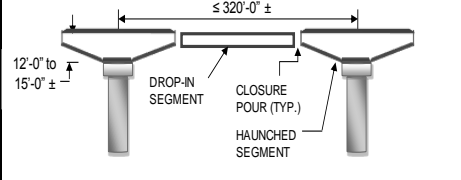
Splice Type	Advantages	Disadvantages
Prestressed for Simple Span and Partially Post-tensioned for Continuity (Caroland et al. 1992)		
<p>Maximum Span length = 250 ft</p> 	<ul style="list-style-type: none"> ▪ Girder segments were made continuous by stressing partial (short) length post-tensioned strands between the adjacent ends of the girder segments. ▪ The partial length post-tensioned strands were found to fully withstand the service stresses and ultimate strength conditions. ▪ Economical solution compared to steel plate girder alternatives in span range of 130 ft to 250 ft. 	<ul style="list-style-type: none"> ▪ No continuity tendons were provided throughout the length of the bridge. Therefore, complete load balancing was not achieved. ▪ Special attention was required in construction of the partially post-tensioned splice connection. ▪ End blocks were needed in the girder segments to anchor the partial post-tensioned strands.

Table 2.2. Continuity PT Load-Balancing Prestress (Hueste et al, 2012).

Splice Type	Advantages	Disadvantages
Prestressed for Simple Span and Post-tensioned for Continuity (Ronald 2001)		
<p>Maximum Span Length = 260 ft</p>  <ul style="list-style-type: none"> ▪ Girder section is Florida bulb-tee with 78 in. depth ▪ Girder spacing = 11 ft 6 in. ▪ Closure pour width = 1 ft 6 in. ▪ Web thickness of bulb-tee = 9 in. ▪ Depth of Haunched segment = 10 ft ▪ Length of Haunched segment = 110 ft 	<ul style="list-style-type: none"> ▪ Stage 1 post-tensioning: Allowed girders to be made continuous. ▪ Stage 2 post-tensioning: Provided residual compression in the deck for serviceability and deflection control. ▪ Cost of post-tensioning was offset by use of few girder lines and greater spacing between girders. ▪ Span lengths were extended beyond the practical limits of standard precast shapes. ▪ No intermediate diaphragms were used. ▪ Fewer massive piers were used for longer spans. ▪ Wide web thickness of 9 in. to accommodate tendons with 16 strands. ▪ Shear key was provided in webs for interlocking. ▪ Blisters were used at closure points to overlap tendons. ▪ Minimum impact on surrounding environment and traffic during construction. 	<ul style="list-style-type: none"> ▪ Cost of superstructure increased with longer spans. ▪ The deeper the haunch, the greater was the negative moment drawn toward interior piers. ▪ Long, slender bulb-tee girders deflected and twisted during handling and erection. ▪ Restriction in the length of the haunched segment based on the amount of prestress that can be provided in the top flange of the girder to resist cantilever bending before post-tensioning. ▪ Difficult to transport heavy haunched girder segments.
<p>Maximum Span Length = 320 ft</p>  <ul style="list-style-type: none"> ▪ Girder section is Florida bulb-tee with 78 in. depth ▪ Girder spacing = 9 ft 6 in. ▪ Closure pour width = 1 ft 8.5 in. ▪ Web thickness of bulb-tee = 9 in. ▪ Depth of Haunched segment = 12 ft ▪ Length of Haunched segment = 115 ft ▪ For Girders and Closure pours: $f'_c = 8500$ psi ▪ For Deck: $f'_c = 6500$ psi ▪ Strands: 0.6 in. diameter, ASTM A416, Grade 270 low relaxation 	<ul style="list-style-type: none"> ▪ No intermediate diaphragms were used. ▪ Fewer massive piers were used for longer spans. ▪ Wide web thickness of 9 in. to accommodate tendons with 16 strands. ▪ Shear key was provided in webs for interlocking. ▪ Blisters were used at closure points to overlap tendons. ▪ Minimum impact on surrounding environment and traffic during construction. 	<ul style="list-style-type: none"> ▪ Difficult to transport heavy haunched girder segments.

2.1.4. Discussions with Industry Stakeholders

The findings were presented to two group meetings consisting of (i) precasters that are responsible for casting the units and transporting them to the construction site and (ii) general bridge contractors that are concerned with the erection, splicing and post-tensioning of the girder components, as well as the construction of the remainder of the bridge including the deck and substructure.

2.1.4.1. Findings from the Precasters

- An increase in the span length will lead to an augmentation of the weight of each precast component. Hauling limit is about 200 kips, that maximum weight needs to be respected.
- Taking the weight limit into consideration, it is possible to define limits for I-girder and U-girder segments. The limit should be set to 140 feet in length and 10 feet in depth for the I-girder and 130 feet in length for the U-girder.
- When considering stability issues, precasters considered the longest span practical length achievable for a spliced girder bridge is 260 feet.
- Although it has been seen that use of haunched sections can be necessary in certain design cases, it is preferred by precasters to use standard section elements as the cost is less important and that it is easier to transport.
- It is possible to widen the web by increasing the spacing between the formwork.
- Because the specimen will be post-tensioned, it will need to have thickened ends. According to the precasters, this is not an issue.
- After investigating different type of splice connection, the precasters said they would prefer a partially prestressed type of spliced connections.
- Of the four different types of splice connections discussed (ranging from fully reinforced/non-prestressed to fully prestressed with PT), the precasters said they would prefer a partially prestressed type of spliced connections.

2.1.4.2. Findings from the Contractors

- Contractors considered a maximum span length of 250 to 270 ft was feasible.

- Contractors prefer unshored construction as they consider it saves a significant amount of time and money.
- The weight of the girder should be kept as low as possible.
- Contractors like the idea of splicing the segments on-pier as it allows in-span splicing to be performed on the ground. Nevertheless, this would lead to heavy weight spliced segments to be lifted.
- Contractors agreed the partial prestressed spliced design option is preferable.
- The contractors raised a concern about the wind forces that can jeopardized the lateral stability of the girders while they are being erected.

2.1.4.3. Additional Findings from the Designer/Owner (TxDOT)

- Engineers from TxDOT stated that the bridge designed for this project would be financially and structurally more advantageous than segmental bridges with shorter spans.
- TxDOT has just started to use the life-cycle cost analysis. They suggest that it would be interesting to use the life-cycle cost analysis in the designs.
- TxDOT engineers preferred solutions where the fascia girder did not possess a widened end at the drop-in splice location. This sentiment was to preserve the clean lines of the side elevation of the bridge deck. However, this presents a significant challenge, with the resulting narrow-web solution it is not possible to terminate and anchor the PT; the PT must run continuously through the splice.

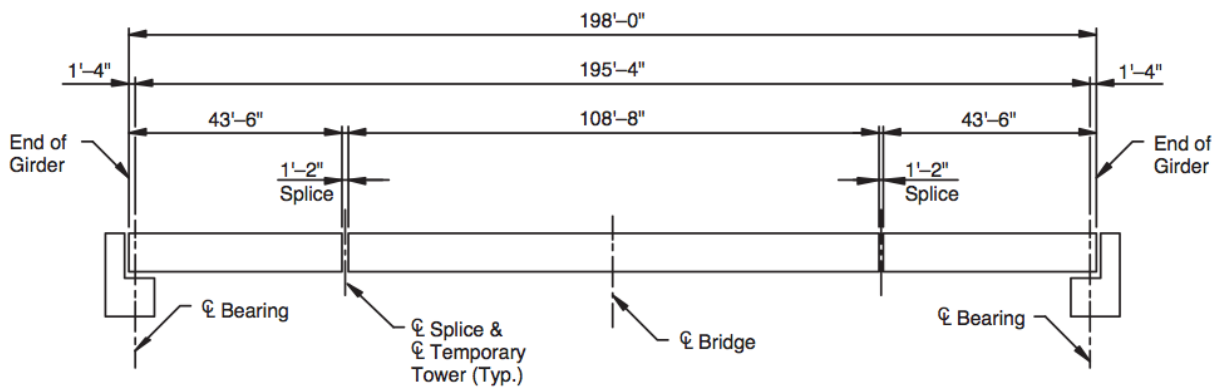
2.1.5. NCHRP Report 517

NCHRP Report 517 (Castrodale and White, 2004) investigated on pier as well as in-span splicing. They went over more than 250 cases where splicing has been used in precast prestressed girders in order to increase the span length. They showed that due to weight and size hauling limitations, the maximum reachable span length is 160 ft.

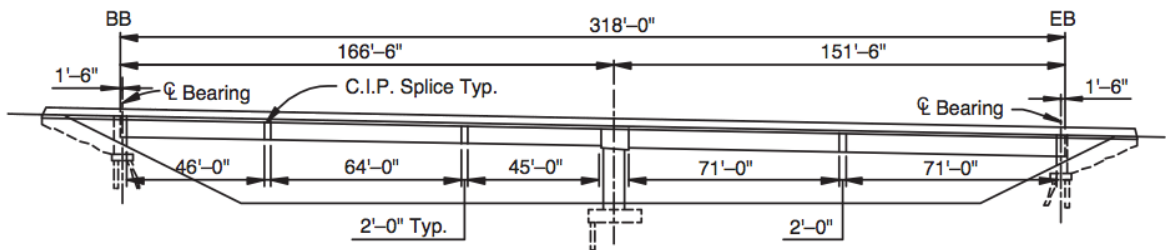
However, the report provided all the information about the technology available in order to expand the span length of precast, prestressed concrete girders up to 300 ft. They also concluded that there was no need to use more expansive segmental box girder alternatives.

Castrodale and White (2004) also listed analogies and differences between spliced girders using precast, prestressed elements and segmental bridge construction. The NCHRP Report 517 presents the changes in material properties and design enhancement that could be done in order to increase the span range of spliced girders using precast, prestressed elements. As far as material properties, the report advises that the strength of the concrete should be increased as well as its density. In addition, the prestressing strands size and strength should be increased as well. The design enhancements include the modification and creation of new standard girder sections, the modification of strand pattern and the enhancement of design methods.

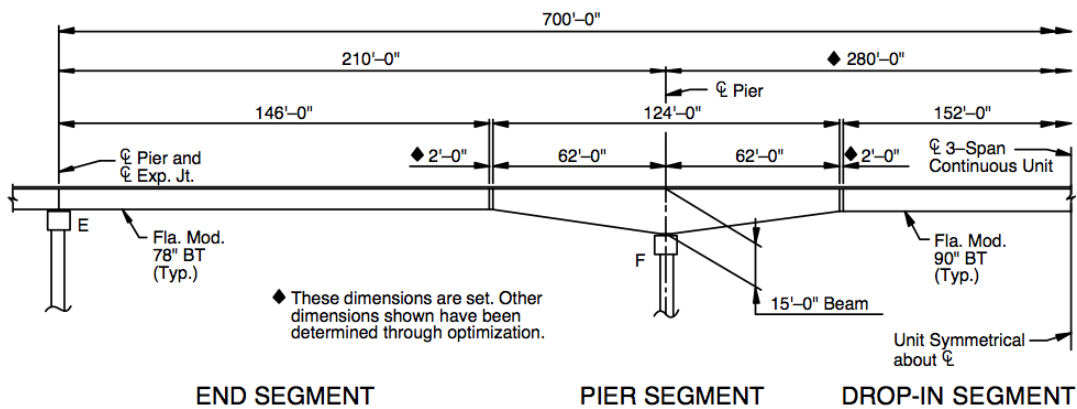
The NCHRP Report 517 provides numerous design examples in order to increase the span length. The three examples present how to design a single span spliced PCI BT-96 Girder, a two-span spliced U-Beam Girder and a continuous three span girder. The three examples have in-span splices. Figure 2.1 presents the three examples.



(a) Simply supported bridge with two in-span splices.



(b) Three-span continuous bridge with two splices within the central span and one splice in each of the side spans. For long central spans, it is often necessary to use haunched girders over the piers in the negative moment regions.



(c) Two-span continuous bridge with one splice within each span.

Figure 2.1. Design Examples from NCHRP Report 517 (2004).

2.1.6. Recent AASHTO (6th Edition) Code Revisions

Based on the NCHRP Project 517 (Castrodale and White, 2004), several modifications and enhancements were recommended for the AASHTO LRFD Bridge Design Specifications. Many of those recommendations have subsequently been adopted by the Code Committee. Apart from numerous editorial changes, the main substantive modifications and additions are outlined below.

First, spliced precast concrete girders are defined to clarify the difference between typical segmental construction and spliced girder construction. Specifically, clause 5.2, in Figure 2.2. states:

Spliced Precast Girder—A type of superstructure in which precast concrete beam-type elements are joined longitudinally, typically using post-tensioning, to form the completed girder. The bridge cross-section is typically a conventional structure consisting of multiple precast girders. This type of construction is not considered to be segmental construction for the purposes of these Specifications. (See Article 5.14.1.3.)

Figure 2.2. Clause 5.2 AASHTO

Spliced girders typically require a combination of both pre and post-tensioned tendons. Clause 5.9.5.2.3c code and commentary state in Figure 2.3.:

5.9.5.2.3c—Combined Pretensioning and Post-Tensioning

In applying the provisions of Articles 5.9.5.2.3a and 5.9.5.2.3b to components with combined pretensioning and post-tensioning, and where post-tensioning is not applied in identical increments, the effects of subsequent post-tensioning on the elastic shortening of previously stressed prestressing tendons shall be considered.

C5.9.5.2.3c

See Castrodale and White (2004) for information on computing the effect of subsequent post-tensioning on the elastic shortening of previously stressed prestressing tendons.

Figure 2.3. Clause 5.9.5.2.3c AASHTO

In order to make a distinction between spliced precast girders and segmental construction, a new section for spliced precast girders has been created. This section

provides additional information on how to classify spliced precast girder bridges from a design stand point. The emphasis is put on not to assimilate them as a segmental construction. For instance, the commentary clause C5.14.1.3.1 enumerates what differentiates spliced precast girder bridges with segmental construction and what design approach shall be used. Clause 5.13.1.3., in Figure 2.4., gives some insight on how to calculate prestress losses in spliced precast girder bridges. It also states that once the splices are poured, the structure may be treated as fully continuous at all limit states for loads applied after splicing.

5.14.1.3.1—General

The requirements specified herein shall supplement the requirements of other sections of these Specifications for other than segmentally constructed bridges. Therefore, spliced precast girder bridges shall not be considered as segmental construction for the purposes of design. For special design cases, additional provisions for segmental construction found in Article 5.14.2 and other Articles in these Specifications may be used where appropriate.

Spliced girder superstructures which satisfy all service limit state requirements of this Article may be designed as fully continuous at all limit states for loads applied after the girder segments are joined.

Prestress losses in spliced precast girder bridges may be estimated using the provisions for other than segmentally constructed bridges in Article 5.9.5. The effects of combined pretensioning and post-tensioning and staged post-tensioning shall be considered.

When required, the effects of creep and shrinkage in spliced precast girder bridges may be estimated using the provisions for other than segmentally constructed bridges in Article 5.4.2.3.

Precast deck girder bridges, for which some or all of the deck is cast integrally with a girder, may be spliced. Spliced structures of this type, which have longitudinal joints in the deck between each deck girder, shall comply with the additional requirements of Article 5.14.4.3.

Spliced precast girders may be made continuous for some permanent loads using details for simple span precast girders made continuous. In such cases, design shall conform to the applicable requirements of Article 5.14.1.4.

C5.14.1.3.1

In previous editions of these Specifications, spliced precast girder bridges were considered as a special case of both conventional precast girders and segmental construction. However, it is more appropriate to classify this type of structure as a conventional bridge with additional requirements at the splice locations that are based on provisions developed for segmental construction. The cross-section for bridges utilizing segmented precast girders is typically comprised of several girders with a composite deck.

Spliced precast girder bridges may be distinguished from what is referred to as “segmental construction” elsewhere in these Specifications by several features which typically include:

- The lengths of some or all segments in a bridge are a significant fraction of the span length rather than having a number of segments in each span. In some cases, the segment may be the full span length.
- Design of joints between girder segments at the service limit state does not typically govern the design for the entire length of the bridge for either construction or for the completed structure.
- Cast-in-place closure joints are usually used to join girder segments rather than match-cast joints.
- The bridge cross-section is comprised of several individual girders with a cast-in-place concrete composite deck rather than precasting the full width and depth of the superstructure as one piece. In some cases, the deck may be divided into pieces that are integrally cast with each girder. A bridge of this type is completed by connecting the girders across the longitudinal joints.
- Girder sections are used, such as bulb tee or open-topped trapezoidal boxes, rather than closed cell boxes with wide monolithic flanges.

Figure 2.4. Clause 5.14.1.3.1 AASHTO

Clause 5.14.1.3.2d provides more information towards the design of joint and what articles and recommendations shall apply. It mentions that the stress and loss limits in joints in precast girder bridges are the same as those used for “Segmentally Constructed Bridges”, as seen in Figure 2.5.

5.14.1.3.2d—Joint Design

Stress limits for temporary concrete stresses in joints before losses specified in Article 5.9.4.1 for segmentally constructed bridges shall apply at each stage of prestressing (pretensioning or post-tensioning). The concrete strength at the time the stage of prestressing is applied shall be substituted for f'_{ci} in the stress limits.

Stress limits for concrete stresses in joints at the service limit state after losses specified in Article 5.9.4.2 for segmentally constructed bridges shall apply. These

stress limits shall also apply for intermediate load stages, with the concrete strength at the time of loading substituted for f'_c in the stress limits.

Resistance factors for joints specified in Article 5.5.4.2.2 for segmental construction shall apply.

The compressive strength of the closure joint concrete at a specified age shall be compatible with design stress limitations.

Figure 2.5. Clause 4.14.1.3.2d AASHTO

The commentary Clause C5.14.1.3.2b presents recommendations regarding the use of diaphragms in Figure 2.6.

C5.14.1.3.2b

When diaphragms are provided at closure joint locations, designers should consider extending the closure joint at the exterior girder beyond the outside face of the girder. Extending the closure joint beyond

the face of the exterior girder also provides improved development of diaphragm reinforcement for bridges subject to extreme events.

Figure 2.6. Clause C5.14.1.3.2b AASHTO

Commentary clause C5.14.1.3.4, Figure 2.7., gives insight on different construction sequence possibilities and how it would affect the concrete strength and number of post-tensioning tendons required in the closure joint.

C5.14.1.3.4

Where some or all post-tensioning is applied after the deck concrete is placed, fewer post-tensioning tendons and a lower concrete strength in the closure joint may be required. However, deck replacement, if necessary, is difficult to accommodate with this construction sequence. Where all of the post-tensioning is applied before the deck concrete is placed, a greater number of post-tensioning tendons and a higher concrete strength in the closure joint may be required. However, in this case, the deck can be replaced if necessary. See Castrodale and White (2004).

See Article 5.10.3.5 for post-tensioning coupler requirements.

Where tendons terminate at the top of the girder, blockouts and pourbacks in the deck slab are required for access to the tendons and anchorages. While this arrangement has been used, it is preferable to anchor all tendons at the ends of girders. Minimizing or eliminating deck slab blockouts by placing anchorages at ends of girders reduces the potential for water seepage and corrosion at the post-tensioning tendon anchors.

This provision is to ensure that ducts as yet unsecured by concrete will not be used for active post-tensioning.

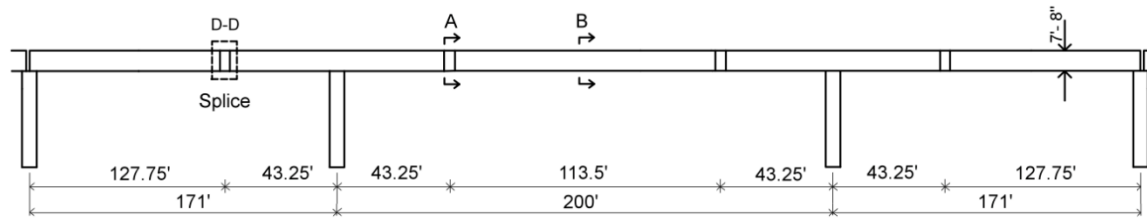
Figure 2.7. Clause C5.14.1.3.4 AASHTO

2.1.7. Sylvan Avenue Bridge

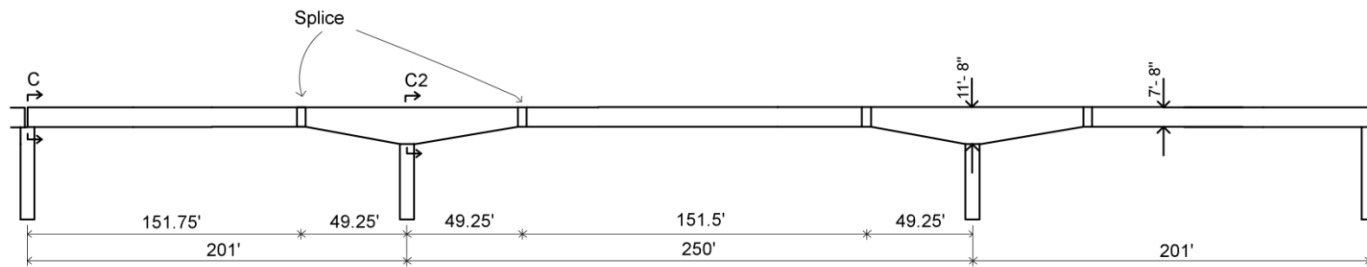
The recent design and construction of the Sylvan Avenue Bridge across the Trinity River near Dallas Texas represents the present state-of-the-practice for the state of Texas. This bridge has 23 spans and utilizes both pre-tensioned simply supported girders, as well as continuous and post-tensioned girder construction with in-span splices. There are three post-tensioned portions amongst the 23 spans that are each composed of three continuous spans as shown in Figure 2.8. Most of the spans use a new Tx-80 prestressed concrete section shape. However, in order to create the 250 ft span river crossing, it was necessary to use haunched girders as shown in Figure 2.8 (b).

The haunch-modified girders were cast on soffits in order to create the centerline haunch. In contrast with TxDOT standard shapes where the girders customarily have a 7-in web, the Tx80 modified girder has 10-in wide web, primarily to accommodate the PT ducts. Figure 2.9 presents details of the cross sections and splice details.

Some steps of the construction process are shown in the photographic record presented in Figure 2.10. Figure 2.10 (a) shows placement of the central drop-in girder in span 11. In order to provide girder stability during construction, it was necessary to provide a shore-tower beneath one splice within a span. This ensures the over pier units are effectively simply supported and stable.

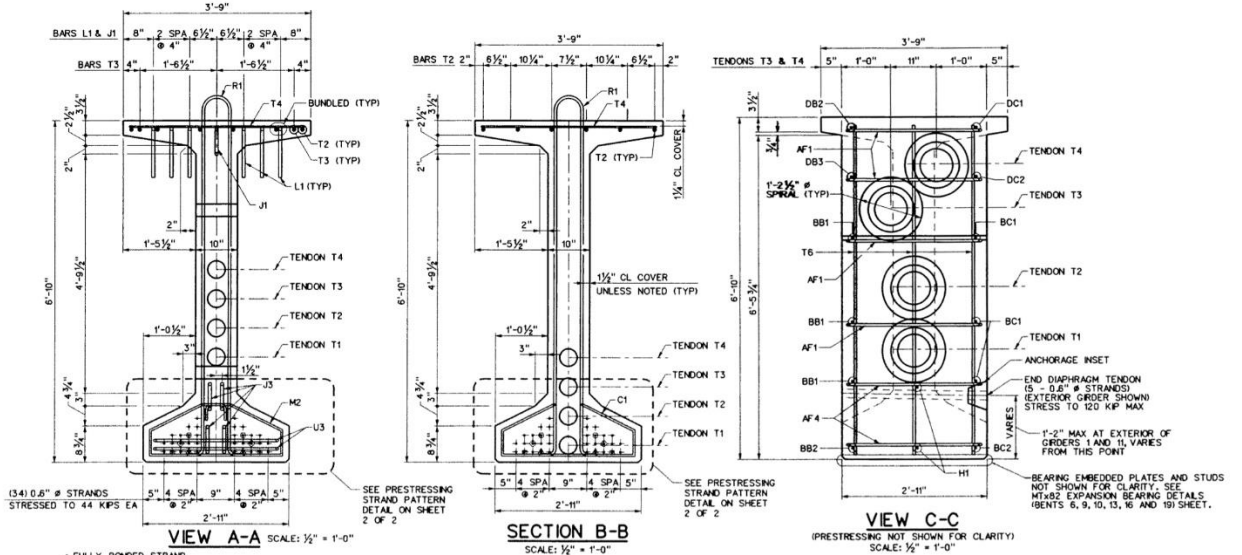


(a) Elevation for Spans 6 to 8 and 16 to 18.

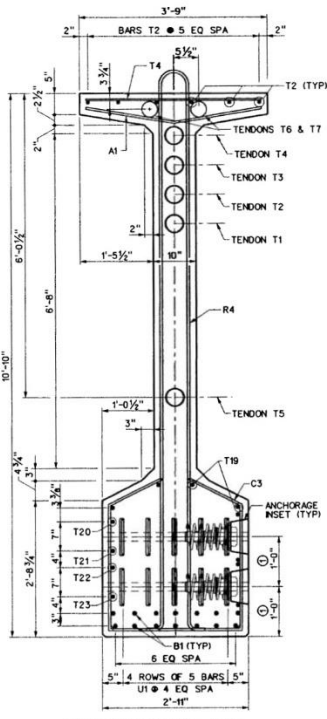


(b) Elevation for Spans 10 to 12.

Figure 2.8. Use of Spliced Girders for the Sylvan Avenue Bridge.



- FULLY BONDED STRAND
- STRAND DEBONDED 24'-0" FROM EACH END OF SEGMENT (2 TOTAL)
- STRAND DEBONDED 20'-0" FROM EACH END OF SEGMENT (2 TOTAL)
- STRAND DEBONDED 16'-0" FROM EACH END OF SEGMENT (2 TOTAL)
- STRAND DEBONDED 12'-0" FROM EACH END OF SEGMENT (2 TOTAL)



① DIMENSION AT EXTERIOR FACE OF EXTERIOR ORDER, VARIES FROM THIS POINT.

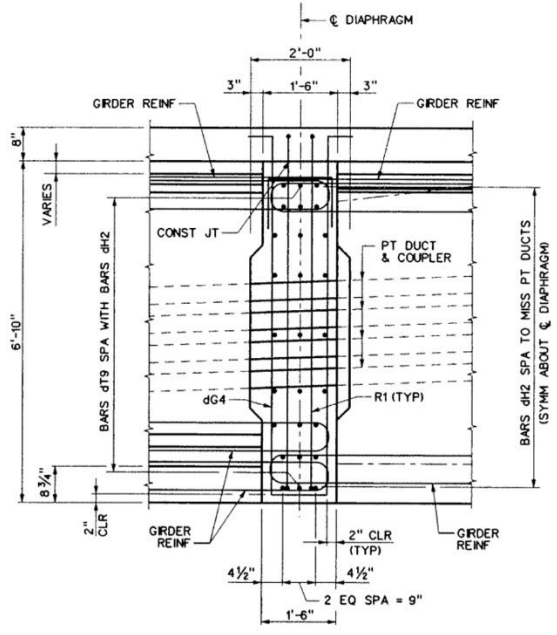


Figure 2.9. Different Sections of the Sylvan Avenue Bridge.



(a) Placing the drop-in segment within Span 11



(b) Shore towers on back spans

Figure 2.10. Pictures of the Construction Process (Webber 2013).

2.2. PRESTRESS LOSSES

Prestress losses are separated into two groups: short term losses and long term losses. The short term losses are assumed to happen instantly as the strands are stressed and released. The main short term loss that can occur with both pre-tensioning and post-tensioning is called elastic shortening and represents the losses experienced by the steel strands as the concrete shorten under the load. For post-tensioned members, friction and anchorage set losses are also part of the short term losses. The long term losses are creep and shrinkage of the concrete as well as relaxation of the steel.

2.2.1. Short Term Losses

2.2.1.1. Elastic Shortening

For a pre-tensioned member, as the stressed strands are released, the stress is transmitted to the concrete which will instantly shorten. The strands, which are also attached to the concrete, will shorten too, leading to a loss of stress in the tendons. Note that for a post-tensioned member, there will be no elastic shortening if the strands are jacked at the same time. However, if the strands are sequentially jacked, only the last strand to be jacked will not experience any loss.

2.2.1.2. Friction Losses

For a post-tensioned member, the tendons are in ducts. Ideally, the tendons are supposed to be at the center of the duct. But in reality, the tendons are in contact with the ducts which creates friction. The friction loss is the difference between the stress at the end of the member and at a section along the member.

2.2.1.3. Anchorage Set

For a post-tensioned, at transfer, there is a loss in the force due to the setting of the wedge. Indeed, the wedge will slip a certain distance before sitting which will create a loss in the tendons. That distance depends on the type of wedge and is usually given by the manufacturer.

2.2.2. Long Term Losses

2.2.2.1. Creep of Concrete

Concrete subjected to any long term compressive stress will deform over time. This will create a strain that will increase over time. The strain will increase rapidly at first and then will tend to a constant value with time. The tendons, which are attached to the concrete, undergo the same strain and will experience a loss of stress. The creep is a very complex process that depends on the concrete mix, the curing conditions, the exterior environment, and the maturity of concrete when loaded as well as the load applied.

2.2.2.2. Shrinkage of Concrete

Concrete contains additional water in its pores that hasn't been used for the hydration process of the cement. The additional water will evaporate over time which will lead the concrete to experience a shortening. This shortening will cause a loss of stress in the strands.

2.2.2.3. Relaxation of Steel

A constant tension is applied to the tendons. Over time, the tendons adapt to the stress applied by deforming. The relaxation of steel represents the losses due to the deformation of the tendons under an applied stress at a constant length.

2.3. METHODS USED TO DETERMINE PRESTRESS LOSSES

Determining all the above losses as accurately as possible is really important to make sure that a structure will stay safe in time and be able to carry the design loads. Different methods exist to predict those losses, from approximate methods to very complex time dependent analysis.

It is important to realize that long term losses are inter-dependent. Indeed, losses due to creep, shrinkage and steel relaxation at a certain time t will lead to reduced stresses in the tendons, which will also decrease the successive losses that arise later. It is for this reason a time-dependent analysis is necessary.

Approximate methods may be used in order to obtain a general measure of the magnitude of losses for design.

2.3.1. Lump Sum Mass

AASHTO LRFD 2004 provides The Lump Sum Mass. This method has been created using a large data base of experiments. The experiments mostly monitored the prestress losses in different types of bridges. By the variety of bridges investigated, the different types of conditions those bridges were exposed to, the data base gives a national trend of what the losses are depending on various material properties. Using linear regression analysis, the lump sum mass model was created to give an approximation of the prestress losses based on all the previous research records. This method is suitable for a first order approximation of the expected magnitude of losses for preliminary design purposes; more accurate methods may be needed for the final design, and certainly during construction.

2.3.2. Approximate Method

The approximate method usually calculates the total losses by adding the losses created by each phenomenon. Each loss is calculated separately and then added to give overall losses. The approximate method gives the losses at the end of service. This method does not allow the designer to calculate the prestress losses at a time t .

2.3.3. Time Dependent Method

In addition to approximate methods, models also provide a time dependent method. Refined methods calculate values for each loss type separately then sum results to obtain the total final loss. Time dependent methods will allow the structural engineer to determine the losses at any time t of the life of the structure. Losses due to creep and steel relaxation are inter-related. Indeed, when losses due to creep or steel relaxation occur, the prestressing strands experience a loss. The actual stress in the tendons decrease, which will decrease the losses over time.

The main advantage of the time dependent method is that it can be implemented step-wise computationally. Such analysis is helpful for complex construction as it permits the aggregation of the various losses during construction sequences such as pretensioning, deck placement, post-tensioning.

2.4. BACKGROUND HISTORY

Various research investigations have been conducted to determine prestress losses and the effects of long term losses like creep, shrinkage and steel relaxation. The following is a background history with the most relevant past research conducted by team of researchers all over the world.

2.4.1. Huo, et al. (2001)

In this study, the researchers worked on the time dependent properties of High Performance Concrete (HPC) including: creep, shrinkage and modulus of elasticity. They investigated the models that allows to predict those properties and compared them to experimental values. The model investigated was ACI-209, they high lightened that the model had the tendency to over-predict the losses in prestress due to shrinkage and creep of high-strength concrete.

The study proposed modification to the ACI-209 model that include the strength of the concrete, those modifications are applicable for both normal strength and high strength concrete.

2.4.2. NCHRP 496 Tadros, et al. (2003)

The goal of this research was to investigate the prestress losses in pretesionned bridge girders using high strength concrete, most of the models used were based on normal strength concrete (<6ksi). But over the years, high strength concrete has become a norm, and is being used in all kind of structures. Knowing the importance prestress losses can have if they are under or over-estimated, the motivation of this study stands clear: Determinate if the models that were used to design conventional concrete structures can still safely be used with high-strength concrete structures.

Seven full scale bridges were investigated in four different states. Data from 31 prestensioned girders from seven states were retrieved from previous tests and used. Data was coming from different states where the meteorological, geographical and practice conditions were different. That information helped to modify AASHTO LRFD formulas to better predict prestress losses for high-strength concrete girders.

First, the data retrieved were compared to the recommendations of ACI-209 and the AASHTO LRFD Specifications. Shrinkage results averaged 174% when using AASHTO-LRFD method and 155% according to the ACI-209 recommendations.

Creep results averaged 161% when using AASHTO-LRFD method and 179% according the ACI-209 recommendations.

Then, they developed a proposed method including correction factors based on the study of the data. The proposed method formula produced results that average 105% of the experimental value for shrinkage and 98% for creep.

2.4.3. Waldron (2004)

Determining effectively prestress losses in the design of a prestressed concrete bridge is primordial. An over prediction of the losses will lead to a very conservative design for service loads whereas an under prediction will lead to cracking at service loads. High performance and high strength concrete demonstrates to have less creep and shrinkage than conventional concrete which leads us to realize than the recommendations given from the codes will over-estimate the losses.

Nine prestressed girders were investigated. Instrumentation recorded the losses over time and those results were compared with the main creep and shrinkage models. It has been shown than the following methods, the PCI-BDM and NCHRP 496, gave a better prediction than AASHTO LRFD 1998. Indeed, the PCI-BDM and NCHRP 496 have been created to be applicable for conventional concrete as well as high strength concrete.

2.4.4. Hale, et al. (2006)

This study investigated the prestress losses in high-performance concrete bridge girders. The data collected were then compared with the AASHTO LRFD 2004 specifications, the PCI Design Handbook method described by Zia et al. (1979) and finally the NCHRP report 496 (2003). AASHTO LRFD (2004) refined method overestimated the total losses by 50 % when compared with the measured losses.

For all the girders investigated, Zia et al (1979) method showed to be more accurate than AASHTO LRFD (2004). The losses estimated with the method detailed in the NCHRP report 496 were, on average, within 6% of the measured losses.

2.4.5. Trejo, et al. (2008)

This project focused on Self Consolidating Concrete (SCC) and its properties compared to Conventional Concrete (CC). Different mix designs were investigated and full-scale girders were fabricated and tested. All of the experimental results were compared with the specifications given by the AASHTO LRFD code. Results demonstrated that the specifications may be used to predict the mechanical properties of SCC concrete with a compressive strength ranging between 5 and 10 ksi.

Creep of the SCC mixtures is lower than that of the CC mixtures, maximum creep for CC is 18 % higher than that of SCC. The AASHTO LRFD (2006) specifications allows predictions models to have ± 50 percent errors in the prediction of creep. The following models, AASHTO LRFD (2004) and (2006), ACI-209 and CEB-FIP, gave good predictions for the creep of both CC and SCC mixtures. Because the AASHTO LRFD (2006) model was calibrated for high-strength concrete with low w/c ratio, the prediction model seems to better predict CC and SCC mixtures evaluated in this study.

The prestress losses were also monitored and compared with models. The losses predicted by AASHTO LRFD (2004) were higher than the measurement for both CC and SCC girders. Maybe because the losses or gains due to deck placement is not included in AASHTO (2004). AASHTO (2006) takes into account the construction sequence, the short term losses were estimated to be within ± 30 percent errors, for the long term losses, the model apparently didn't give any good results at 140 days. Researcher said that it might be due to the fact that the girders were tested soon after being casted and that might interfere with the models.

2.4.6. Al-Omaishi, et al. (2009)

The research reported in this paper were included in the latest AASHTO revisions published in 2007. After comparing models available, they concluded that the

AASHTO LRFD 2007 refined method is more precise compared to older AASHTO LRFD specifications or PCI Bridge design methods when it comes to estimate prestress losses structures using concrete that have a compressive strength between 5 ksi and 15 ksi. It has also been proven to be applicable to both composite and non-composite members.

Even the approximate method given in AASHTO LRFD 2007 has been proven to be more accurate than any pre-2005 ASSHTO LRFD method. It is a good method for preliminary design but a refined method will have to be used in order to validate the final design.

2.4.7. NCHRP 628 Khayat, et al. (2009)

This research was intended to provide some guidelines toward the use of SCC in precast, prestressed concrete bridge elements by recommending some changes to the ASSHTO LRFD 2004 and 2007 specifications. SCC samples with different properties and mix design were created and investigated. In order to check the structural performance of SCC, four full scale AASHTO Type II precast, pretensioned girders using SCC were built. Two girders were built with SCC with a compressive strength included between 8 and 10 ksi, and two girders with HPC with similar compressive strength. They showed that SCC mixtures containing Type I/II cement develop less creep and shrinkage than those containing Type III.

The following modifications were proposed:

- Modifications of the coefficients to calculate creep using AASHTO LRFD 2007.
- Modifications of the coefficients to calculate shrinkage using AASHTO LRFD 2004.
- Current CEP-FIP MC90 can be used to predict shrinkage.

2.4.8. Pan, et al. (2013)

This paper focused on the CEP-FIP 90 model. This model has been used to predict creep and shrinkage effects on structures. It helped predicting the losses due to creep and shrinkage and helped designing structures. The study conducted by Pan, et al (2013) compared the CEP-FIP 90 model with a large database containing data from the

literature and data collected in China. All the concrete investigated had a compressive strength included between 30 MPa (4.35 ksi) and 80 MPa (11.6 ksi). He stressed the fact that most of the models available were established on statistical regression analysis of tests that were mostly using normal strength concrete. For high strength concrete, it was shown on one hand that the CEP-FIP 90 model greatly underestimates the shrinkage strain, on the other hand the CEP-FIP 90 model slightly overestimates the effects of creep.

Modification were proposed to make the model more reliable for high strength concrete. The results were closer to the experimental data than the original CEP-FIP 90 model especially for high strength concrete.

2.4.9. Summary

The study of the past research showed that numerous models are available when it comes to predict effects of short and long term losses. The main concern raised by the researchers is that most of those models were developed using experimental data where normal strength concrete was used.

The global trend has been the use of high strength concrete and most of the models have shown to not be reliable in those conditions. Researchers have been updating models by adding correction factors that would made the models applicable for higher strength of concrete.

2.5. MODELS

2.5.1. AASHTO LRFD (2004)

2.5.1.1. Lump Sum Method

AASHTO LRFD (2004) provides an approximation method for determining the time-dependent losses called the lump sum estimate of prestress losses. The lump sum is based on trends obtained by researchers using a time-step method on different beam sections. (NCHRP 496) (8-32)

For a I-girder, the long term losses due to creep of the concrete, shrinkage of the concrete and relaxation of the prestressing steel is given by:

$$33 \left(1 - 0.15 \frac{f'_c - 6}{6} \right) + 6PPR \quad (2.1)$$

In which:

$$PPR = \frac{A_{ps} f_{ps} (d_p - \frac{a}{2})}{A_{ps} f_{ps} (d_p - \frac{a}{2}) + A_s f_y (d_s - \frac{a}{2})} \quad (2.2)$$

Where:

A_{ps} = Area of prestressing steel (in.²).

f_{ps} = Stress in the prestressing steel at nominal bending resistance (ksi).

d_p = Distance from extreme compression fiber to centroid of prestressing tendons (in.).

A_s = Area of non-prestressed reinforcement (in.²).

f_y = Yield Strength of non-prestressed reinforcement (ksi).

d_s = Distance from extreme compression fiber to centroid of non-prestressed reinforcement (in.).

a = Depth of equivalent rectangular stress block (in.).

f'_c = Compressive strength of concrete (ksi).

2.5.1.2. Approximate Method

2.5.1.2.1. Total Loss Due to Shrinkage

The total losses due to the shrinkage are given by:

For prestensioned members:

$$\Delta f_{ps} = (17 - 0.15H) \quad (2.3)$$

For post-tensioned members:

$$\Delta f_{pS} = (13.5 - 0.123H) \quad (2.4)$$

2.5.1.2.2. Total Loss Due to Creep

The total losses due to the shrinkage are given by:

$$\Delta f_{pC} = 12f_{cgp} - 7\Delta f_{cdp} \quad (2.5)$$

Where:

Δf_{cdp} = Change in concrete stress at center of gravity of prestressing steel, due to permanent loads, with the exception of the load acting at the time the prestressing force is applied. So essentially the self-weight of the member is not considered (ksi).

2.5.1.2.3. Total Loss Due to Relaxation

Between jacking and transfer:

$$\Delta f_{pR1} = \frac{\log(24t)}{10} \left(\frac{f_{pJ2}}{f_{py}} - 0.55 \right) f_{pJ2} \quad (2.6)$$

Where:

t = Time estimated in days from stressing to transfer (days).

f_{pJ2} = Initial stress in the tendon at the end of stressing or jacking (ksi).

f_{py} = Specified yield strength of prestressing steel (ksi).

After transfer:

For pretensioning with stress-relieved strands:

$$\Delta f_{pR2} = 20 - 0.4\Delta f_{pES} - 0.2(\Delta f_{pS} + \Delta f_{pC}) \quad (2.7)$$

For post-tensioning with stress-relieved strands:

$$\Delta f_{pR2} = 20 - 0.3\Delta f_{pF} - 0.4\Delta f_{pES} - 0.2(\Delta f_{pS} + \Delta f_{pC}) \quad (2.8)$$

Where:

Δf_{pF} = Friction loss (ksi).

Δf_{pES} = Loss due to elastic shortening (ksi).

Δf_{pS} = Loss due to shrinkage (ksi).

Δf_{pC} = Loss due to creep of concrete (ksi).

For pretensioning with low relaxation properties:

Use 30 percent of Δf_{pR2} .

2.5.2. AASHTO LRFD (2006)

AASHTO LRFD (2006) provides two methods in order to determine the prestress losses. The short term losses are determined the same way for the two methods. The difference lies in the determination of the long term losses. The first method, called approximation estimate of time-dependent losses, calculate all the long term losses at the end of service life as one term.

The second method, called refined estimate of time-dependent losses, calculate each term separately and sum them up at the end.

2.5.2.1. Short Term Losses

The short term losses, as demonstrated previously, are constituted of the losses due to elastic shortening, friction and anchorage set.

2.5.2.1.1. Elastic Shortening

For pretensioned members:

$$\Delta f_{pES} = \frac{E_p}{E_{ci}} f_{cgp} \quad (2.9)$$

For post-tensioned members:

$$\Delta f_{pES} = \frac{(N-1)}{2N} \frac{E_p}{E_{ci}} f_{cgp} \quad (2.10)$$

Where:

Δf_{pES} = Prestress loss due to elastic shortening (ksi).

f_{cgp} = Concrete stress at the center of gravity of prestressing tendons due to the prestressing force immediately after transfer and the self-weight of the member at the section of maximum moment (ksi).

E_p = Modulus of elasticity of prestressing steel (ksi).

E_{ci} = Modulus of elasticity of concrete at transfer or time of load application (ksi).

N = Number of identical prestressing tendons.

2.5.2.1.2. Friction losses

The losses due to friction can be determined as:

$$\Delta f_{pF} = f_{pj}(1 - e^{-(Kx+\mu\alpha)}) \quad (2.11)$$

Where:

Δf_{pF} = Prestress loss due to friction (ksi).

f_{pj} = Stress in the prestressing steel at jacking (ksi).

x = Length of a prestressing tendon from the jacking end to any point under consideration (ft).

μ = Coefficient of friction.

α = Sum of the absolute values of angular change of prestressing steel path from jacking end, or from the nearest jacking end if tensioning is done equally at both ends, to the point under investigation (rad.).

e = Base of Napierian logarithms.

2.5.2.1.3. Anchorage set

Anchorage set losses depend on the type of equipment used, the value for anchor set is usually provided by the manufacturer. Once the value of the anchor set is known, it is possible to determine the loss.

2.5.2.2. Approximate Estimate of Time-Dependent Losses

This method calculate the long term losses due to creep, shrinkage and steel relaxation as one term.

$$\Delta f_{pLT} = 10.0 \frac{f_{pi} A_{ps}}{A_g} \gamma_h \gamma_{st} + 12.0 \gamma_h \gamma_{st} + \Delta f_{pR} \quad (2.12)$$

$$\gamma_h = 1.7 - 0.01H \quad (2.13)$$

$$\gamma_{st} = \frac{5}{(1+f'_{ci})} \quad (2.14)$$

Where:

Δf_{pLT} = Approximate losses due to long term losses (ksi).

f_{pi} = Prestressing steel stress immediately prior to transfer (ksi).

H = The average annual ambient relative humidity (%).

γ_h = Correction factor for the relative humidity of the ambient air.

γ_{st} = Correction factor for specified concrete strength at time of prestress transfer to the concrete member.

Δf_{pR} = An estimate of relaxation loss taken as 2.4 ksi for low relaxation strand, 10.0 ksi for stress relieved strand.

2.5.2.3. Refined Estimate of Time-Dependent Losses

The long term losses in the refined estimates of time-dependent losses is determined by calculating each loss separately and adding them at the end. The total long term losses is obtained with the following equation:

$$\Delta f_{pLT} = (\Delta f_{pSR} + \Delta f_{pCR} + \Delta f_{pR1})_{id} + (\Delta f_{pSD} + \Delta f_{pCD} + \Delta f_{pR2} - \Delta f_{pSS})_{df} \quad (2.15)$$

Where:

Δf_{pSR} = Prestress loss due to shrinkage of girder concrete between transfer and deck placement (ksi).

Δf_{pCR} = Prestress loss due to creep of girder concrete between transfer and deck placement (ksi).

Δf_{pR1} = Prestress loss due to relaxation of prestressing strands between time of transfer and deck placement (ksi).

Δf_{pR2} = Prestress loss due to relaxation of prestressing strands in composite section between time of deck placement and final time (ksi).

Δf_{pSD} = Prestress loss due to shrinkage of girder concrete between time of deck placement and final time (ksi).

Δf_{pCD} = Prestress loss due to creep of girder concrete between time of deck placement and final time (ksi).

Δf_{pSS} = Prestress gain due to shrinkage of deck in composite section (ksi).

2.5.2.3.1. Shrinkage Losses before Deck Placement

The Losses due to the shrinkage of the concrete of the girder between transfer and deck placement is given by:

$$\Delta f_{pSR} = \varepsilon_{bid} E_p K_{id} \quad (2.16)$$

In which:

$$K_{id} = \frac{1}{1 + \frac{E_p A_{ps}}{E_c I_g} (1 + \frac{A_g e_{pg}^2}{I_g}) (1 + 0.7 \Psi_b(t_f, t_i))} \quad (2.17)$$

$$\varepsilon_{bid} = k_s k_{hs} k_f k_{td} 0.48 \times 10^{-3} \quad (2.18)$$

$$\Psi_b(t_f, t_i) = 1.9k_s k_{hc} k_f k_{td} t_i^{-0.118} \quad (2.19)$$

$$k_s = 1.45 - 0.13\left(\frac{V}{S}\right) \quad (2.20)$$

$$k_{hc} = 1.56 - 0.008H \quad (2.21)$$

$$k_f = \frac{5}{1+f'_{ci}} \quad (2.22)$$

$$k_{td} = \frac{t_f}{61-4f'_{ci}+t} \quad (2.23)$$

$$k_{hs} = 2.00 - 0.014H \quad (2.24)$$

Where:

- ε_{bid} = Concrete shrinkage strain of girder between the time of transfer and deck placement.
- K_{id} = Transformed section coefficient that accounts for time-dependent interaction between concrete and bonded steel in the section being considered for time period between transfer and deck placement.
- e_{pg} = Eccentricity of prestressing force with respect to centroid of girder (in.); positive in common construction where it is below girder centroid.
- $\Psi_b(t_f, t_i)$ = Girder creep coefficient at final time due to loading introduced at transfer.
- t_f = Final age (days).
- t_i = Age at transfer (days).
- H = Relative humidity (%).
- k_s = Factor for the effect of the volume –to-surface ratio for the component.
- k_f = Factor for the effect of concrete strength.
- k_{hc} = Humidity factor for creep.
- k_{hs} = Humidity factor for shrinkage.
- k_{td} = Time development factor.

- t = Maturity of concrete (day), defined as age of concrete between time of loading for creep calculation, or end of curing for shrinkage calculations, and time being considered for analysis of creep or shrinkage effects.
- t_i = Age of concrete at time of load application (day).
- V/S = Volume-to-surface ratio (in.).
- f'_{ci} = Specified compressive strength of concrete at time of prestressing.

2.5.2.3.2. Creep Losses before Deck Placement

The prestress loss due to creep between the time of transfer and the placement of the deck is given by:

$$\Delta f_{pCR} = \frac{E_p}{E_{ci}} f_{cgp} \Psi_b(t_d, t_i) K_{id} \quad (2.25)$$

Where:

- $\Psi_b(t_d, t_i)$ = Girder creep coefficient at time of deck placement due to loading introduced at transfer.
- t_d = Age of concrete at time of load application (day).

2.5.2.3.3. Relaxation of Prestressing Strands before Deck Placement

The prestress loss due to the relaxation of steel between the time of transfer and the placement of the deck is given by:

$$\Delta f_{pR1} = \frac{f_{pt}}{K_L} \left(\frac{f_{pt}}{f_{py}} - 0.55 \right) \quad (2.26)$$

Where:

- f_{pt} = Stress in prestressing strands immediately after transfer (ksi).
- K_L = 30 for low relaxation strands and 7 for other prestressing steel.

2.5.2.3.4. Shrinkage Losses after Deck Placement

The prestress loss due to the shrinkage of girder concrete between the time of deck placement and the final time is given by:

$$\Delta f_{pSD} = \varepsilon_{bdf} E_p K_{df} \quad (2.27)$$

In which:

$$K_{df} = \frac{1}{1 + \frac{E_p A_{ps}}{E_{ci} A_g} \left(1 + \frac{A_c e_p^2}{I_c}\right) (1 + 0.7 \Psi_b(t_f, t_i))} \quad (2.28)$$

Where:

ε_{bdf} = Concrete shrinkage strain of girder between the time of deck placement and final time.

K_{df} = Transformed section coefficient that accounts for time-dependent interaction between concrete and bonded steel in the section being considered for time period between deck placement and final time.

e_{pc} = Eccentricity of prestressing force with respect to centroid of composite section (in.).

A_c = Composite section (in.2).

I_c = Moment of inertia of the composite section (in.4).

2.5.2.3.5. Creep Losses after Deck Placement

The prestress loss due to the creep of girder concrete between the time of deck placement and the final time is given by:

$$\Delta f_{pCD} = \frac{E_p}{E_{ci}} f_{cgp} \left(\Psi_b(t_f, t_i) - \Psi_b(t_d, t_i) \right) K_{df} + \frac{E_p}{E_c} \Delta f_{cd} \Psi_b(t_f, t_d) K_{df} \quad (2.29)$$

Where:

Δf_{cd} = Change in concrete stress at centroid of prestressing strands due to long-term losses between transfer and deck placement (ksi).

$\Psi_b(t_f, t_d)$ = Girder creep coefficient at final time due to loading at deck placement.

2.5.2.3.6. Relaxation of Prestressing Strands after Deck Placement

The prestress loss due to the relaxation of steel between the time of deck placement and the final time is given by:

$$\Delta f_{pR2} = \Delta f_{pR1} \quad (2.30)$$

2.5.2.3.7. Shrinkage of Deck Concrete

The prestress gain due to shrinkage of deck composite section is given by:

$$\Delta f_{pSS} = \frac{E_p}{E_c} \Delta f_{cdf} K_{df} (1 + 0.7 \Psi_b(t_f, t_d)) \quad (2.31)$$

In which:

$$\Delta f_{cdf} = \frac{\varepsilon_{ddf} A_d E_{cd}}{(1 + 0.7 \Psi_b(t_f, t_d))} \left(\frac{1}{A_c} - \frac{e_{pc} e_d}{I_c} \right) \quad (2.32)$$

Where:

Δf_{cdf} = Change in concrete stress at centroid of prestressing strands due to shrinkage of deck concrete.

ε_{ddf} = Shrinkage strain of deck concrete between placement and final time.

A_d = Area of deck concrete (in.²).

E_{cd} = Modulus of Elasticity of deck concrete (ksi).

e_d = Eccentricity of deck with respect to the gross composite section. (in.).

$\Psi_b(t_f, t_d)$ = Creep coefficient of deck concrete at final time.

2.5.3. CEB-FIP (1993)

The CEB-FIP (1993) defines the creep coefficient as follows:

$$\phi(t, t_0) = \phi_0 \beta_c (t - t_0) \quad (2.33)$$

Where:

ϕ_0 = Notional Creep.

β_c = Coefficient that takes into account the development of creep with time.

t = Age of concrete at the moment considered (days).

t_0 = Maturity of concrete at time of loading (days).

The notional creep is defined as follows:

$$\phi_0 = \phi_{RH} \beta(f_{cm}) \beta(t_0) \quad (2.34)$$

In which:

$$\phi_{RH} = 1 + \frac{1 - \frac{RH}{RH_0}}{0.46 \left(\frac{h}{h_0} \right)^{1/3}} \quad (2.35)$$

$$\beta(f_{cm}) = \frac{5.3}{(f_{cm}/f_{cm0})^{0.5}} \quad (2.36)$$

$$\beta(t_0) = \frac{1}{0.1+(t_0/t_1)^{0.2}} \quad (2.37)$$

Where:

f_{cm} = Compressive strength at 28 days (MPa).

f_0 = 10 MPa.

RH = Relative humidity in percent.

RH_0 = 100%.

h = Notional size of the member (mm).

h_0 = 100 mm.

t_1 = 1 day.

The development of the creep with time is given by:

$$\beta_c(t - t_0) = \left(\frac{(t-t_0)/t_1}{\beta_H+(t-t_0)/t_1} \right)^{0.3} \quad (2.38)$$

In which:

$$\beta_H = 150 \left\{ 1 + \left(1.2 \frac{RH}{RH_0} \right)^{18} \right\} \frac{h}{h_0} + 250 \quad (2.39)$$

The CEB-FIP (1993) defines the shrinkage strain as follows:

$$\varepsilon_{cs}(t, t_s) = \varepsilon_{cs0} \beta_s(t, t_s) \quad (2.40)$$

In which:

$$\varepsilon_{cs0} = \varepsilon_s(f_{cm}) \beta_{RH} \quad (2.41)$$

$$\beta_{RH} = -1.55(1 - (RH/100)^3) \quad (2.42)$$

$$\varepsilon_s(f_{cm}) = \left(160 + 10\beta_{sc} \left(9 - \frac{f_{cm}}{10} \right) \right) \times 10^{-6} \quad (2.43)$$

$$\beta_s(t - t_0) = \sqrt{\frac{(t-t_0)}{350\left(\frac{h}{4}\right)^2 + (t-t_0)}} \quad (2.44)$$

Where:

β_{sc} = Factor for the type of cement used, 4 for slow hardening cement, 5 for normal or rapid cement, and 8 for rapid hardening cement.

3. EXPERIMENTAL WORK

3.1. SPLICED GIRDER CONSTRUCTION

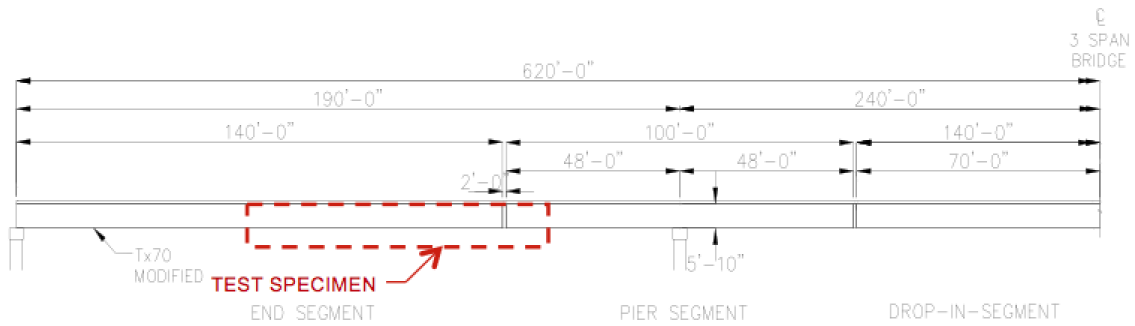
3.1.1. Introduction

From Chapter 2, on-pier and in-span splicing has been presented. On-pier splicing limits the span length reachable because of hauling limitations. In-span splicing is a more appropriate method to increase the span length.

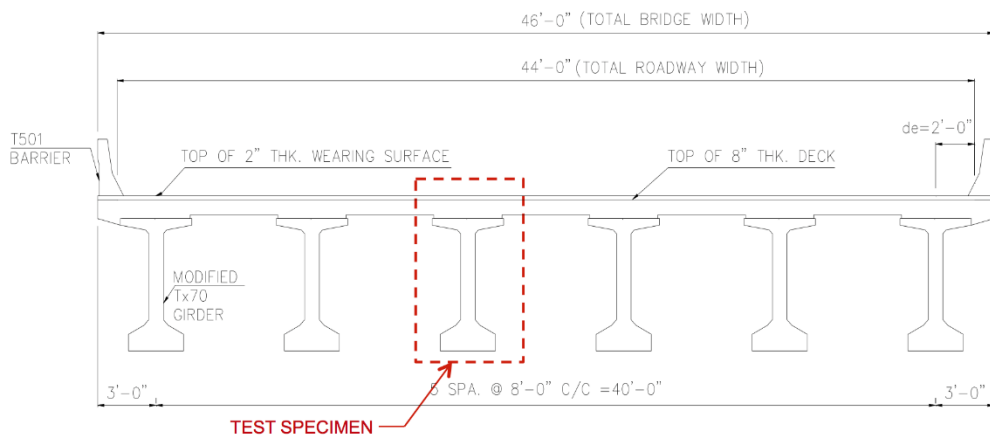
The use of precast prestressed segments is predominant in Texas bridges. They are often mass produced in a precasting plant as the shapes have been standardized. Therefore, the research motivation to implement new splicing technologies in order to extend the length of the spans is important.

Different splicing methods have been investigated over the years and they all have their merits. Some of them include only mild steel, others include only prestressing steel but after investigating design requirements, it appeared that a mixed design would be more relevant in order to increase the span length.

According to TxDOT recommendations, a three-span continuous spliced girder system was chosen for the prototype bridge. The cross-section used is the Tx70 but it had to be modified. The web was thickened in order to better accommodate the stirrups and the three ducts. Figure 3.1 represents the prototype three-span continuous bridge. The middle span reaches 240 ft whereas the first and third spans are 190 ft long. The end and drop-in segments are 140 ft long and the on-pier segments are 96 ft long. The splices are designed to be 2 ft wide. The prototype bridge has six lines of girder segments spaced 8 ft apart and allow three traffic lanes. Figure 3.1 also presents the test specimen and its position relative to the prototype bridge. The size of the High Bay Laboratory (HBL) governed the length of the test specimen that could be assembled. Working on the design of a prototype bridge and the loads it would be subjected to, the design team came up with a precast prestressed spliced concrete girder that was 71 ft long.



(a) Prototype bridge



(b) Prototype bridge cross section

Figure 3.1. Prototype Bridge and the Test Specimen (Hueste et al, 2014).

3.1.2. Test Specimen Properties

3.1.2.1. Geometrical Properties

According to Figure 3.1, the specimen is required to only have one splice but due to the crane limitation in the High Bay Laboratory, two additional splices were added. Indeed, the crane used to move elements in the laboratory has a weight limit set at 36 kips. The final test specimen was constructed using four segments and three splices as shown in Figure 3.2.

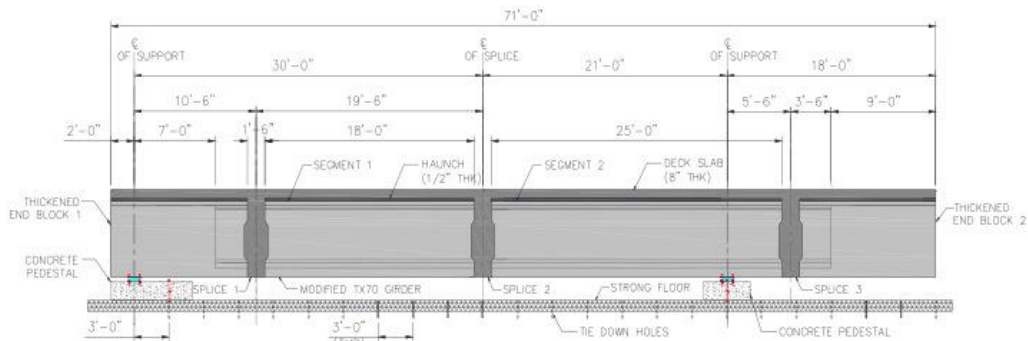


Figure 3.2. Test Specimen (Hueste et al. 2014).

Because the specimen was post-tensioned, the end segments were thickened in order to accommodate the post-tensioning anchorage system.

Figure 3.3 represents the cross-section of the test specimen. As mentioned before, the original Tx70 had to be modified by widening the web to 10 in., increasing the thickness of the top flange to 5 in. and widening the top and bottom flanges to 45 in. and 35 in.. Table 3.1 presents the section properties of the Modified Tx70 girder.

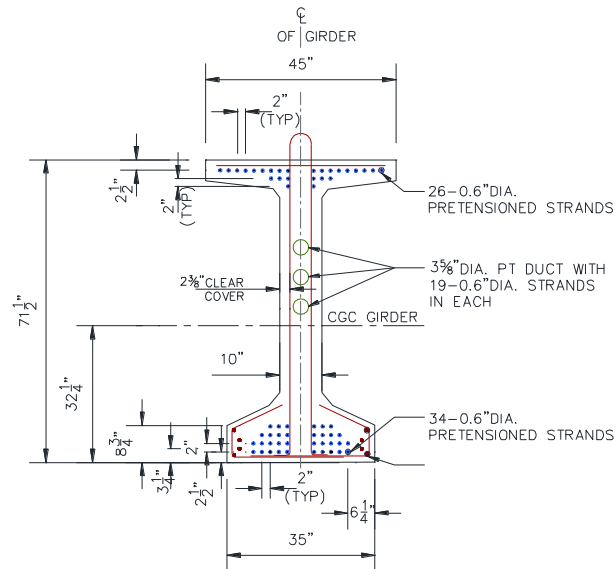


Figure 3.3. Cross Section of Modified Tx70 Girder (Hueste et al. 2014).

Table 3.1. Section Properties of the Modified Tx70 Girder (Hueste et al. 2014).

Girder	Depth of Neutral Axis from Top (in.)	Depth of Neutral Axis from Bottom (in.)	Area (in. ²)	Moment of Inertia (in. ⁴)	Weight (plf)
Modified Tx 70	37	34.5	1243.5	817,093	1295

3.1.2.2. Deck Properties

The deck was 8 in. thick and 92 in. wide and reinforced with mild steel following the recommendations from TxDOT standard construction practice. The cover used for the deck was 2 in. for the top bars and 1.25 in. for the bottom bars. The 28-day concrete compressive strength used for the deck design was 4 ksi.

3.1.2.3. Splice Details

The splices are cast-in-place after the girder segments are set, and are not pretensioned. They are partially prestressed as the post-tensioning ducts run through the splices and additional mild steel reinforcement is provided. Several 180-degree bent hooked bars are anchored in the segments and extend into the cast-in-place splice location, overlapping each other. In addition, vertical reinforcement was provided at each splice location. The detailing of the splice is shown in Figure 3.4.

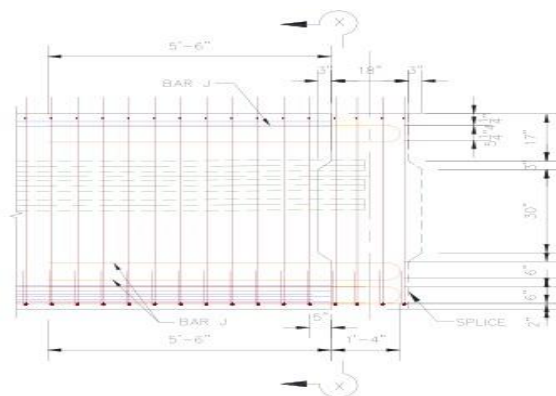


Figure 3.4. Detailing of the Splice (Hueste et al. 2014).

3.1.2.4. Concrete Properties

Different types of concrete were used in to cast the girder segments, the splices and the deck. The following tables present a summary of the concrete properties. This information was important as it was used in all the subsequent calculations to predict all prestress losses, strain profiles and numerical analysis. Table 3.2 and Table 3.3 present the properties of the concrete used for the girder.

Table 3.2. Compressive Strength of SCC used for Girder Segments.

Compressive Strength (ksi)							
Age (Days)	3	7	28	56	91	222	294
Batch 1	-	7.77	10.03	-	-	-	-
Batch 2	6.65	7.60	9.35	10.81	10.60	11.73	-
Batch 3	-	7.63	9.65	-	-	-	-
Batch 4	6.50	7.87	9.38	11.03	10.87	-	11.43
Batch 5	-	7.72	9.65	-	-	-	-
Batch 6	6.97	7.91	9.82	10.56	11.07	-	11.13
Batch 7	-	8.32	10.47	-	-	-	-
Batch 8	-	8.34	10.53	-	-	-	-
Average	6.71	7.89	9.86	10.8	10.84	11.73	11.33

Table 3.3. Modulus of Elasticity of SCC used for Girder Segments.

MOE (ksi)				
Age (Days)	7	28	56	294
Batch 2	4239	4607	5091	-
Batch 4	4240	4772	5158	5368
Batch 6	4224	4845	5128	5494
Average	4234	4741	5126	5452

Table 3.4 presents the properties of the concrete used for the splices. Table 3.5 presents the properties of the concrete used for the deck.

Table 3.4. Properties of Concrete used for Splices.

Age (Days)	1	5	7	28	56	103
Compressive Strength (ksi)	4.50	7.11	7.62	8.79	9.46	9.50
MOE (ksi)	x	x	5548	5895	5954	x

Table 3.5. Properties of Concrete used for Deck.

Age (Days)	1	14	28	56	95
Compressive Strength (ksi)	2.04	5.27	5.36	6.66	6.81
MOE (ksi)	3981	x	5052	4684	x

3.1.2.5. Steel Properties and Layout

All segments were pretensioned when they were cast in San Antonio. Once the splices and deck were cast in the High Bay Lab, the full length of the specimen was post-tensioned. Figure 3.3 represents the cross-section of the girder and shows where the pretensioning strands were placed in the top and bottom flanges. Table 3.6 presents the detailing of the pretensioning. The post-tensioning layout is presented in Figure 3.5.

Table 3.7 gives additional information regarding the post-tensioning details. The post-tensioning has been designed to balance the weight of the deck. Table 3.8 presents the characteristics of the prestressing and mild steel used for design.

Table 3.6. Pretensioning Details.

Pre-tensioning	Top Layer	Bottom Layer
Strands (0.6 in. diameter)	26	34
Force at Transfer, kips	1142	1494
Eccentricity (girder only), in.	33.7	29.4
Eccentricity (composite), in.	20.5	42.7

Table 3.7. Post-Tensioning Details.

Post-Tensioning	Duct #1 (Top)	Duct #2 (Middle)	Duct#3 (Bottom)
Tendons	19	19	19
PT Force Transfer (Design value), kips	779	779	779
Real PT value, kips	850	843	823
e_c in.	3.2	3.8	10.8

Table 3.8. Steel Properties.

Parameters		Values
Mild Reinforcing Steel	f_y	60 ksi
Prestressing Steel	Strand Diameter	0.6 in.
	f_{pu}	270 ksi
	Duct diameter	3.625 in.
	Coeff. of friction, μ	0.25
	Coeff. of wobble loss	0.0002/ft
	Anchor Set	0.375 in
	Elastic Modulus, E_p	28,500 ksi

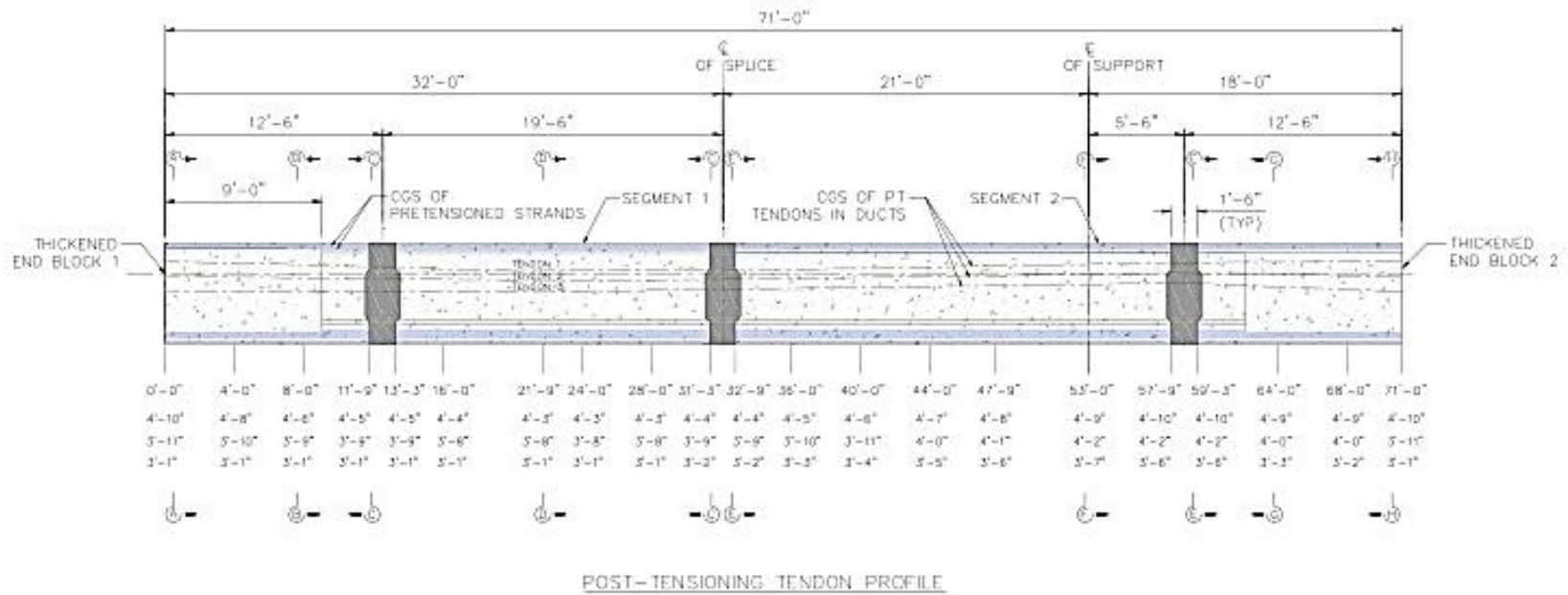


Figure 3.5. Post-Tensioning Layout (Hueste et al. 2014).

3.1.3. Instrumentation

In order to investigate the behavior of the specimen and especially the splices, five different tests were performed. The first two tests were nondestructive tests, the goal was to investigate the behavior of the test specimen under service loads in the maximum positive and negative moment regions. The following three tests were destructive tests, where the post-cracking behavior of the specimen was investigated until the ultimate strength was reached.

Numerous instruments were used to monitor any changes in strain over time in the specimen. The instrumentation included both internal and external instruments, such as: strain gages on mild steel, embedded concrete gages, surface strain gages, string potentiometers, Linear Variable Differential Transformers (LVDTs), and DEMEC points.

3.1.3.1. Strain Gages

The strain gages were positioned on the rebar. They were used in the thickened end of the segments but mostly in the splices which is the main zone of interest.

3.1.3.2. Surface Strain Gages

The surface strain gages were positioned all over the deck, directly on the concrete and also on the north side of the girder on both the top and bottom flanges. Those gages allowed the determination of the compressive or tensile strain that the girder was undergoing at certain locations. Figure 3.6 presents the locations of the surface strain gages on both the deck and the north face of the specimen.

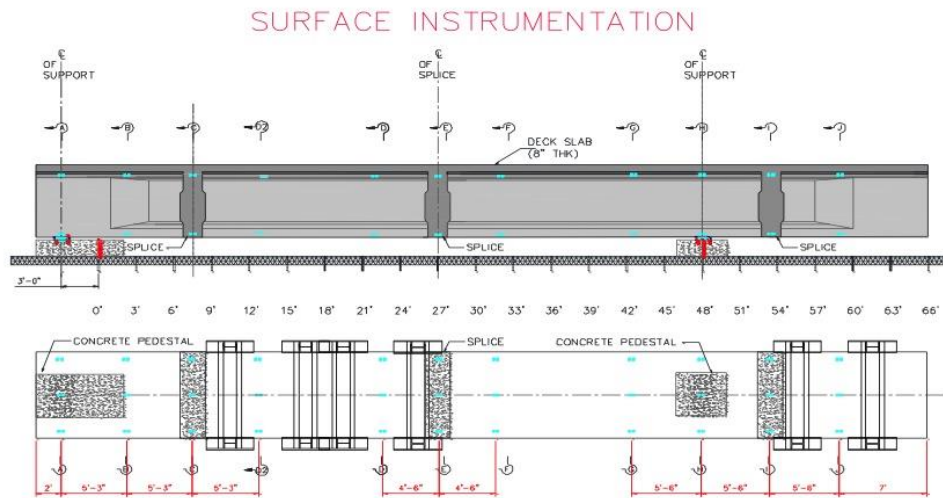
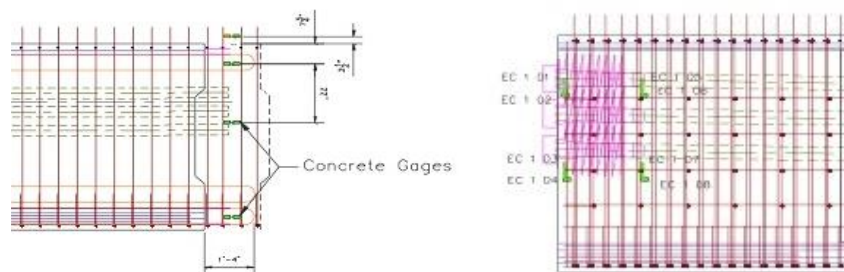


Figure 3.6. Surface Strain Gages (Hueste et al. 2014).

3.1.3.3. Embedded Concrete Gages

The embedded strain gages are directly in the concrete. They are located in the thickened ends of the end segments and at each splice location. For each splice location, there are four embedded concrete gages, in the deck, top flange, web and bottom flange. Those gages provide measurements to plot the full strain profile at each time of interest. Figure 3.7 presents the locations of the embedded concrete gages.



(a) *Embedded concrete gages in splice* (b) *Embedded concrete gages in girder*

Figure 3.7. Embedded Concrete Gages (Hueste et al, 2014).

3.1.3.4. String Potentiometers

The string potentiometers were positioned below the girder along its full length every 2 ft. They provided information to determine the deflection profile of the girder under any load applied. The string potentiometers were attached to the floor of the High Bay Laboratory and directly to the bottom of the specimen as shown in Figure 3.8.

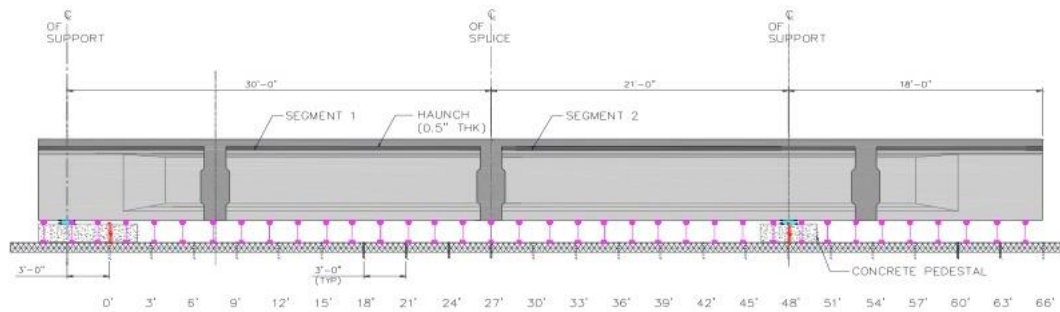


Figure 3.8. String Potentiometers Locations (Hueste et al. 2014).

3.1.3.5. Linear Variable Differential Transformers (LVDTs)

Eight LVDTs were mounted at the location of each splice. The LVDTs monitor the deformation of the splices by placing vertical, horizontal and diagonal LVDTs. Figure 3.9 presents the position of each LVDT at each splice location.

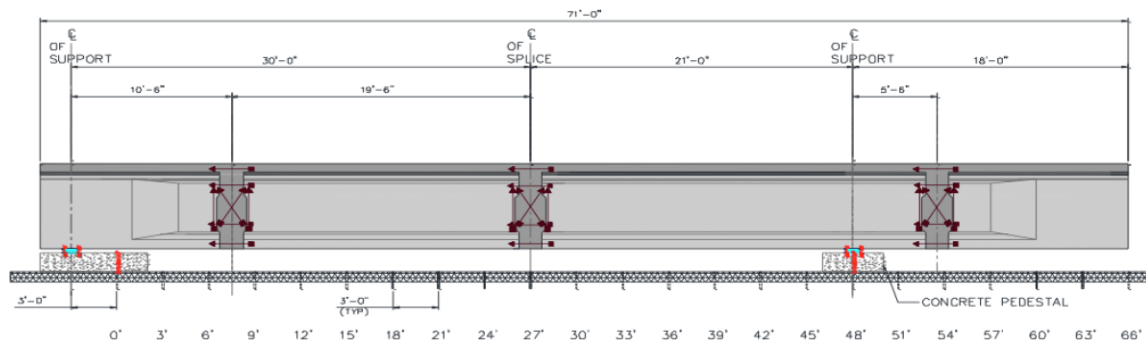


Figure 3.9. Positiones of LVDTs (Hueste et al. 2014).

3.1.3.6. Demountable Mechanical (DEMEC) Points

The DEMEC points were part of a grid that was drawn on the girder at three different locations. Each intersection point of the grid was used as a DEMEC point. The distances between DEMEC points are measured over time during testing. This method can be interesting when it comes to determining how the girder deforms but it is time consuming as readings need to be taken at each time of interest. In addition, DEMEC measurements contain errors as they are performed manually. However, an electronic device was used to capture the measurements and improve accuracy.

3.1.4. Construction Process

In order to build the specimen, precast prestressed concrete segments were cast in San Antonio and brought to the TAMU High Bay Structural Laboratory. The segments were aligned and seated on temporary supports. The experimental work in the laboratory spanned from the time the segments were brought into the laboratory until the specimen was decommissioned and taken out of the laboratory; a period of nine months to perform the following tasks.

3.1.4.1. Installation of the Girder Segments in the High Bay Lab

Figure 3.10 show the precast prestressed segments being installed in the High Bay Laboratory. Each segment was placed on supports at each end. Segments had to be perfectly aligned and spaced. Figure 3.11 (a) and (b) present the installation of the ducts in the splices. Once the ducts were placed, strands were run along the full length of the specimen as presented in Figure 3.11 (c) and (d).



(a) Setting the second segment



(b) Aligned segments

Figure 3.10. Alignment of Girder Segments.



(a) Placing bottom duct



(b) Ducts placed and sealed



(c) Running strands in top duct



(d) Top duct completed

Figure 3.11. Placing Ducts between Segments.

3.1.4.2. Preparing the Splices

Figure 3.12 (a) shows the transverse steel reinforcement installed in the Splice connection. In addition, strain gages are attached to steel reinforcement in the top and bottom flange. Those gages were used to monitor the stresses that the steel undergoes under certain loading conditions. Those strain gages can be seen in Figure 3.12 (b). Moreover, embedded concrete gages are installed at three locations in the splice (top flange, web and bottom flange). A typical concrete gage is shown in Figure 3.12 (c).



(a) Reinforcement in the splice



(b) Strain gages on bars



(c) Embedded concrete gage in the splice

Figure 3.12. Splice Details.

3.1.4.3. Mix Design

Different mix designs were mixed and poured in order to test the material properties and find an adequate mix for the splices. Different types of cement and type of aggregates were used to determine their effects on material properties. After mixing more than 10 batches, a satisfactory mix was selected for the splices. The deck concrete was specified as TxDOT Class 5.

3.1.4.4. Formwork

In order to cast the splices, formwork was designed to adapt to the shape of the specimen. The formwork for the splices was made of two pieces that were attached to each other by four threaded bars. Maintaining the two opposite pieces firmly attached and sealed to prevent any leaks during casting. Figure 3.13 shows two photographs of the splice formwork.



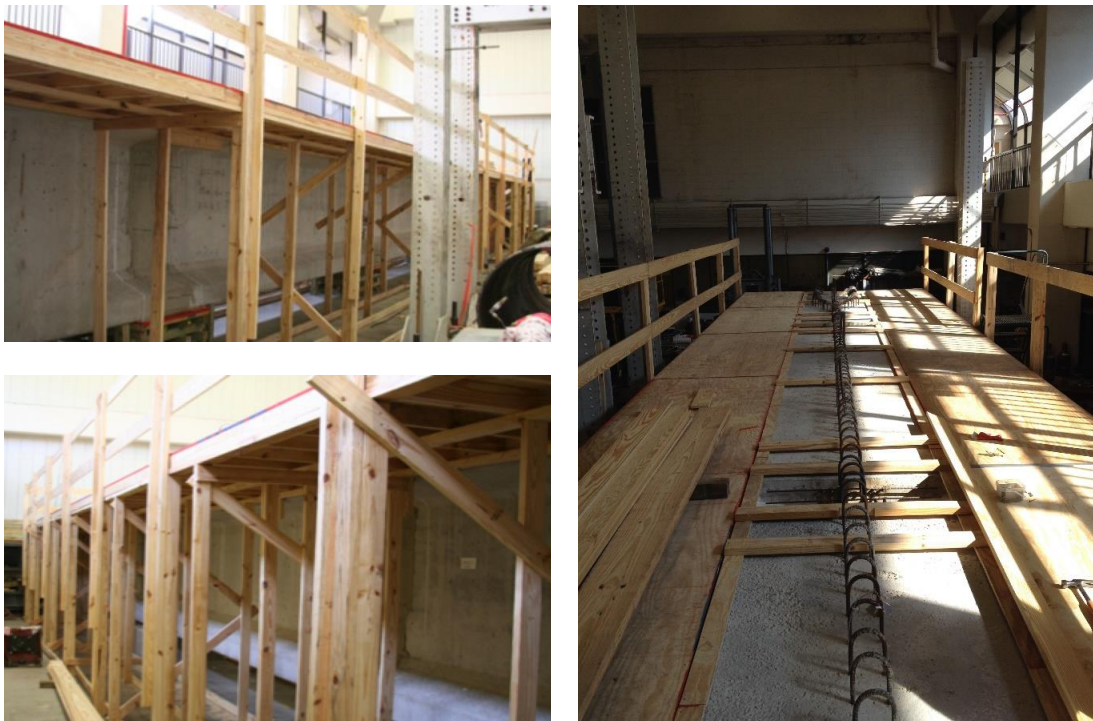
(a) Splice formwork



(b) View from the top

Figure 3.13. Splice Formwork.

The next step was to build formwork for the deck and a timber falsework structure was constructed to support the formwork in place. The falsework was made of numerous timber frames that were braced. After the formwork for the deck was erected, a guard rail was added for security purposes. Figure 3.14 presents the deck formwork and its falsework.



(a) Falsework view from the sides

(b) Formwork view from the top

Figure 3.14. Deck Formwork.

3.1.4.5. Cast Splices

Once the formwork was in place and secured, the splices were cast according to the mix design determined earlier. In addition, cylinders and beams were made to perform hardened property testing over time. Figure 3.15 presents the casting of the splices and students making concrete cylinders for further testing.



(a) Pouring concrete



(b) Preparing concrete cylinders and beams

Figure 3.15. Casting the Splices and making Cylinder and Beam Samples.

3.1.4.6. Deck

Several days after the splices were successfully cast, the formwork for the deck was finalized. The steel reinforcement for the deck was installed as well as embedded concrete gages at each splice location. The deck was cast and samples were taken in order to make test cylinders and test prisms for further testing of hardened concrete properties testing as presented in Figure 3.16.



(a) *Finished formwork*



(b) *Installation of deck reinforcement*



(c) *Casting of the deck*

Figure 3.16. Deck Preparation and Casting.

3.1.4.7. Installation of Gages and Other Measurement Equipment

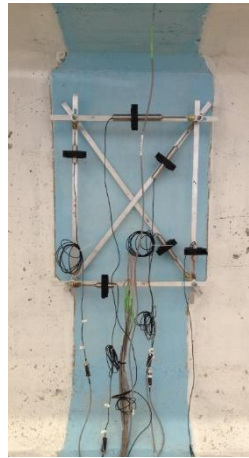
Once the deck was cast, all of the external instrumentation was installed. Surface strain gages were positioned on the top of the deck as seen in Figure 3.17 (a). Surface strain gages on the north side of the specimen on both the top and bottom flanges are presented on Figure 3.17 (c). LVDTs were installed at each splice location to record the deformations that could occur vertically, horizontally and at 45 degrees, as presented on Figure 3.17 (b). String potentiometers installed under the specimen in order to obtain a precise profile of the deflections at any time can be seen on Figure 3.17 (d). The DEMEC points on the south side of the specimen are presented on Figure 3.17 (e).

3.1.4.8. Post-Tensioning of the Specimen and Grouting

After all the instrumentation has been installed, the specimen was post-tensioned. The company Dywidag Systems International (DSI) performed the post-tensioning of the specimen as presented in Figure 3.18. In addition, Figure 3.19 presents the grouting process and the making of grout cubes and cylinders for further testing.



(a) Surface strain gages on top of the deck



(b) LVDTs at splice location



(c) Surface strain gages on top and bottom flanges



(d) String pots under the specimen



(e) DEMEC Points on the south side of the specimen

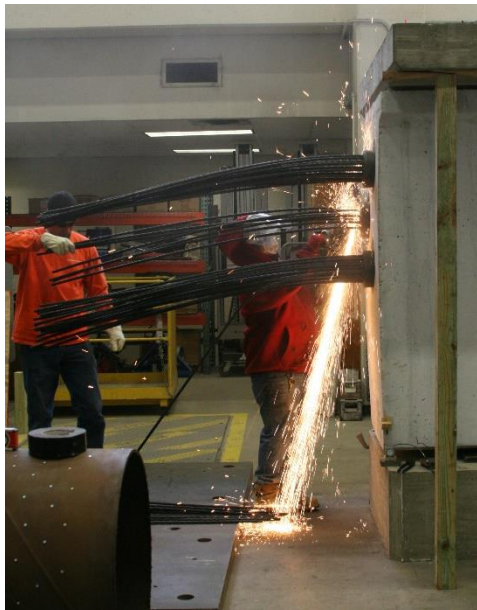
Figure 3.17. External Instrumentation.



(a) Post-tensioning



(b) Global view post-tensioning



(c) Cutting the strands

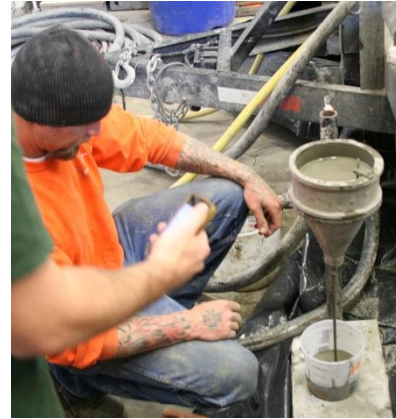


(d) Post-tensioning completed

Figure 3.18. Post-Tensioning Operation.



(a) Mixing the grout



(b) Checking the viscosity



(c) Pressure grouting the ducts



(d) Preparing grout cubes and cylinders

Figure 3.19. Grouting Operation.

3.2. CREEP FRAMES

Cylinders from batch 2, 4 and 6 (taken on the 7th of August 2013) from the precast girder concrete were used to perform the creep testing. Three creep frames were used. Figure 3.20 shows the setup used for the creep frames. Each frame was composed of three steel plates, four rods and two springs. The two springs were located at the bottom of the frame between two of the three steel plates. Four concrete cylinders were stacked between two half concrete cylinders (top and bottom) and all the cylinders were compressed by two steel plates. Each frame required seven cylinders, five which were loaded in compression in the creep frame (four plus two halves) and two that were outside of the frame and used as a reference for shrinkage. Every cylinder (except the half cylinders) was gaged longitudinally on opposite sides. Cylinders compressed in the frame were sulfur capped to make sure that alignment between them was maintained.

In addition, two steel plates were gaged (six gages per plate) to compensate for the temperature strains. To summarize, each creep frame requires seven cylinders, two steel plates and 24 strain gages total.

Table 3.9 summarize the composition of each frame, showing which batch was used for each cylinder. As mentioned previously, three different batches were used. Batch 2 and 4 were both used for Frame 1 and 2. Frame 1 and 2 both included three cylinders from Batch 2 and three cylinders from Batch 4. The third frame was totally composed of cylinders from Batch 6.

Table 3.10 shows the loading that was applied to each frame using an MTS machine. The loading was chosen in order to represent the stresses experienced by the girder when pretensioning and post-tensioning was applied.

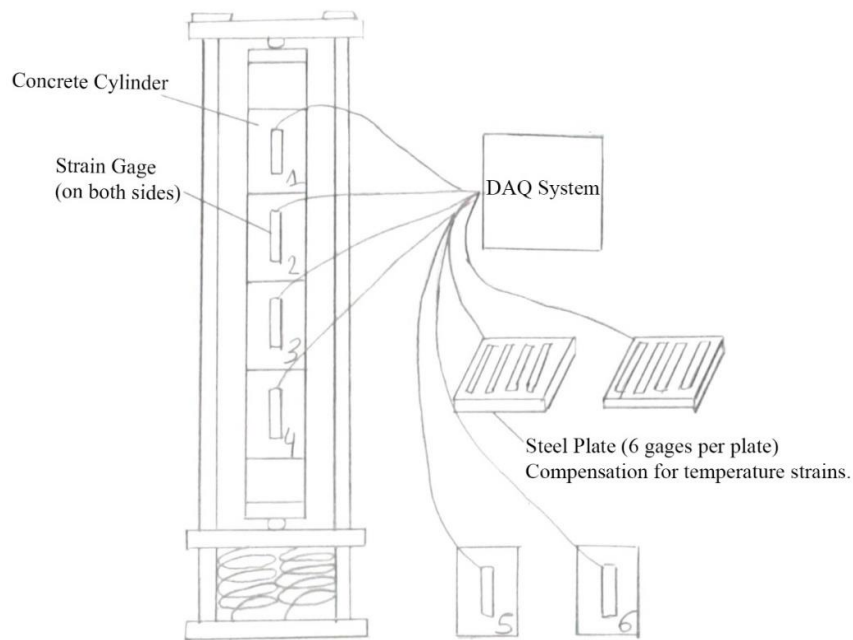


Figure 3.20. Creep Frame Test Setup.

Table 3.9. Batches used for the Creep Frames.

Frame	Cylinder 1	Cylinder 2	Cylinder 3	Cylinder 4	Cylinder 5	Cylinder 6
1	B2	B4	B2	B4	B2	B4
2	B2	B4	B2	B4	B2	B4
3	B6	B6	B6	B6	B6	B6

Table 3.10. Loading applied to each Creep Frame.

Frame	Loading	Description
1	$0.15f'_c = 21.5 \text{ k}$	Pretensioning
2	$0.25f'_c = 36 \text{ k}$	Post-tensioning
3	$0.35f'_c = 50.3 \text{ k}$	Pre + Post

Creep frames that were used for a past project in 2008 were unloaded in order to be used again. Numerous tasks had to be performed to get the frames ready. Below is the description of the most important tasks.

3.2.1. Sulfur Capping

Figure 3.21 (a) shows the material used for sulfur capping the concrete cylinders. The list of equipment is as follows:

- A melting pot to melt the sulfur.
- A capper to receive the melted sulfur and cap the concrete cylinder.
- The sulfur material to be melted.
- A capping ladle.
- Mineral oil to grease the capper.

The sulfur takes usually 2 to 3 hours to melt completely under 275 degrees Fahrenheit. Some extra concrete cylinders were used to practice before capping the actual specimens. After capping 8 to 10 cylinders, it appeared that the capper was not totally plane. As a result, the capping done were neither flat nor centered.

If a cap is not in accordance with the ASTM Standard C617/C617M (2012), it was easily breakable and replaceable with a new one. It was important to check that when the cylinder is placed in the capper, it is completely centered at its base. The capper used was misaligned. The alignment of each cylinder had to be done manually, it was the only way to obtain reasonable results.

Figure 3.21 (b) shows the twelve capped cylinders ready to be gaged. The entire procedure has to be done under the hood as the sulfur fumes could be toxic for anyone to breathe. In addition, the capper has to be oiled numerous times with mineral oil in order for the sulfur not to adhere to the capper.



(a) Sulfur capping equipment



(b) Capped cylinders

Figure 3.21. Capping Cylinders.

Sulfur capping is a procedure that takes time and requires precision. Capping in a hurry or without any rigorous method leads to mis-aligned specimens which are detrimental for the creep testing; capping is an important step and must not be overlooked.

3.2.2. Gaging Cylinders and Steel Plates

The steel plates were sanded to make the surface as flat as possible since numerous gages were going to be placed on them. After using a sanding machine and manually sanding them using higher grade sanding paper, the six plates were ready to be gaged. Six steel plates were gaged with six gages on each plate, giving a total of thirty six gages.

The gaging process consists of cleaning up the area as much as possible using M-prep Conditioner A followed by the use of M-prep Neutralizer A. Those products clean the surface and create optimum conditions for an adhesive to be used. After that, a piece of tape is used to place the gage at the right location avoiding contact with fingers and other external elements. The gages are very fragile and require a great care in order to be placed properly.

Once the gage is in the right location, the tape is removed from one side and then M-bond Catalyst C is applied to the gage. Once dry, special M-bond Adhesive is applied along the gage and the gage needs to be pressed for a couple of minutes. The tape can then be removed.

After all the gaging is done, the gages need to be protected using a coating. The coating depends on the environmental conditions to which the gages will be exposed. A type M-coat A coating was used; the creep frames will be exposed to the same conditions as the girder, which is the lab environment. The humidity is approximately equal to 50 percent, so there is no need to use a more protective coating. Figure 3.22 presents the finished steel plates where six gages have been placed and coated.

There were a total of 18 cylinders for three creep frames. Each cylinder was gaged longitudinally at two opposite faces (180 degrees apart). There was a total of an additional 36 gages to be applied. Twelve cylinders were sulfur capped, as they were part of the creep frames, the other six cylinders were placed next to the frames as a reference but were not subject to any loading.



Figure 3.22. One Gaged Steel Plate.

Cylinders were prepared in order to be gaged. On each opposite side of the cylinders, an area was sanded manually to make the concrete surface as flat as possible. Sanding the cylinders revealed some air pockets, it was necessary to use epoxy to fill up those gaps. After drying, cylinders had to be sanded again to eliminate the extra epoxy and leave a totally flat surface ready to be gaged. Figure 3.23 shows a cylinder that has been sanded, then epoxy has been applied and it has been sanded again. The surface is completely flat and ready to be cleaned with the chemicals products.



Figure 3.23. Concrete Cylinder Ready for Gaging.

The gaging process of the cylinders is the same as for the steel plates; it is more difficult as the surface is a cylinder and not a plate. It required more precision to place the gages correctly. The same product were used to clean the surface and to bond the gage to the concrete cylinder.

Also, gaging capped cylinders was more difficult as there was less room to execute the work. The caps are also fragile and need to be protected in order to not be damaged during the gaging process.

3.2.3. Half Cylinders

For each creep frame, half-cylinders were used at the top and bottom to protect the main test cylinders from being directly adjacent to the steel plate. The half-cylinders (six pieces) were retrieved from the previous creep frames and came from six different batches of concrete. It was necessary to perform compressive strength tests on those cylinders to make sure that the compressive strength was sufficient. Two cylinders from each batch were tested. Table 3.11 shows the results obtained and shows that the half cylinders can be used in the creep frame. Indeed, they exhibited a compressive strength superior or equal to 12 ksi, which is higher than for the specimens from the girder.

Table 3.11. Compressive Strength of the Half Cylinders.

Half Cylinder	1	2	3	4	5	6
Average f'_c (ksi)	13.3	13.0	12.9	12.1	12	13.5

The half cylinders were then sulfur capped to be ready for use in the creep frames. Figure 3.24 presents all the cylinders and steel plates after being gaged and coated. The next step was the assembly of the creep frames and the wiring between the frames and the data acquisition system (DAQ).



Figure 3.24. Cylinders and Plates, Gaged and Coated.

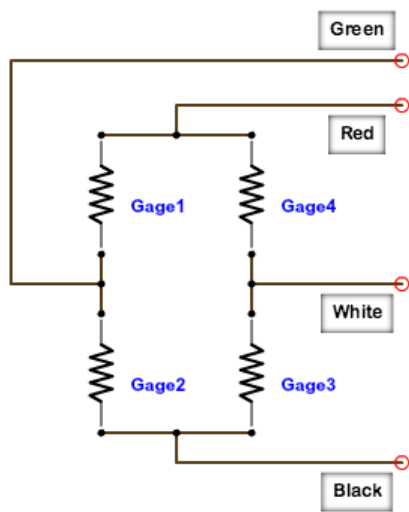
3.2.4. Wiring and DAQ

As the wires provided with the strain gages were not shielded. Thus, to prevent noise, the bridge to connect the gages together, shielded wires were used to reach the DAQ system. The same length of shielded wire was used for each gage to maintain consistency.

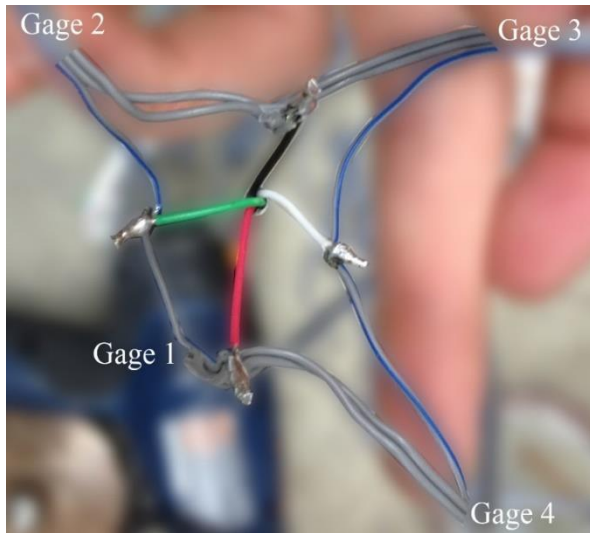
3.2.5. Assembling Creep Frames

Once all the cylinders were capped, gaged and coated, the creep frames were assembled. As mentioned before, a creep frame consist of four cylinders stacked on top of each other held between two half cylinders. The whole set is loaded in the frame, while two additional cylinders are left unloaded. In addition, two steel plates are used for temperature compensation. After assembling the creep frame, the connection was made between the gages and the shielded wires using a bridge circuit.

The bridge is represented on Figure 3.25 (a). This bridge contains four gages, two gages from a cylinder (gage 1 and 3) and two compensation gages from the steel plate (gage 2 and 4). The circuit is as follows, the four colors, green,red,white and black represents each of the component of the shielded wire. This wire was connected to the DAQ system to monitor the gages' activity.



(a) Bridge circuit schematic view



(b) Bridge circuit

Figure 3.25. Bridge Circuit.

Assembling the creep frames required a lot of soldering, each wire coming from the gages needed to be connected with the shielded wire according to the bridge circuit above. The circuit can be seen in Figure 3.25 (b). There were 72 connections to solder separately; connectors could have been used but it would have created some noise in the data acquisition. Since the strain measured were so small (microstrains), any type of noise had to be avoided. Soldering the connections was the best option available, because it is not easily modifiable as a connector would be.

3.2.6. Loading the Creep Frames and Recording Data

The creep frames were loaded using a MTS machine as shown in Figure 3.26 (a). The frames were still connected to the DAQ system while being loaded. They stayed connected and recorded data for a couple of days before they were moved to a storage room. Data were first recorded every 5 minutes but after a month, the frequency was dropped to every 20 minutes. Figure 3.26 (b) shows the three creep frames after being loaded. They are connected to the DAQ system which takes readings continually.



(a) Loading the creep frame



(b) Creep frames loaded and recording data

Figure 3.26. Loading of the Creep Frames.

3.3. SHRINKAGE READINGS

The three batches used for the girder (Batch 2, 4 and 6) were used to cast prisms in order to measure shrinkage according to ASTM Standard C157 (2008) as a function of time. Four prisms were made per batch. The device in Figure 3.27 is used to measure shrinkage. Before each measurement, the device needs to be calibrated using a steel rod. Each side of the prism needs to be measured and the average will give the final value. Measurements were taken from the time the prism were created to about twenty five days and from two hundred and fifty five days to around four hundred days.



Figure 3.27. Shrinkage Measurement Device.

4. RESULTS AND DISCUSSION

Results are presented in four parts: (i) the prediction obtained using AASHTO LRFD 2006 implemented using Matlab; (ii) the girder data; (iii) the creep data; (iv) the shrinkage data. The goal herein is to predict the state of strain of the girder at any time prior to testing and compare that prediction with the available data from the girder itself. Additional data from the shrinkage readings and creep frames serve as a parallel corroboration and way to better understand the importance of long-term losses in a complex, sequentially constructed, girder.

4.1. PREDICTIONS FROM AASHTO LRFD 2006

Test data in this study was first recorded during the post-tensioning (PT) operations; no prior data is available in order to track the evolution of the strain profile of the girder during construction. Table 4.1 presents the chronology of events from the construction of the precast segments to the first test. Each of these events modify the state of strain within the girder. It is important to consider the evolution of the girder's state of strain during the design process, to ensure adverse outcomes do not lead to catastrophic consequences during the construction.

Table 4.1. Chronology of Girder's Life.

Day	Event
1	Segments are pretensioned
126	Splices are cast
134	Deck is poured
209	Girder PT applied
221	The temporary supports are removed
231	First day of testing
251	Completion of testing

As described in chapter 2, long-term losses may be over-predicted and are inter-dependent of each other. Following the recommendations and equations from AASHTO LRFD 2006, a Matlab code was written to determine the prestress losses in the pretensioning at the location of maximum positive moment. A one-day time step method was used to provide adequate accuracy. The state of stress was determined for each day including the losses from the previous iteration. Successive iterations were based on the updated values of the modified force from the previous step. The graph obtained is presented in Figure 4.1, which clearly shows the phases of short and long-term losses. Table 4.2 gives more detail by explaining the different events occurring.

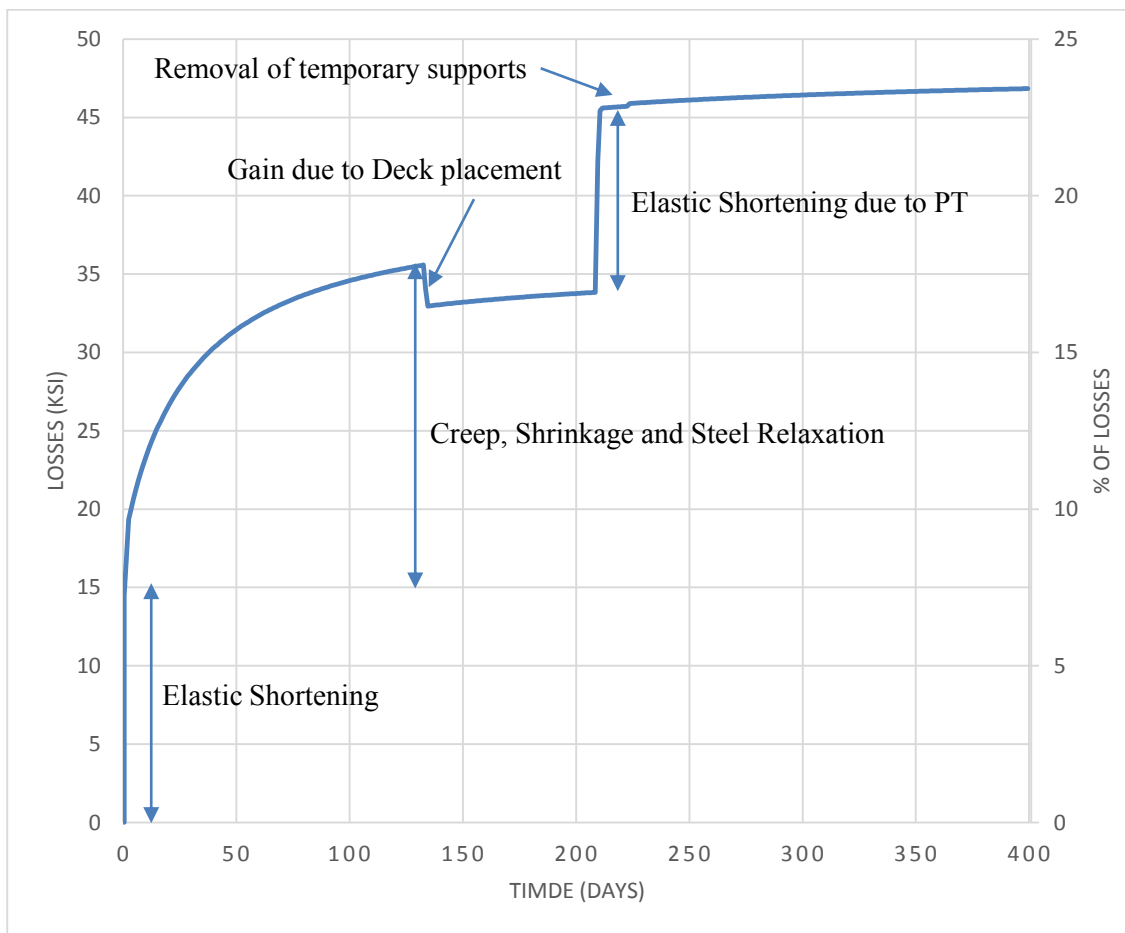


Figure 4.1. Prestress Losses in Pretensioning.

From the graph in Figure 4.1, it is possible to determine the percentage each loss event represents. The results are presented in Table 4.3. The design recommendations provided by AASHTO LRFD 2006 advise to use 20% for the losses which is comparable to the Matlab code results.

The Matlab code also provides the state of stresses at each time step which helps building stress profiles of the section at important times. Figure 4.2 presents the evolution of the stress profile over time in a sequential way. The top row presents the change in stress caused by different events while the bottom row sums every event together in order to obtain the final stress profile presented at the bottom right.

Table 4.2. Description of Losses.

Day	Type of Loss	Losses
Day 1	Short-Term	Elastic shortening
Day 1-133	Long-Term	Creep, Shrinkage and Steel Relaxation
Day 134	Short-Term	Gain from Deck Placement
Day 134-208	Long-Term	Creep, Shrinkage and Steel Relaxation
Day 209	Short-Term	Elastic shortening due to PT
Day 222	Short-Term	Removal of supports
Day 209-400	Long-Term	Creep, Shrinkage and Steel Relaxation

Table 4.3. Percentage of Losses.

	Value (ksi)	Percentage of losses
0.75Fpu	203	0%
Total losses before PT	34	17%
Total losses after PT	47	23%

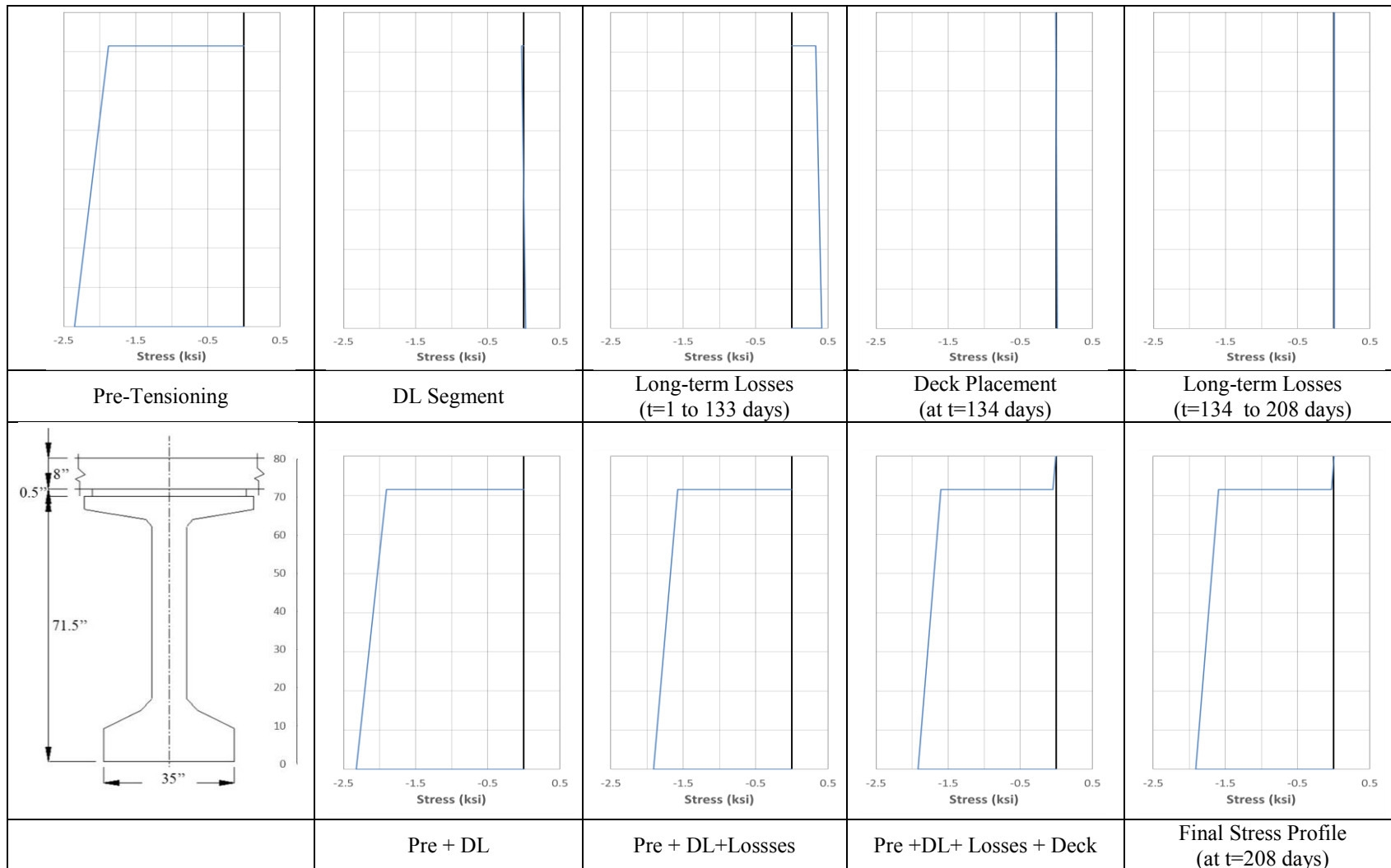


Figure 4.2. Stress Profiles from t=1 day to t=209 days.

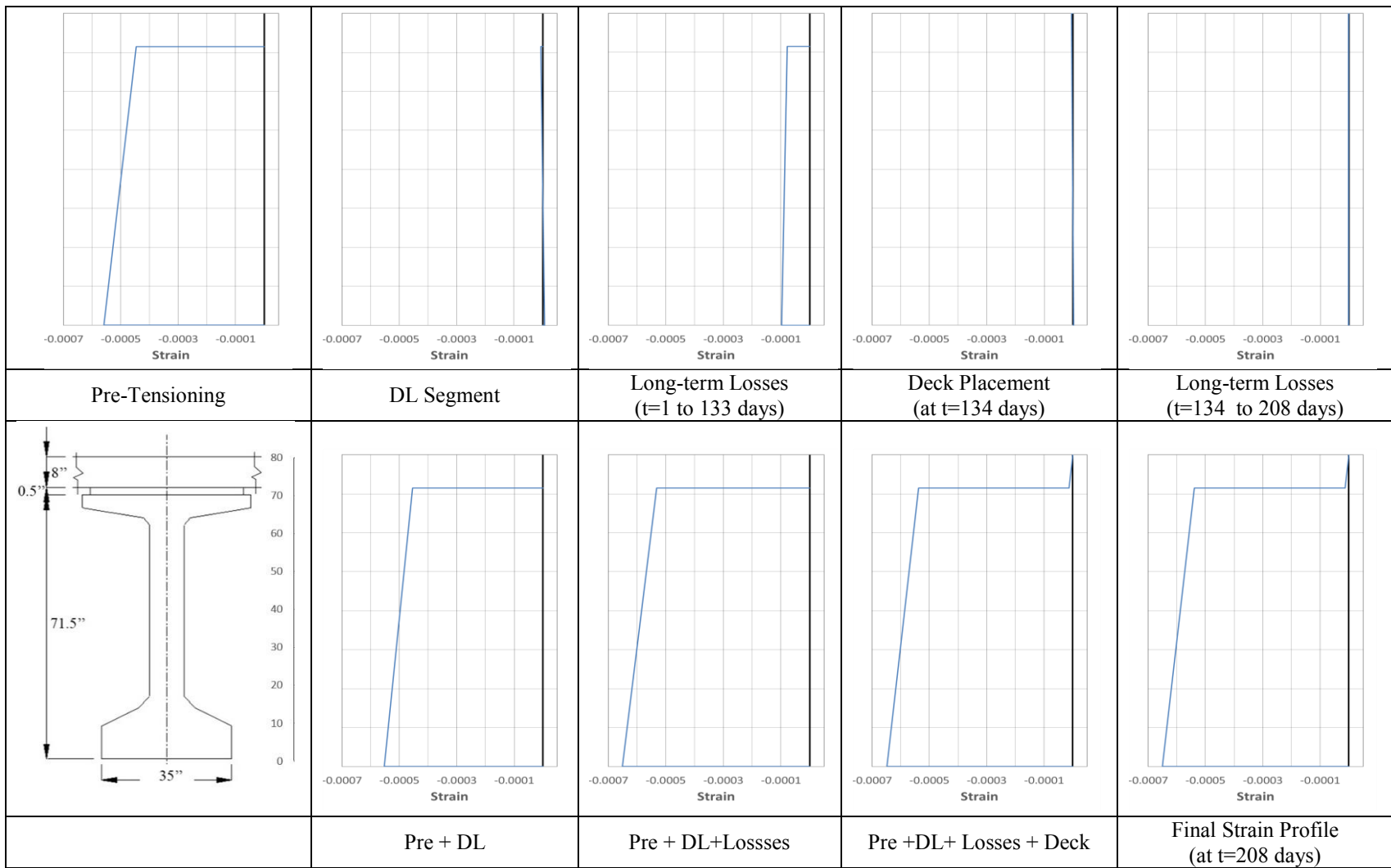


Figure 4.3. Strain Profiles from t=1 day to t=209 days.

Figure 4.2 shows how small the stresses induced by the dead weight of the segment and the deck are. That is because the segment span between shored supports is small. The maximum moments created by the dead weight were almost negligible. In addition, the strain profiles can be inferred from the stresses profiles. Figure 4.3 presents the strain profiles from $t=1$ day to $t=209$ days. These results are later used as a starting point when investigating the effects of imposed girder loads.

4.2. DATA FROM THE GIRDER

During the PT process and for an additional 19 days, data was recorded at 1.0 Hz in order to investigate the response of the specimen and capture the effects of the long-term deformations. The PT process was sequentially applied to the each of the three bundled 19-strands tendons. The central duct was the first to be post-tensioned, then the top duct and finally the bottom duct. Figure 4.4 represents the different stages of loading, the graph clearly shows the three stages of loading. The PT process spanned about 100 minutes.

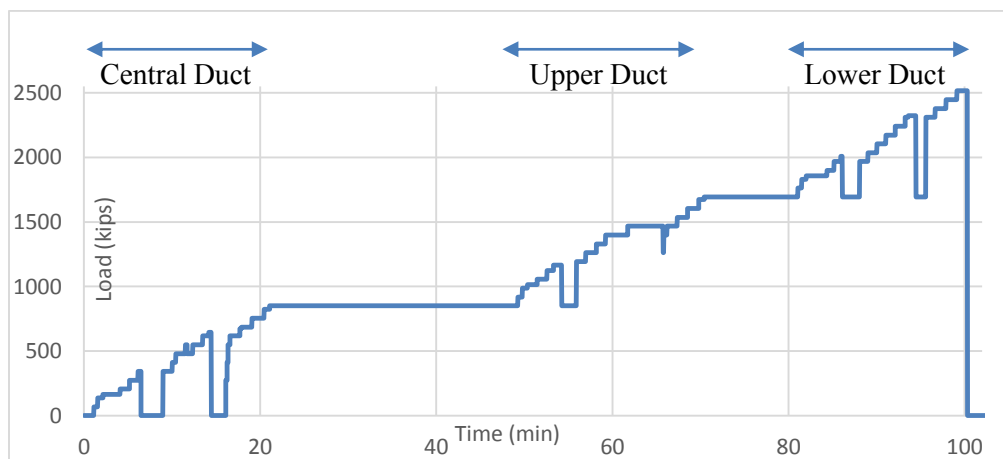


Figure 4.4. Post-Tensioning Load.

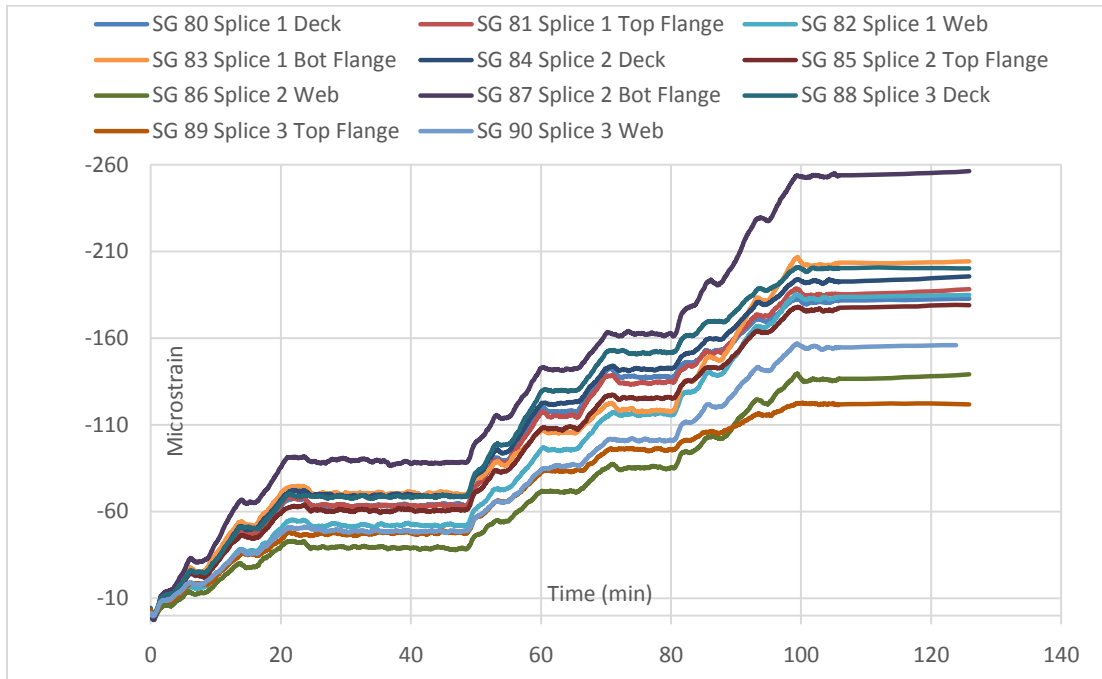
The force applied for the post-tensioning of each duct was not the same. Indeed, the first duct to be post-tensioned experienced elastic shortening from the post-

tensioning of the second and third duct whereas the second duct experienced elastic shortening from the post-tensioning of the third duct. The third duct did not experience any elastic shortening. As a result, the force applied to the first duct was greater than the force applied to the second duct. Table 4.4 presents a summary of the stress applied for each duct as well as the losses experienced to give the final PT forces and the total PT force. The final force (2302 kips) has been used in each of the prediction models. The three values of the final forces are within 1% of each other.

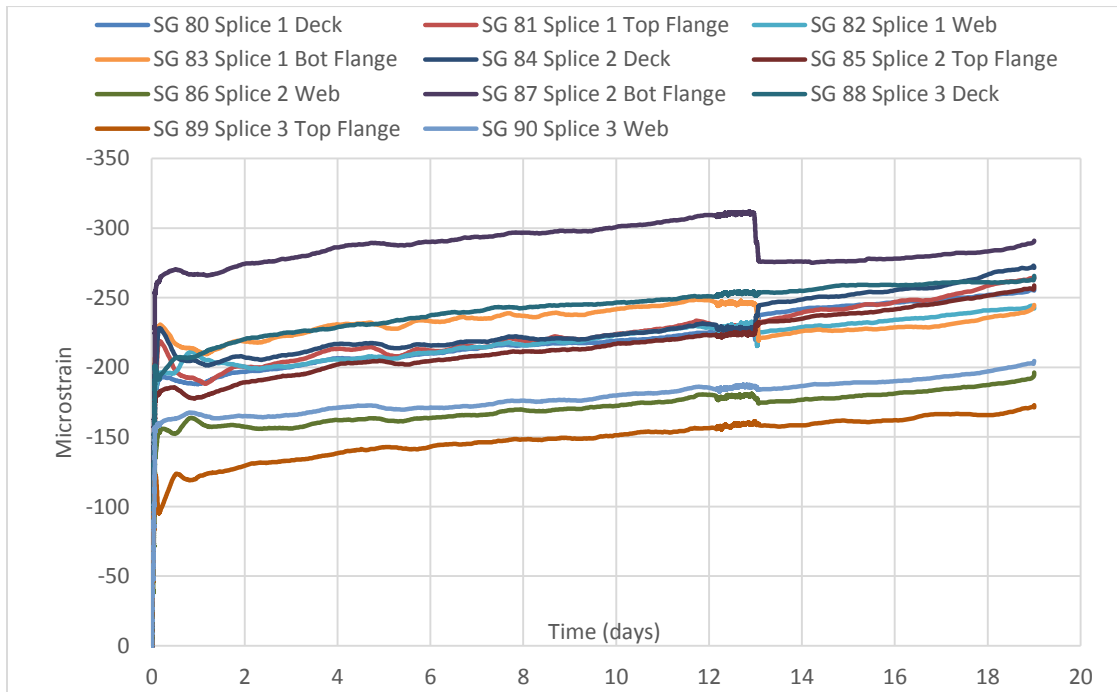
Table 4.4. Post-Tensioning Force

Duct	Stress Applied (ksi)	Elastic Shortening (ksi)	Friction Losses	Anchorage Losses	Final Stress (ksi)	Final Force (kips)
1	206	5.1	4.78%	2.67%	186	768
2	205	2.6	4.78%	2.67%	187	772
3	200	0	4.78%	2.67%	185	762
					Total	2302

As discussed in Chapter 3, embedded concrete gages were placed at each splice location. Figure 4.5 presents the data obtained by the embedded concrete gages in the splices while the PT process occurred. Figure 4.5 shows the elastic shortening that occurred during the PT process. After the PT was applied, the strain continued to increase over time exhibiting the long term creep deformation process. Around 13 days, the temporary supports were removed, modifying the state of stresses in the girder and the splices. Indeed, the full dead weight was applied to the structure, showing sudden change as depicted in Figure 4.5. Data can be divided per splice location to make it easier to visualize as shown in Figure 4.7. The long term deformation seems to have the same trend as the slopes appear to be equal but they are all offset.



(a) Effect of post-tensioning when applied



(b) Effect of post-tensioning over 19 days

Figure 4.5. Effect of Post-Tensioning with Time.

In order to explain and understand what is happening, the time frame was separated between the main events happening: The PT of the girder, creep effects over time, removal of the temporary supports and more creep effects. Each event was separated and the change of strain due to each event was investigated. Splice 2 is the splice of principal interest. Splice 2 region is also compared with data obtained of section D and F. Figure 4.6 presents the test specimen and the location of section D and F.

Figure 4.8 to Figure 4.12 present the strain profiles of Splice 2, section D, section F and the average of section D and F. The top row strain profiles of each figure presents every independent event and the change of strain it created. The bottom row strain profiles presents the sequential addition of those events to reach the final strain profile state. Each strain profile represents all the data available at the section of interest. The splices present more data as they were containing embedded concrete gages in addition to the surface strain gages. Section D and F only had surface concrete gages on the top and bottom flanges as well as on the surface of the deck. The data obtained from the surfaces gages is not as reliable as embedded concrete gages but can still give an idea of the deformations happening at each section. In addition, surface gages are prone to experience a higher compressive strain as the rate of shrinkage is higher on the surface of the concrete than inside.

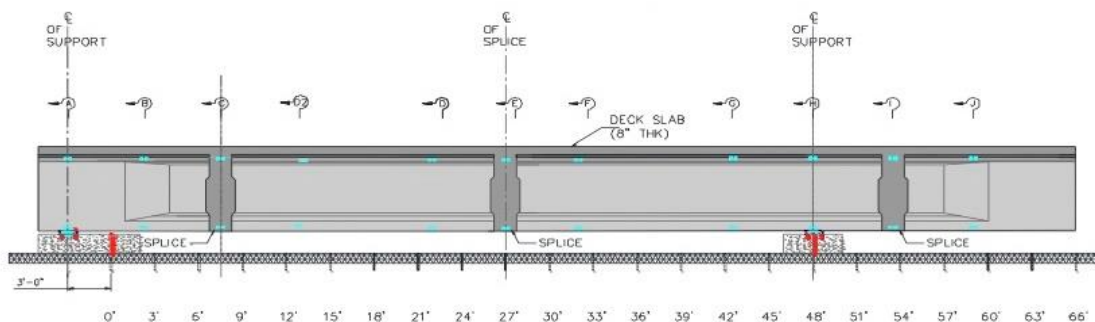


Figure 4.6. Test Specimen (Hueste et al. 2014).

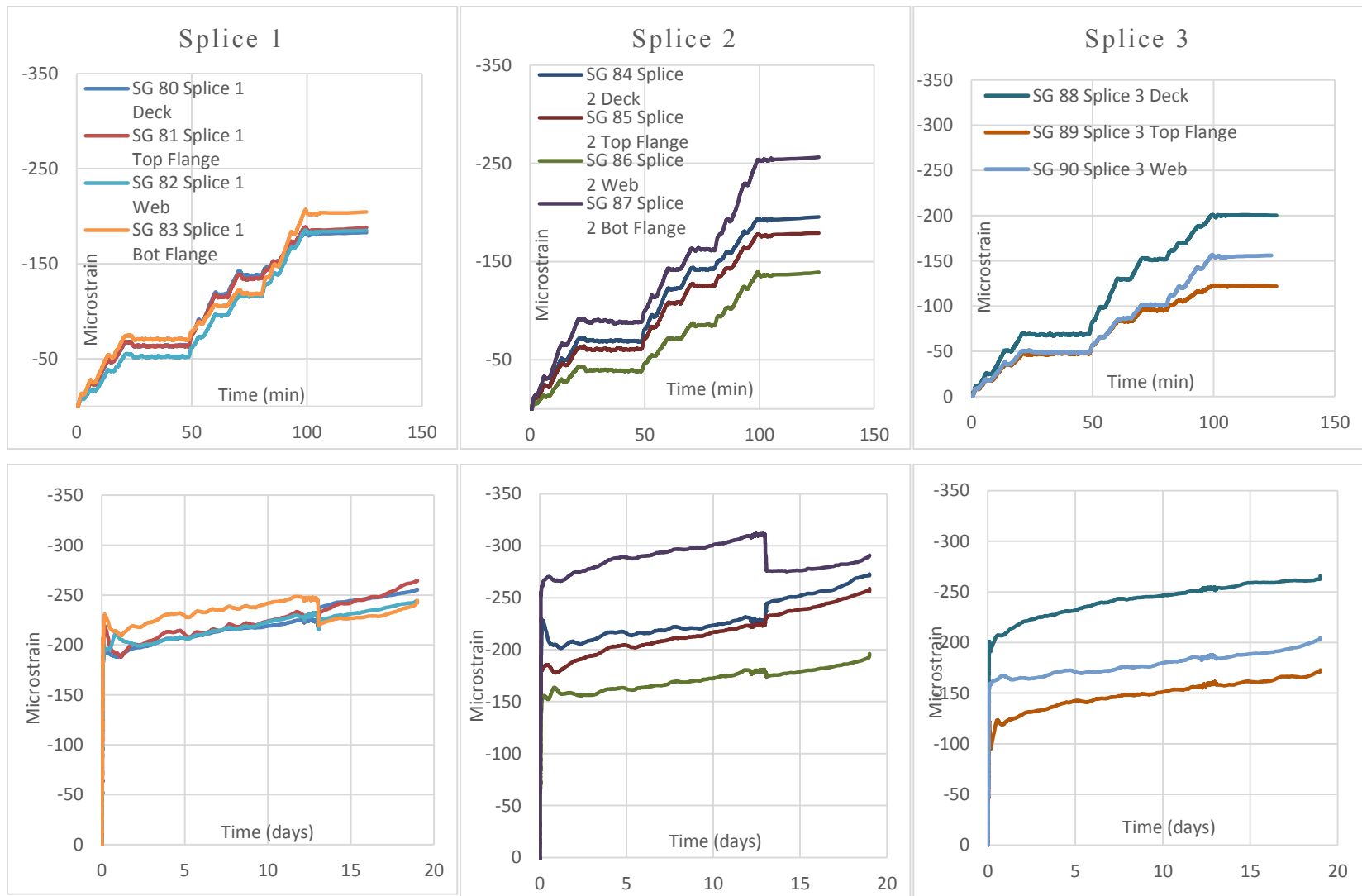


Figure 4.7. Effect of Post-Tensioning on the Splices.

From a design standpoint, the prestressing was designed to ideally balance the dead weight. In the reality, it is observed on the PT strain profile of Figure 4.8 that the strain profile is not a straight line which means that a certain eccentricity of the post-tensioning is creating a bending moment. This bending moment is supposed to oppose the full dead weight of the specimen. But when the temporary supports were removed, and that the full dead weight was applied to the structure, it can be seen on the bottom right strain profile of Figure 4.8 that the result is not a perfect vertical line but close. The design may be considered a success by essentially balancing dead load actions leaving the specimen under an almost constant compression.

A numerical analysis was performed for each state and plotted in order to compare it with the experimental data. The numerical analysis agrees the experimental observations for Section 2 quite well. The differences may be explained by the fact that the numerical analyses include the data from the creep models and it has been shown that creep models overestimate the actual experimental data.

Section D and F show similar results when compared with the Splice 2. The lack of instrumentation at the splice sections makes it harder to fully compare the strain profiles but Figure 4.12 shows that the values are still within a similar range demonstrating that the specimen behaves as a continuous structure.

Figure 4.13 includes the prediction from Figure 4.3 and Figure 4.12 and presents the final state of strain and stress before the beginning of test 1. It includes the effects of the pretensioning, post-tensioning, dead loads and all the losses. The section is fully under compression and give a best understanding of the effect of prestressing on the section. Table 4.5 presents the limits in compression and tension in ksi for the concrete of the girder.

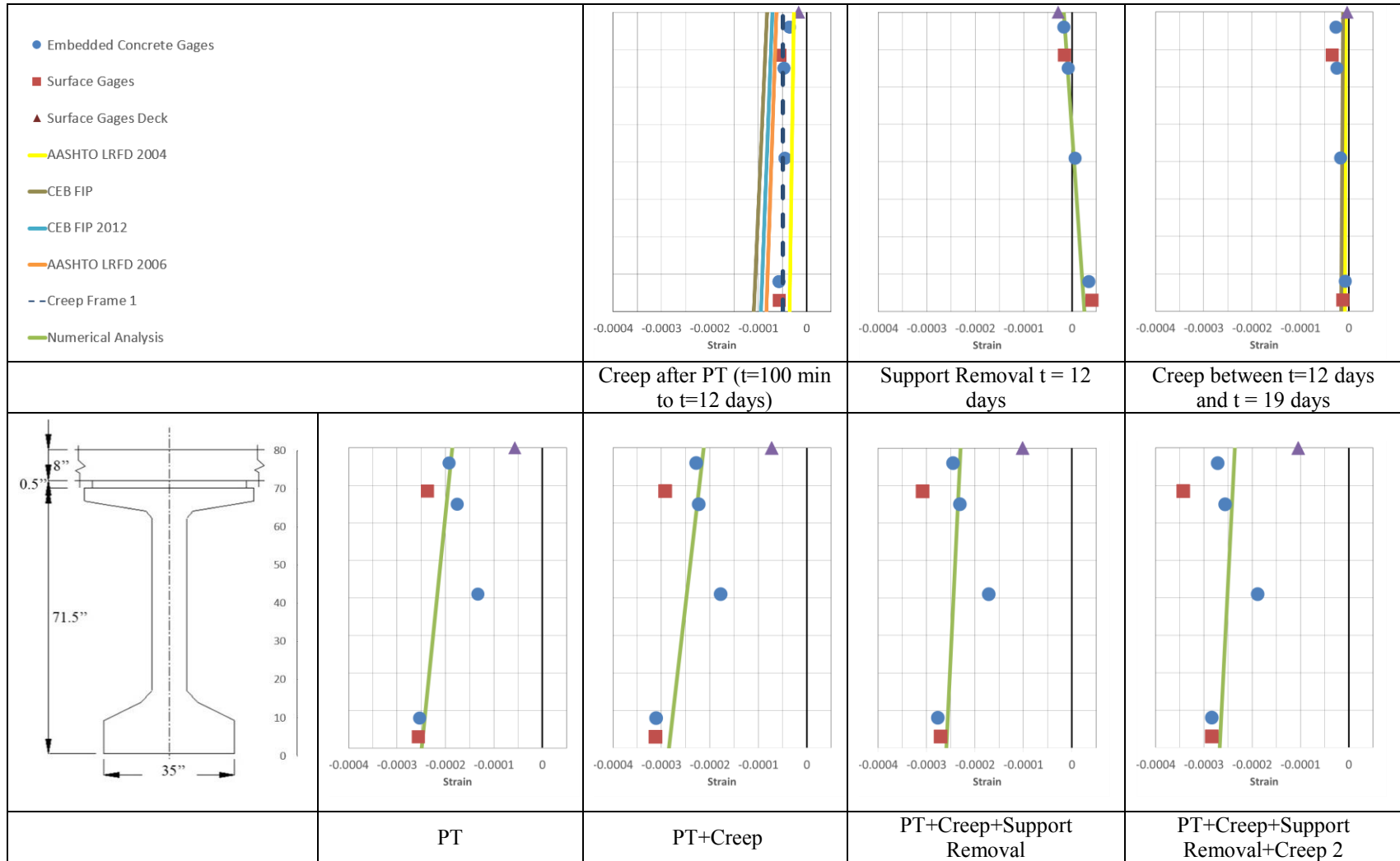


Figure 4.8. Strain Profile for Splice 2.

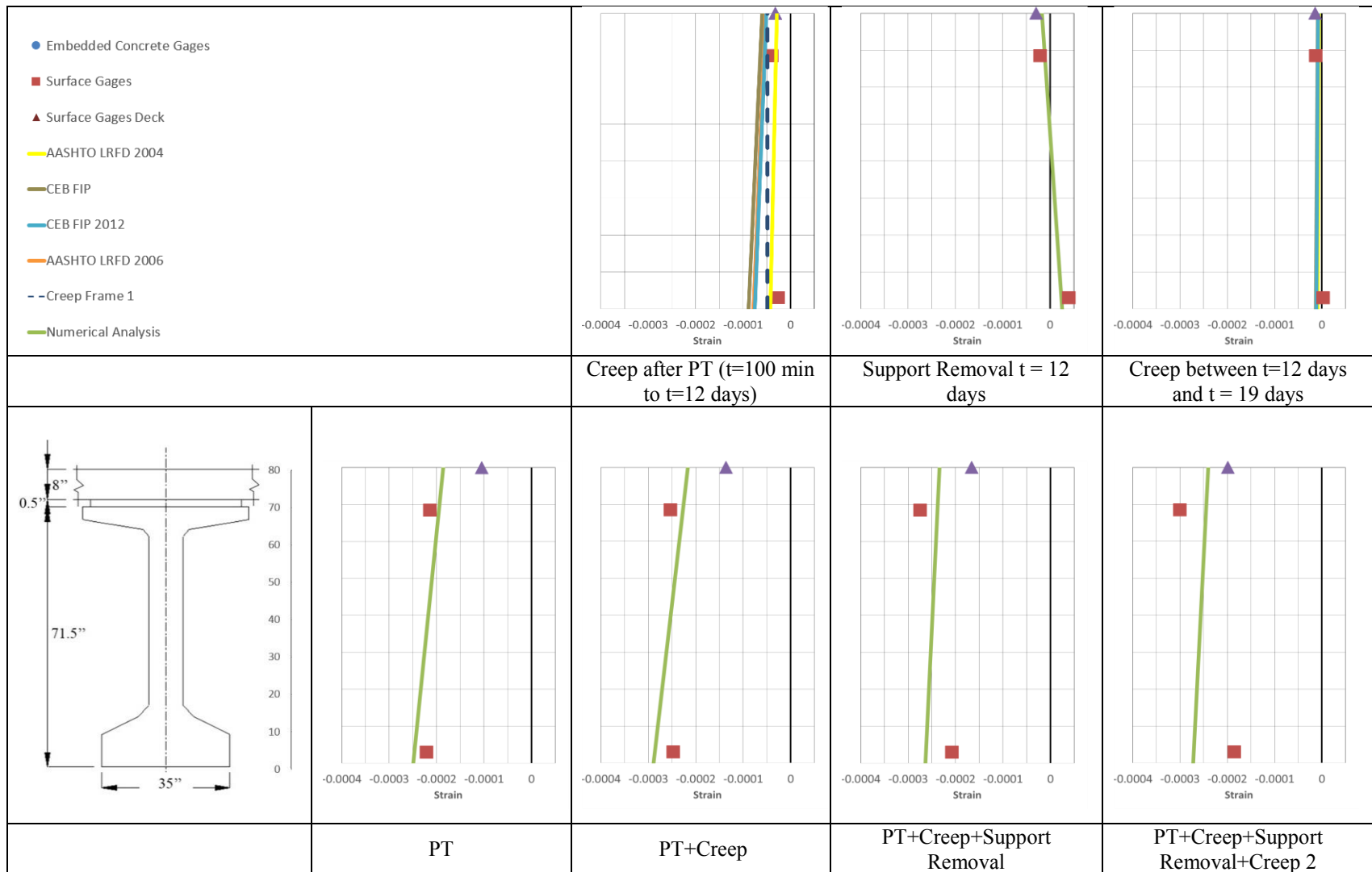


Figure 4.9. Strain Profile Average of Section D & F.

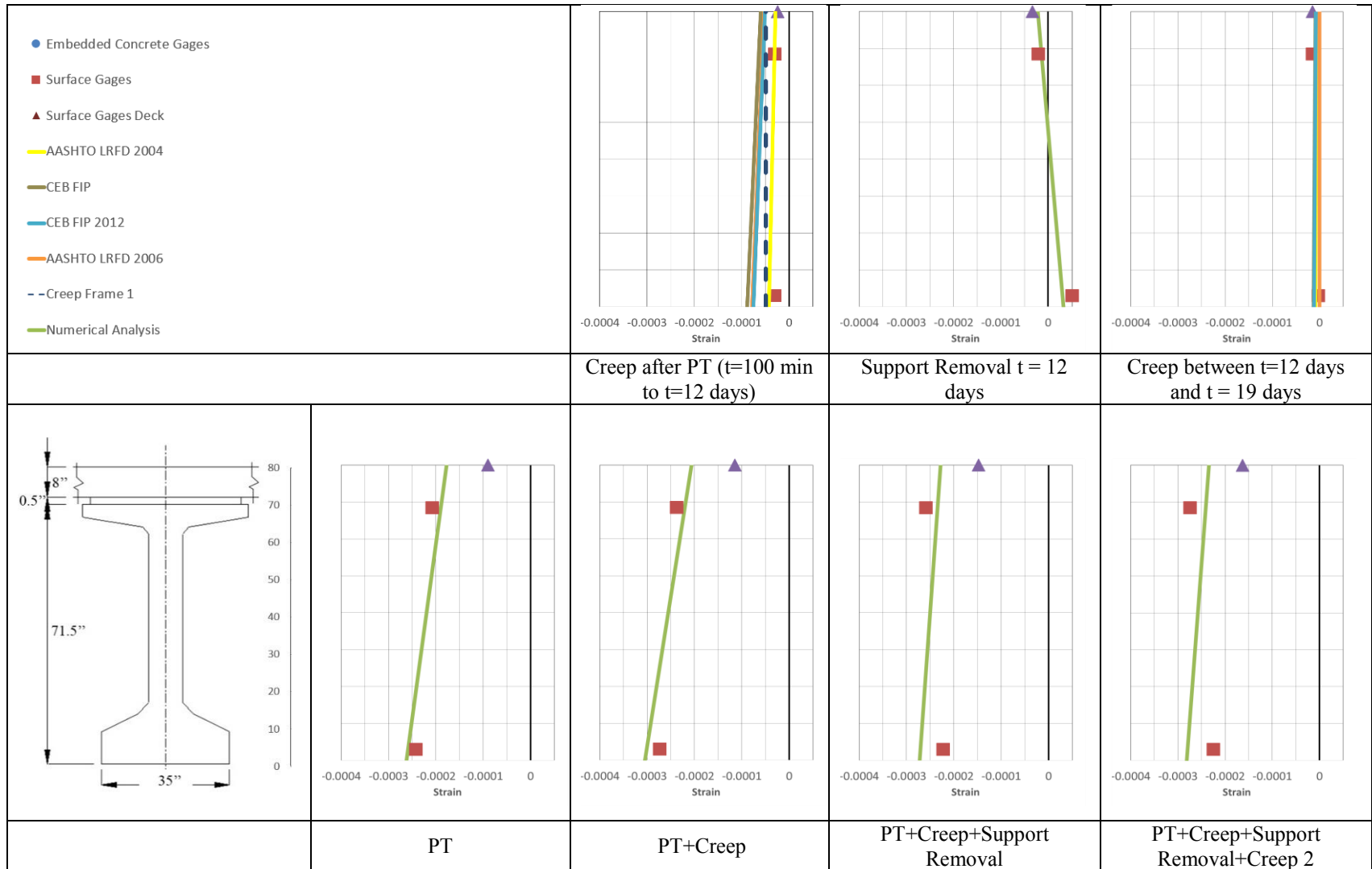


Figure 4.10. Strain Profile for Section D.

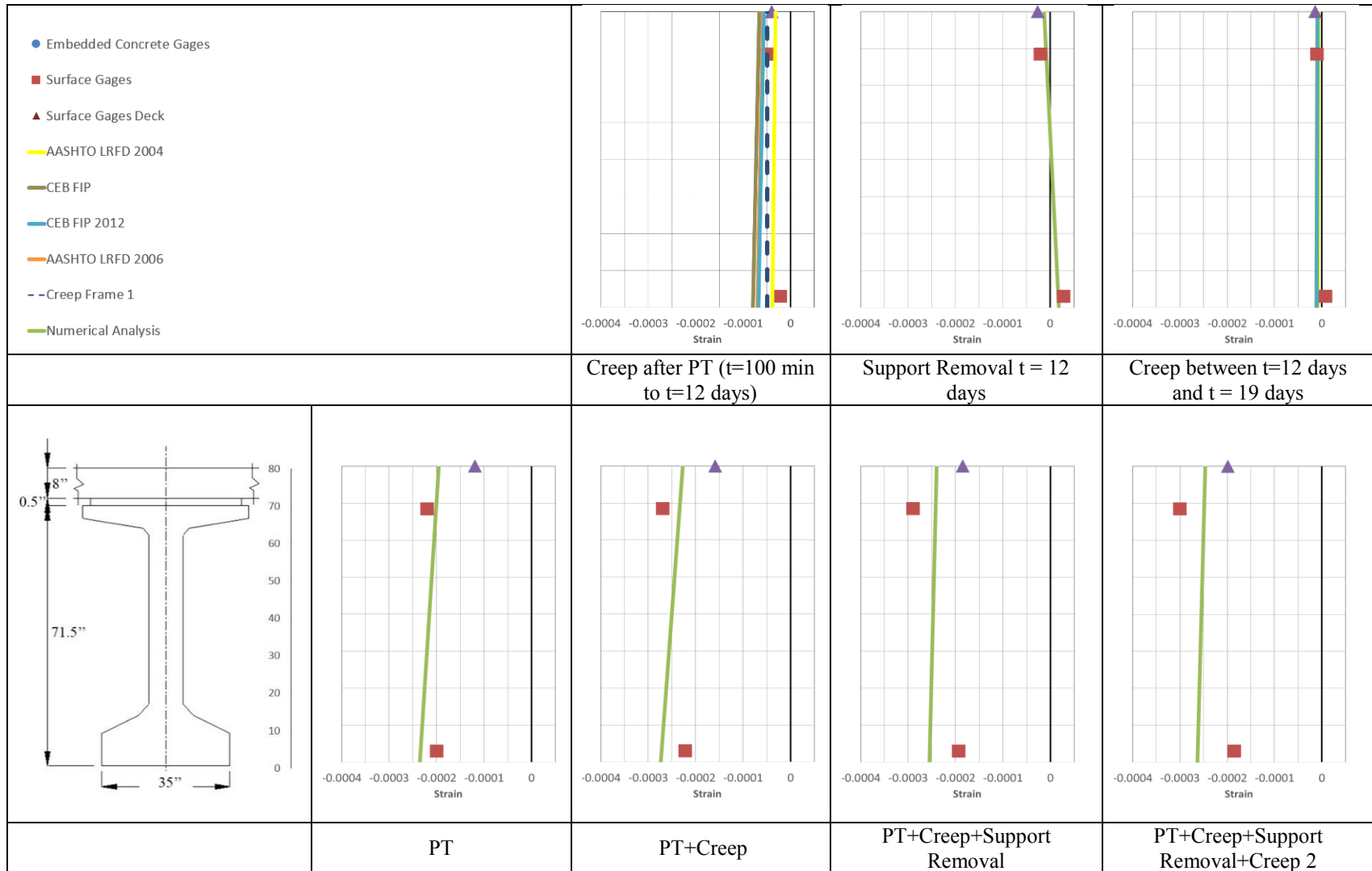


Figure 4.11. Strain Profile for Section F.

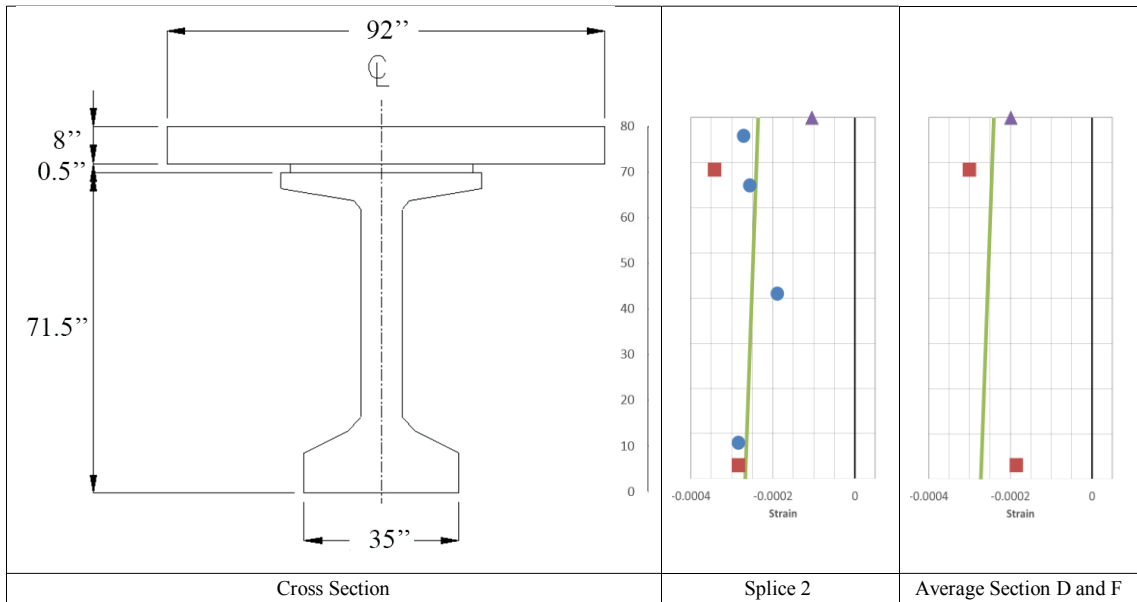


Figure 4.12. Strain Profile Summary.

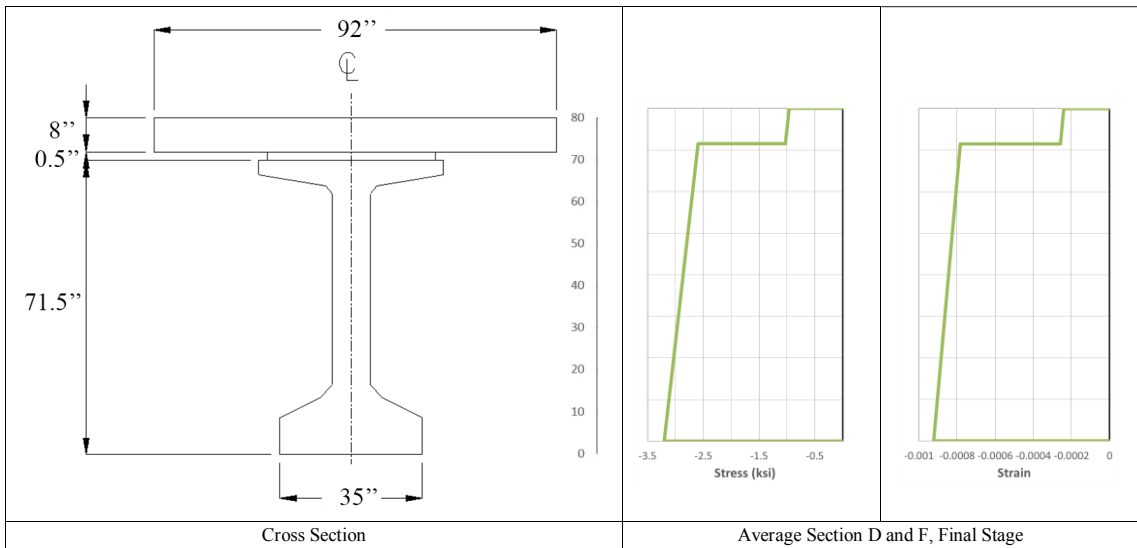


Figure 4.13. Final Stress and Strain Profiles Including Predictions from 4.1.

Table 4.5. Limits in Compression and Tension.

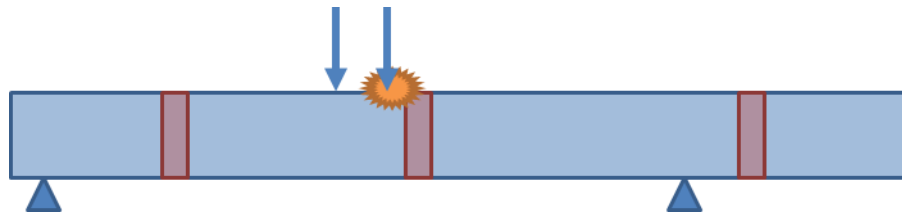
Limit	Compression	Tension
As a function of $f'c$	$0.45f'c$	$0.19\sqrt{f'c}$
For $f'c=11.3$ ksi	5.1 ksi	0.64 ksi

Table 4.5 shows that since the section is in compression already, it might fail in compression rather than in tension. In order to quantify this idea, Table 4.6 presents the stresses available in both compression and tension for cases of maximum positive moment and negative moment. For the maximum positive moment case, the table shows that it requires less additional stress to reach the limit for compression rather than for tension. For the maximum negative moment case, the additional amount of stress to reach the limit in compression or tension is similar. The outcome of Test 3 and Test 4 which tested the structure for maximum positive and negative moments, respectively, follows those predictions.

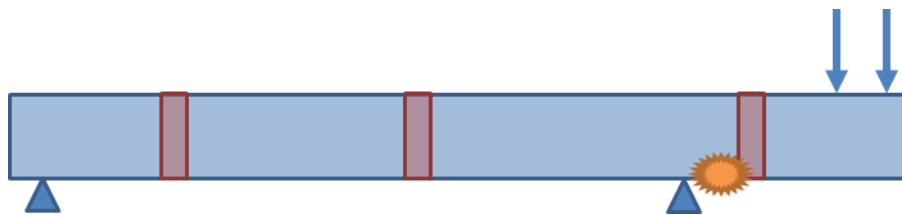
Table 4.6. Compression and Tension Available before Limit

Case	Positive Moment	Negative Moment
Compression Available before Limit	2.4 ksi	1.8 ksi
Tension Available before Limit	3.7 ksi	1.6 ksi

Figure 4.14 (a) presents the failure for Test 3 which investigated performance positive moment. It appears that the structure failed in compression in the deck. Figure 4.14 (b) presents the failure for test 4 which tested the structure for negative moment. The structure also failed in compression between the third splice and the support.



(a) Test 3



(b) Test 4

Figure 4.14. Failure in Compression.

4.3. DATA FROM SHINKAGE READINGS

Shrinkage readings were taken every week. Unfortunately, data were not taken between 25 and 259 days as another student did the readings between 1 and 25 days but did not persist over time.

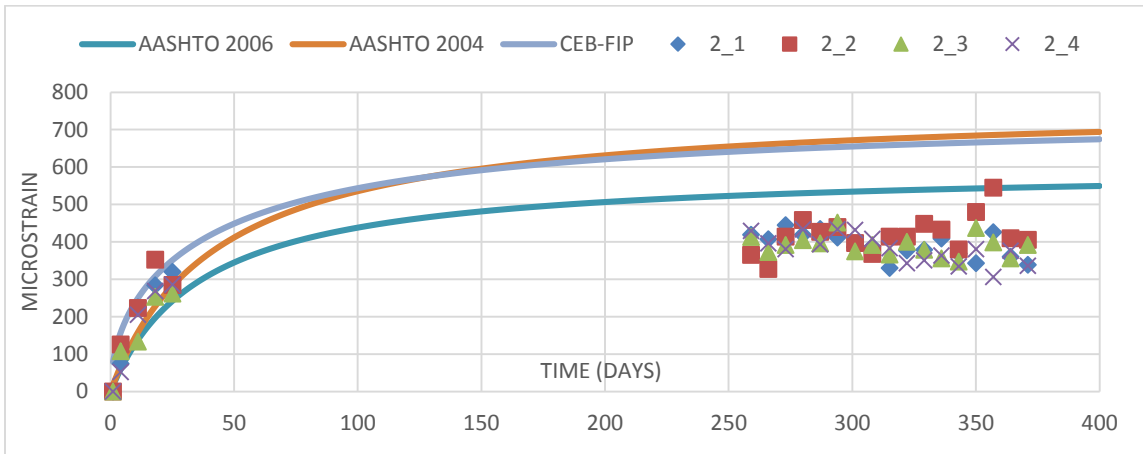
A total of 12 prisms were cast, from batches 2, 4 and 6 of the girder. When the readings were plotted, they exhibit similar trends but seem to be offset. By adjusting for a zero offset, it was possible to compare results with the available shrinkage models such as AASHTO LRFD (2004), AASHTO LRFD (2006) and CEB-FIP (1994). Figure 4.15 presents the data after the zero offset correction was made. Results show the trends are similar and that it can be compared to shrinkage models.

In addition, Figure 4.15 presents the data in comparison with the models. The compressive strength was set to approximately 6 ksi which is the compressive strength of the girder when the pretensioning was released. The models make a good fit in the early days between 0 and 25 days. Beyond 250 days, the models seem to over-predict the experimental data, however AASHTO LRFD (2006) provides the best fit, especially for the specimens from batch 4.

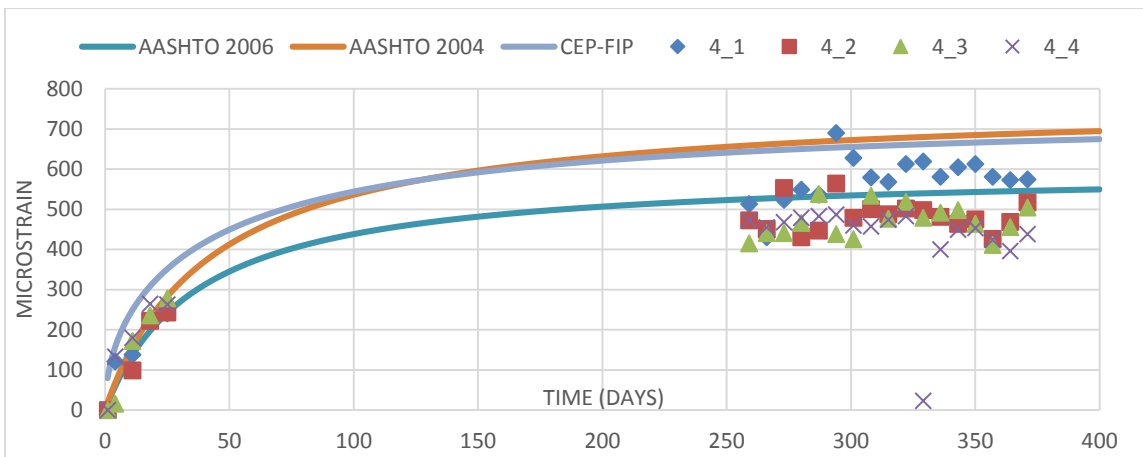
It is important to quantify by how much the models over-predict the experimental results. From Figure 4.15, the percentage of overestimation between the models and the actual experimental data is calculated and presented in Table 4.7. AASHTO LRFD 2006 present the best approximation with an overestimation of 20%.

Table 4.7. Overestimation of Shrinkage Readings by Shrinkage Models.

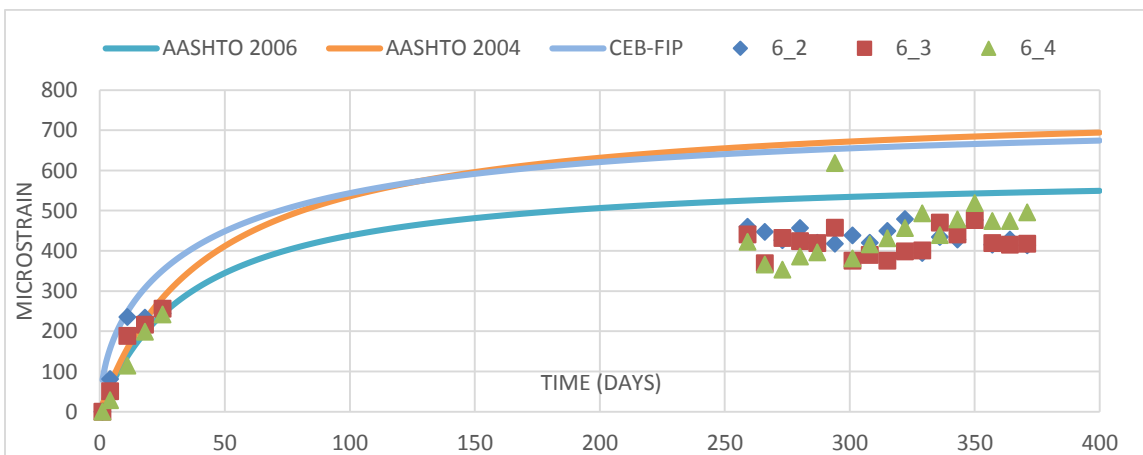
Models	AASHTO LRFD 2004	AASHTO LRFD 2006	CEB-FIP
Shrinkage Experimental Data	151%	120%	147%



(a) Shrinkage readings from batch 2



(b) Shrinkage readings from batch 4



(c) Shrinkage readings from batch 6

Figure 4.15. Shrinkage Readings Compared to Shrinkage Models.

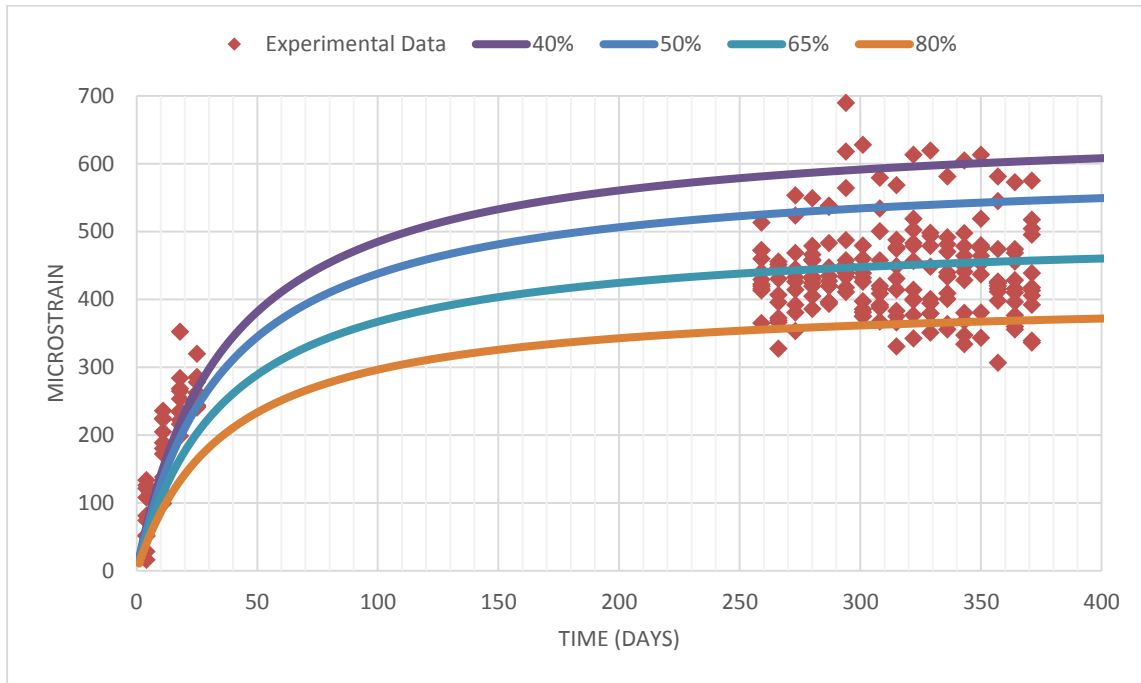


Figure 4.16. Comparison of Shrinkage Models with Experimental Data.

Models predicting shrinkage strain requires numerous inputs like the age of concrete, the humidity percentage and the volume to surface ratio. By modifying those inputs, it is shown that the shrinkage strain is somewhat sensitive to the humidity percentage. In Figure 4.16, AASHTO LRFD 2006 was used with four specific levels of relative humidity: 40, 50, 65 and 80 percent. It can be seen that the 40% humidity fits the initial experiment results but over-estimates them over time. When using 65%, the prediction fits the experimental results over time but under-estimates them in early age. This shows how critical it is to know the humidity percentage of the environment the concrete is subjected to. It may be concluded that shrinkage predictions are quite sensitive to the humidity factor, a slight change of the factor may induce noticeable changes in the strain.

4.4. DATA FROM THE CREEP FRAMES

The frames recorded data from the time they were loaded. Data were recorded each second while the frames were loaded in order to capture the effect of elastic shortening on the concrete cylinders. After loading, the frequency of data recording was decreased to 20 minutes to capture the effect of creep over time. Figure 4.17 presents the evolution of negative compressive strain as a function of time. Figure 4.17 (a) represents the evolution of compressive strain during the loading of each frame. It can be seen that the strain in Frame 3 dropped after it got loaded, it can be explained by the fact that the top half cylinder of the third frame cracked. It can be seen on Figure 4.18. Table 4.8 presents the desired and actual force values used for each creep frame. Those data were used as inputs for the creep models.

Table 4.8. Force Applied on the Creep Frames

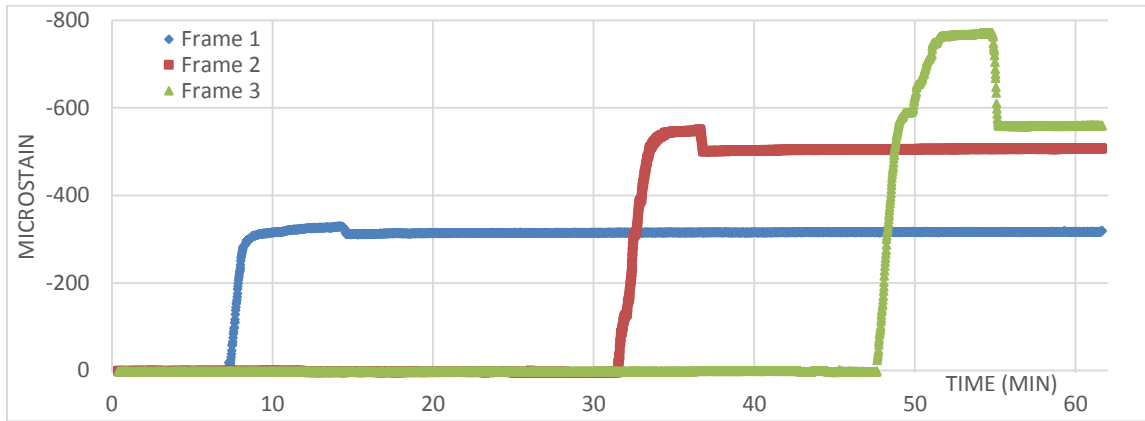
Loading	Desired Value (kips)	Actual Value (kips)
Frame 1	21.5	21.5
Frame 2	35.9	34.6
Frame 3	50.3	38.2

Figure 4.17 (b) represents the data obtained after 126 days. The effect of creep is clear as the compressive creep strain increases over time. In addition, shrinkage effect recorded by the unloaded cylinders is shown as well. The three frames show the same rate of shrinkage as the three shrinkage plots are overlapping each other. This effect has been subtracted from the actual data in order to show the effect of creep only. In addition, the data from each frame were compared to the available creep models presented in Chapter 2 as shown in Figure 4.19. The models seem to over predict the experimental data but it can be seen that the trend is similar. Indeed, the rate of increase of the creep effect seem to be the same for both the experimental data and the creep

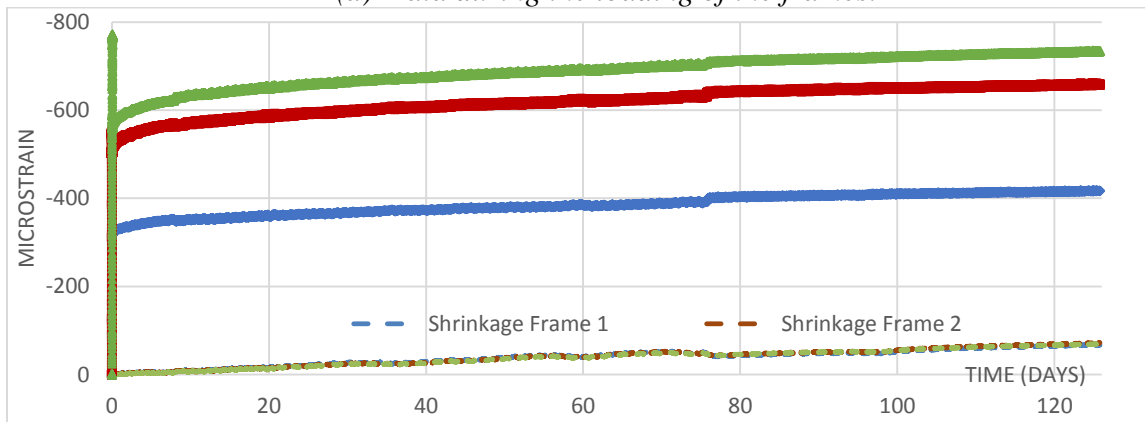
models. Note that the slight jump in the data around day 75 can be attributed to the creep frames being physically moved to another room in the lab.

The cylinders used for the creep testing were 294 days old when they were loaded, meaning that they got the time to shrink before being loaded. Another way to compare results with available models is to include the effect of both shrinkage and creep. The full life of the cylinders is taken into account, from the time they were casted to the time they were loaded. Figure 4.20 and Figure 4.21 present the evolution of strain with time for each frame. Between day 1 and day 294, only shrinkage is used for the models. On day 294, when the creep frames were loaded, the creep is also taken into account when modeling the prediction of strain. Since different models give different predictions, the models were plotted separately. Figure 4.20 presents the comparison between the experimental data and AASHTO LRFD 2006 while Figure 4.21 compares the experimental data to both AASHTO LRFD 2004 and CEB-FIP. Both models were plotted on the same graph because they give similar predictions. The models seem to overestimate the experimental data but the trend are similar, especially on Figure 4.21 where the rate of growth of the strain is similar.

The latest version of AASHTO LRFD which takes into account the strength of concrete, has also been adapted for high strength concrete. Better prediction results are evident. The older ASSHTO LRFD and CEB-FIP models both overestimate the experimental results. The over-estimation of the creep models is consistent with the research project of Trejo, et al. (2008), and (in part) can be attributed to the fact that the concrete is SCC. It seems that the over-estimation obtained is greater than the Trejo, et al. (2008) observation but it may be explained by the fact that the cylinders used for the creep frames were 294 days old whereas those used by Trejo, et al. (2008) were only 7 days old when loaded.



(a) Data during the loading of the frames.



(b) Data from the creep frames over 126 days.

Figure 4.17. Data from the Creep Frames.

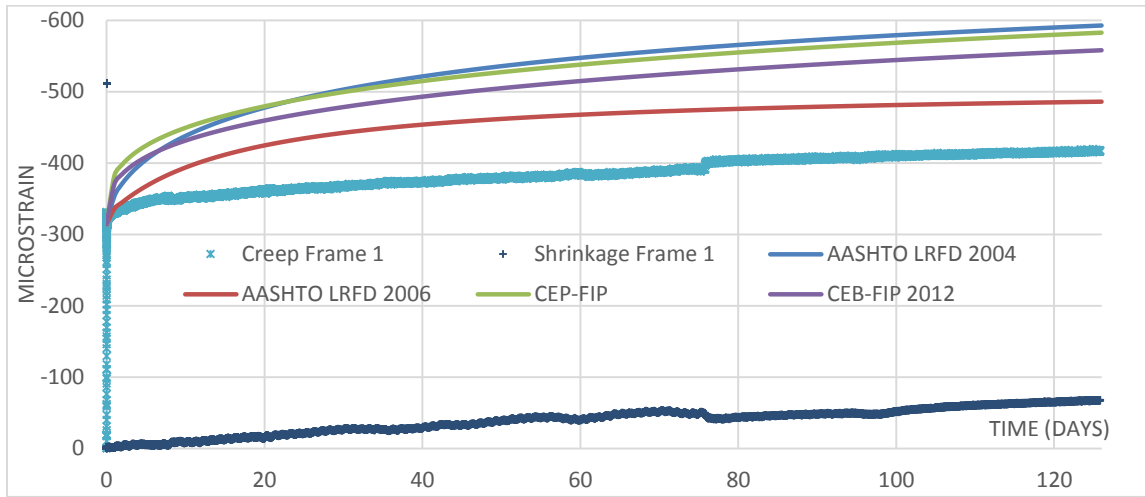


(a) Cracked face of the top half cylinder

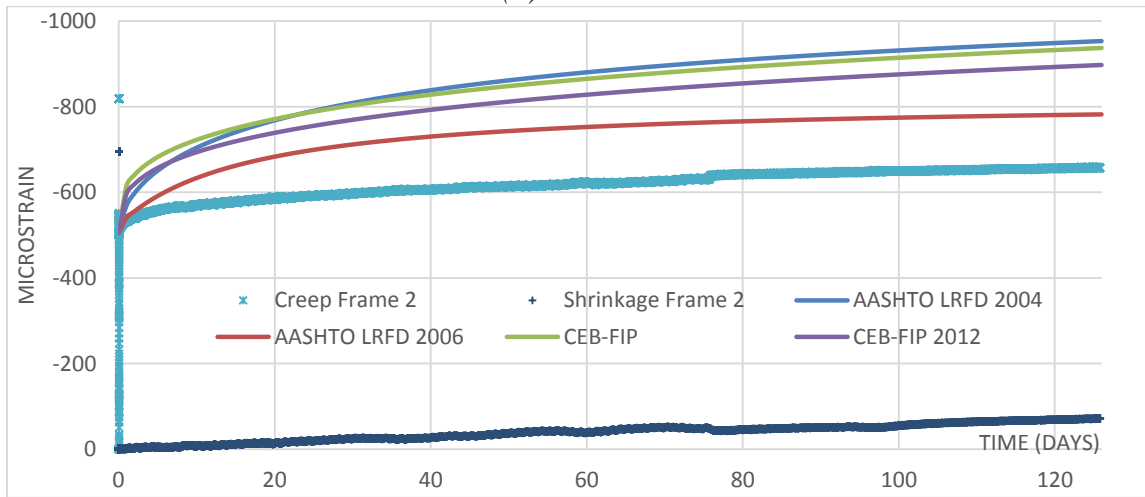


(b) Opposite face cracked

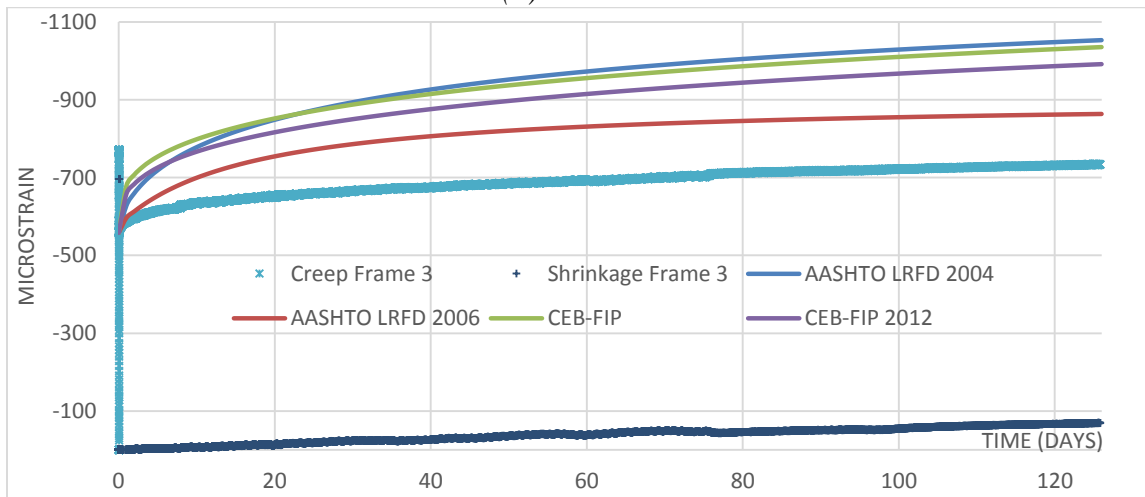
Figure 4.18. Cracked Top Half Cylinder of the Third Frame.



(a) Frame 1

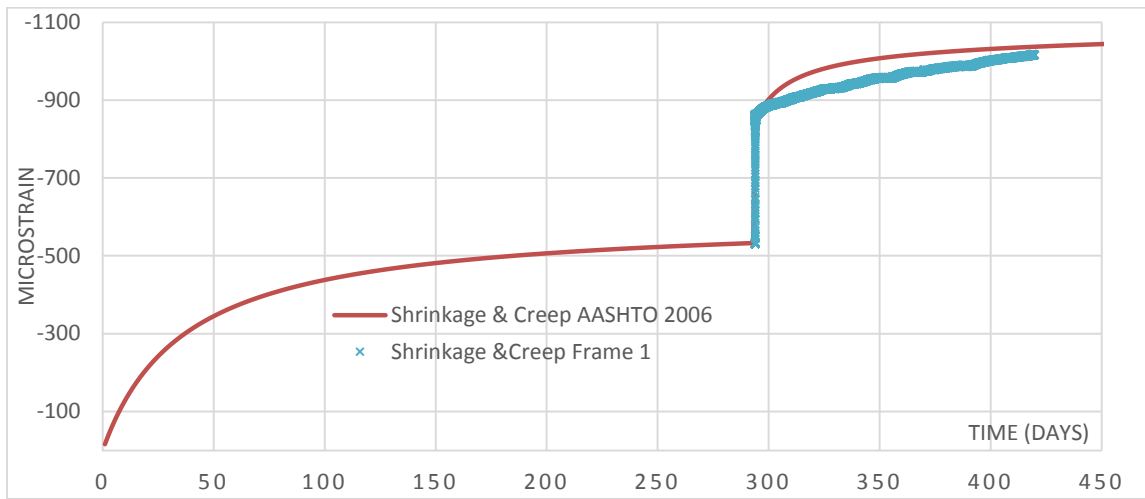


(b) Frame 2

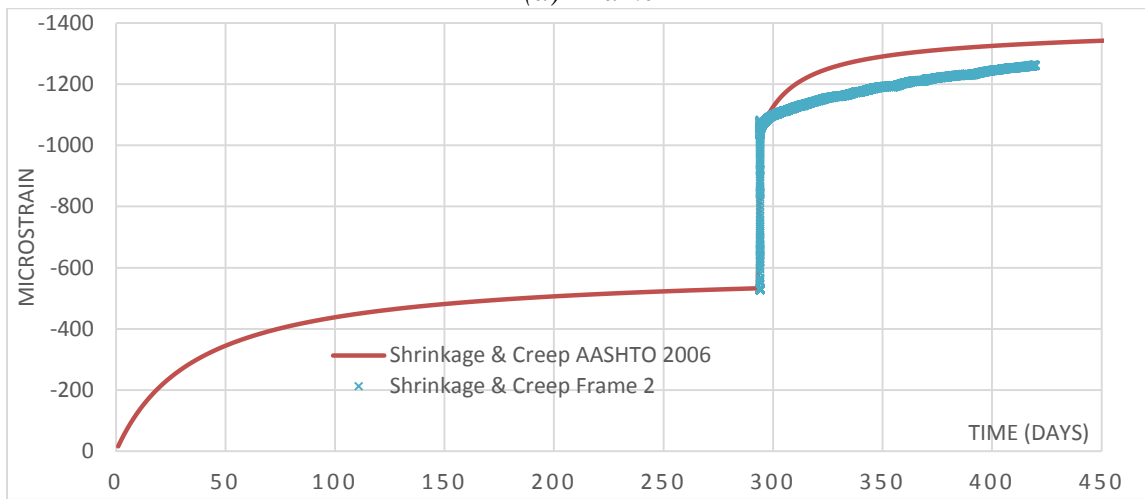


(c) Frame 3

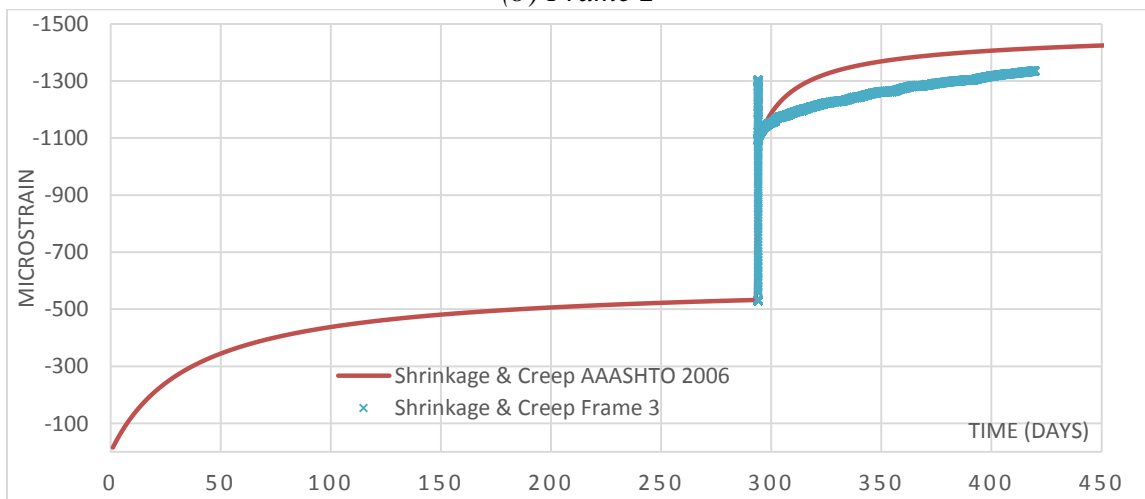
Figure 4.19. Creep Frames Data Compared to Creep Models.



(a) Frame 1



(b) Frame 2



(c) Frame 3

Figure 4.20. Creep Frames Data Compared to ASSHTO LRFD 2006 Model

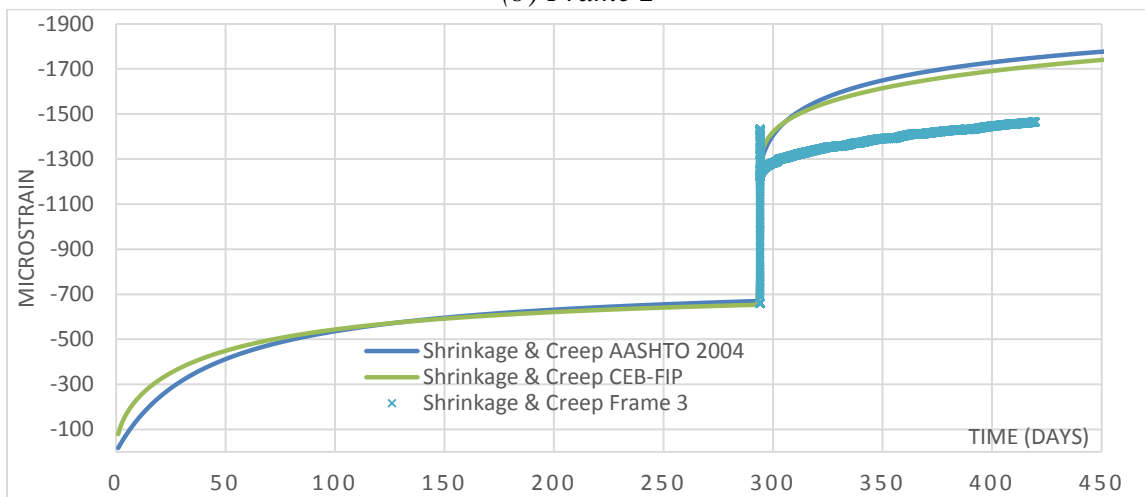
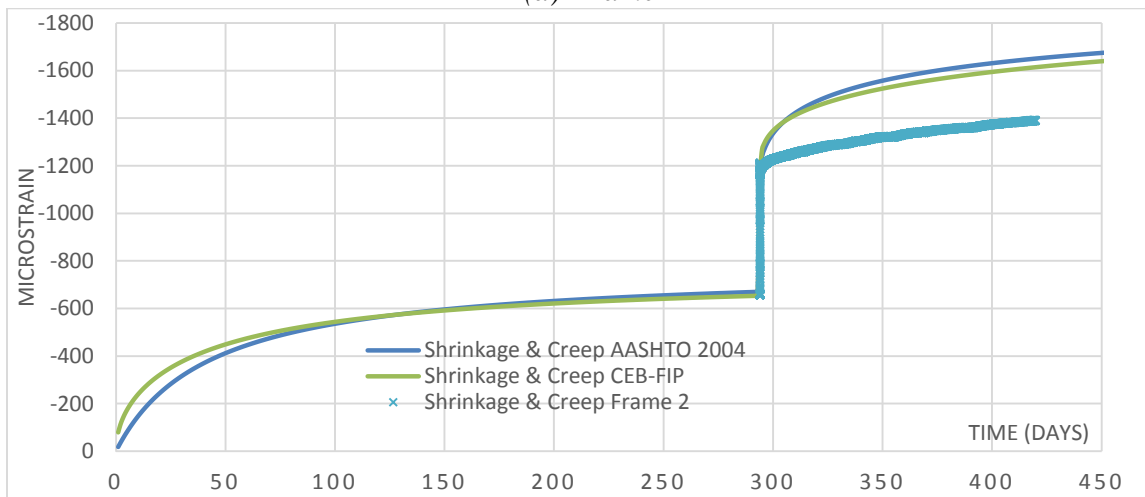
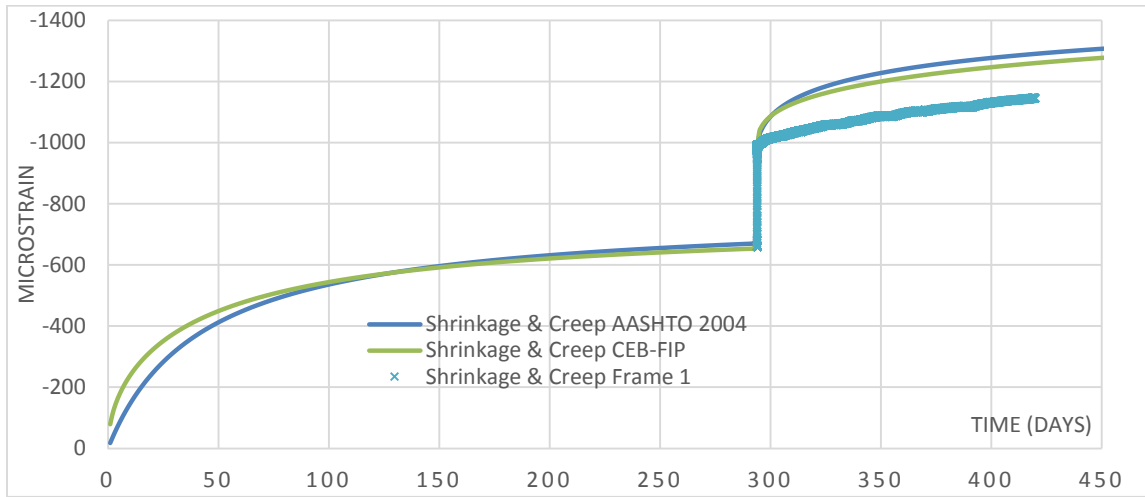
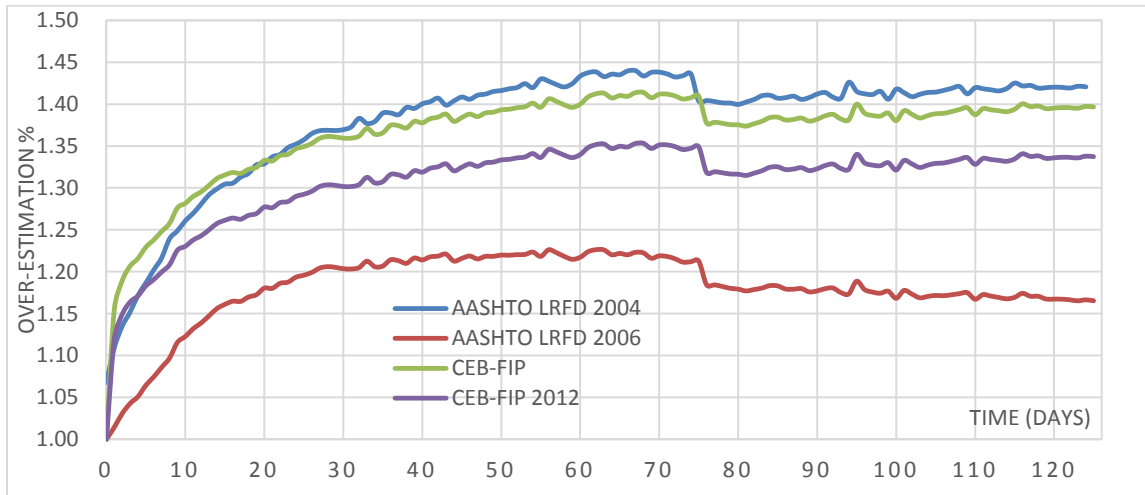


Figure 4.21. Creep Frames Data Compared to AASHTO 2004 & CEB-FIP Models

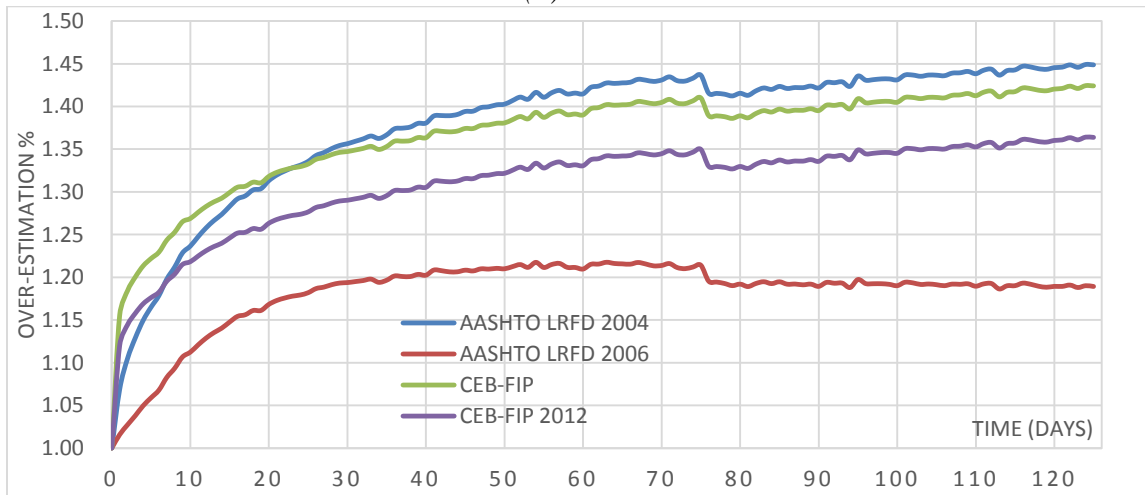
In order to quantify how well the models predict the observed results, it is of interest to plot the over-estimation percentage as a function of time. Figure 4.22 presents the overestimation made by each model for each frame as a function of time. The first thing that can be seen is that the three graphs look similar meaning that the models do not depend on the intensity of the force applied. The overestimation increases quickly at the beginning and starts to diminish with time. But it is interesting to underline that AASHTO LRFD 2004, CEB-FIP and CEB-FIP 2012 overestimation keeps increasing with time while AASHTO LRFD 2006 overestimation is more or less constant after 40 days. Table 4.9 presents a summary of the percentage of overestimation that the different models are exhibiting, the value has been taken at 126 days which is the latest data available from the creep frames. AASHTO LRFD 2006 is the most accurate model available, CEB-FIP 2012 shows an improvement compared to older version of CEB-FIP but won't provide an approximation as good as AASHTO LRFD 2006.

Table 4.9. Overestimation of the Creep Strain by Creep Models

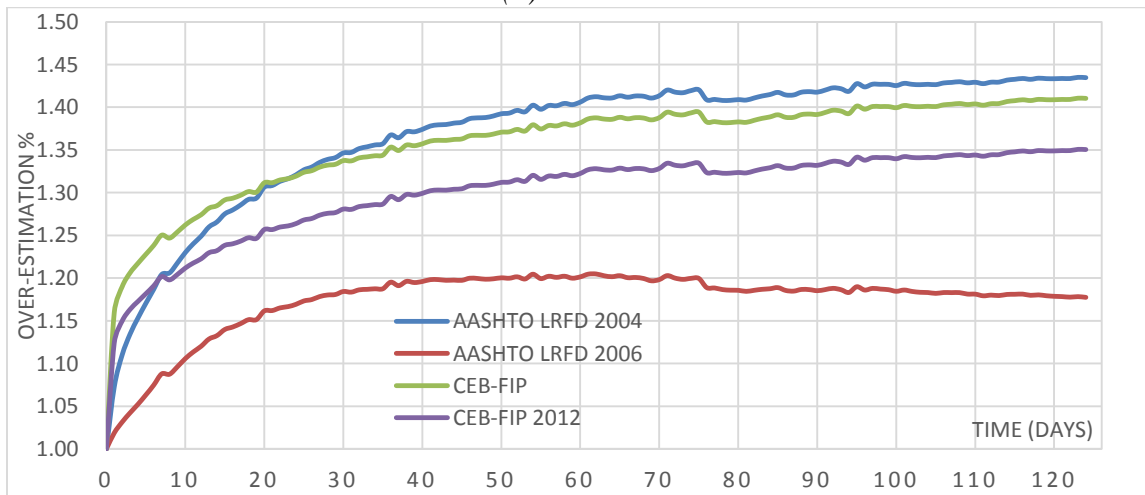
Models	AASHTO LRFD 2004	AASHTO LRFD 2006	CEB-FIP	CEB-FIP 2012
Frame 1	142%	117%	139%	133%
Frame 2	144%	119%	142%	136%
Frame 3	143%	118%	141%	135%
Average	143%	118%	141%	135%



(a) Frame 1



(b) Frame 2



(c) Frame 3

Figure 4.22. Overestimation of Creep Strain

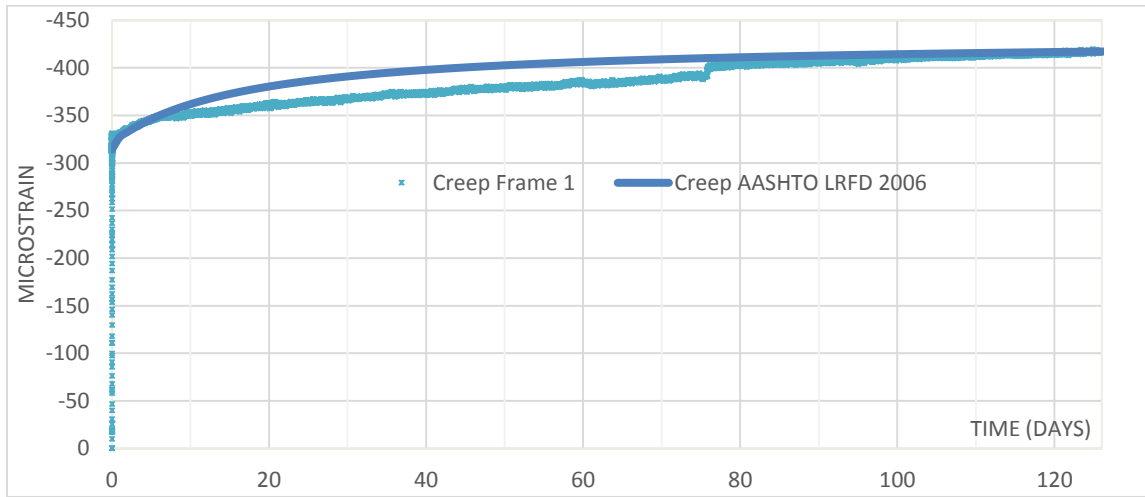
The available models over predict the experimental data for creep effects. Those results are consistent with the past research reviewed in Chapter 2. We can attribute those over prediction to the fact that the concrete used for the girder was SCC. Indeed, SCC is composed of smaller aggregates and a lower water to cement ratio. SCC use is not wide spread and most of the models have not been updated for SCC or any type of high strength concrete.

AASHTO LRFD 2006 is evidently the most accurate model available but still presents a modest over-estimation of creep and shrinkage of about 20%. From the equations of Chapter 2, equation (2.19) gives the definition of the creep coefficient. Inputs were modified in order to fit the experimental creep data. Modifying the compressive strength or maturity of concrete lead to unrealistic results. The best way to fit the experimental data was to add a correction faction of 0.6 in the expression of the creep coefficient. The creep coefficient expression becomes:

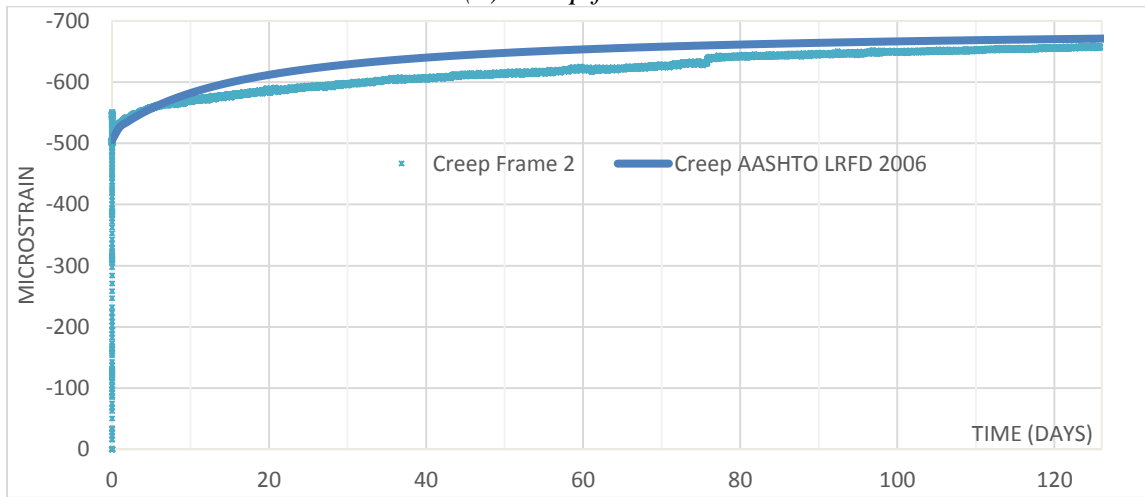
$$\Psi_b(t_f, t_i) = 1.9k_s k_{hc} k_f k_{td} t_i^{-0.118} k_{scc} \quad (4.1)$$

Where it is recommended: $k_{scc} = 0.6$

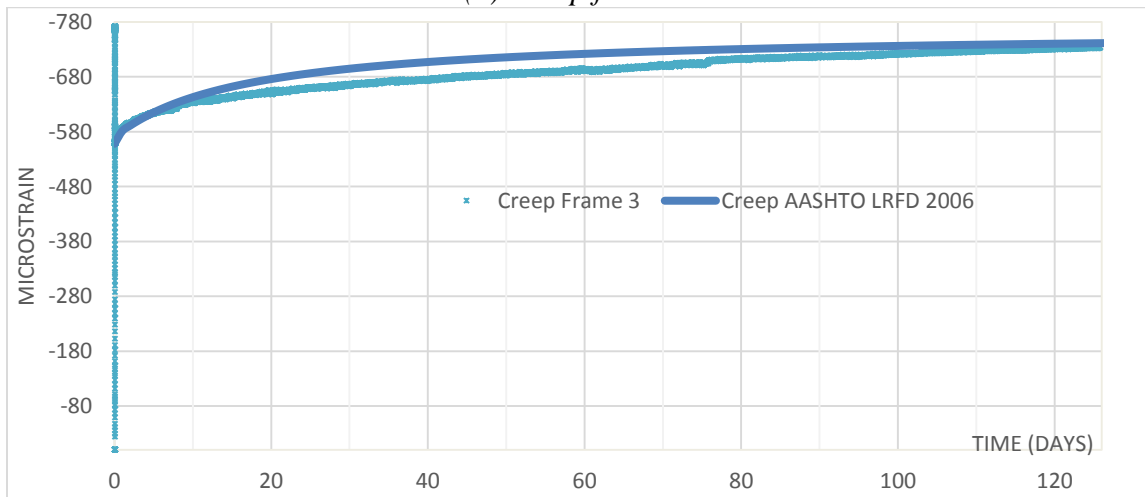
By applying that correction coefficient, the corrected AASHTO LRFD 2006 is plotted along with the experimental creep data as presented in Figure 4.23. The corrected model fits the experimental data reasonably well, generally within 5%.



(a) Creep frame 1



(b) Creep frame 2



(c) Creep frame 3

Figure 4.23. Modified AASHTO LRFD 2006 Compared to Creep Data

5. SUMMARY, CONCLUSION AND RECOMMENDATIONS

5.1. SUMMARY

This thesis reviewed and studied the prediction of short and long term deformations and compared predictions with observed experimental data from a precast prestressed concrete spliced girder. The first chapter provided an introduction of the project and presented the motivation behind this thesis. The second chapter provided a review of the literature for both spliced girders and the prediction of short and long term deformations. The third chapter described the specimen as well as the construction process in the laboratory. Lastly, the fourth chapter provided a detailed analysis of the data from the girder, the shrinkage readings and the creep frames. Each experimental data set available was compared to code-based predictive model results. The predictive results followed the trends well but correction factors were found necessary to align predictions with observations. Creep and shrinkage models overestimated the experimental data and further research is necessary to disambiguate the differences.

5.2. CONCLUSION

The following conclusions may be drawn from this research project:

- 1- The predictions before data were available
 - a. The simulations made to predict the evolution of strain from day 1 to the day of post-tensioning gave a satisfactory (conservative) approximation for design purposes but may not be accurate as a realistic assessment is required as part of the construction process. Unfortunately, data from the girder were not available to compare.
 - b. Final predictions that provided the state of stress (and strain) prior to testing showed that the specimen was more likely to fail in compression rather than in tension. Compression failure occurred during Test 3 and 4.
- 2- The girder

- a. The observed evolution of the strain profile from the post-tensioning to the beginning of Test 1 agreed with the code-based predictions made. The strain profile of the Splice 2 was similar to the strain profile in the neighboring girder (Section D&F) demonstrating that the girder was effectively continuous.
 - b. The final strain profile being almost a rectangular block demonstrated that the design objective of dead load balancing was effectively achieved.
- 3- The shrinkage readings
- a. Overestimation of the shrinkage for SCC for all the models available.
 - b. The current AASHTO provisions provided the closest prediction for shrinkage with an over-estimation of 120%.
 - c. The predictive models are somewhat sensitive to the humidity input and a slight modification can lead to better predictions. Increasing the humidity percentage by 15% provided results in better agreement with the experimental data.
 - d. Those changes might not be applicable in a general way as the concrete used was self-consolidating and that the humidity percentage was not known with precision.
- 4- The creep frames
- a. All predictive models over-estimated the creep for SCC material, however the best result was obtained from the current AASHTO provisions the best prediction for creep with an over estimation of 118%
 - b. The over-estimation provided by most creep models continue to increase with time, while the over-estimation predicted from current AASHTO provisions converge and then plateau over time.

- c. Multiplying the creep coefficient by a correction factor of 0.6 provides a modified creep model that better fits experimental data for SCC. However, it is difficult to assess the cause for the differences as the concrete used was SCC that was already 294 days old when loaded.

A slight over-estimation of long term creep and shrinkage deformations are desirable from a design standpoint as the predictions are conservative. However, during construction, creep and shrinkage deformations need to be predicted as accurately as possible. Thus local knowledge of material specific properties is needed for a more accurate prediction.

5.3. RECOMMENDATIONS

The models used mostly overestimated the experimental data. This can be explained by the fact that the concrete used was self-consolidating concrete and that the creep frames were loaded with 294 days old cylinders. In addition, the conditions the concrete has been exposed to were pretty sterile, quite different from what would happen in the field with rain, sudden temperature changes, and inconsistent humidity percentage. By using additional correction factor or modifying inputs, it was possible to fit the predictions given by AASHTO LRFD 2006 with the experimental data. Unfortunately, in order to validate the use of additional correction factors and/or modified inputs, it needs to be applied to many other cases using self-consolidating concrete and higher maturity.

Further work on SCC would help validating or refuting the use of additional correction factors to correct the over estimation of the long term effect of creep and shrinkage.

In addition, recording data as soon as the structure is pretensioned would be helpful in understanding the evolution of the strain profile of the section from day 1. Unfortunately, recording data from day 1 might be challenging as the precast elements

are usually built by precasters and then hauled to the construction site. It would require the research team to do the precast and construction work in the same location.

Another way to predict accurately the losses due to creep and shrinkage would be to set up creep frames and shrinkage readings before starting the construction process. This would allow a realistic prediction of the short and long term deformations and would allow the construction process to be very precise.

REFERENCES

- AASHTO (2012). *AASHTO LRFD Bridge Design Specifications*. 6th Edition, American Association of State Highway and Transportation officials (AASHTO), Customary U.S. Units, Washington, D.C.
- AASHTO (2004). *AASHTO LRFD Bridge Design Specifications*. 3rd Edition, American Association of State Highway and Transportation officials (AASHTO), Customary U.S. Units, Washington, D.C.
- Abdel-Karim, A. and Tadros, M.K. (1992). Design and Construction of Spliced I-Girder Bridges. *PCI Journal*, Vol. 33, pp. 114–122.
- Abdel-Karim, A. and Tadros, M.K. (1995). State-of-the-Art of Precast/Prestressed Concrete Spliced I-Girder Bridges. *Precast/Prestressed Concrete Institute*, Chicago, IL, 143 pages.
- Al-Omaishi, N., Tadros, M.K., and Seguirant, S. J. (2009). Estimating Prestress Loss in Pretensioned, High-Strength Concrete Members. *PCI Journal*. Vol. 54, No. 4 (Fall): pp. 132–159.
- ASTM C157/C157M (2008). "Standard Test Method for Length Change of Hardened Hydraulic-Cement Mortar and Concrete." In *Annual Book of ASTM standards*. West Conshohoken, Pennsylvania: The American Society for Testing and Materials.
- ASTM C512/C512M (2010). "Standard Test Method for Creep of Concrete in Compression." In *Annual Book of ASTM standards*. West Conshohoken, Pennsylvania: The American Society for Testing and Materials.
- ASTM C617/C617M (2012). "Standard Practice for Capping Cylindrical Concrete Specimens." In *Annual Book of ASTM standards*. West Conshohoken, Pennsylvania: The American Society for Testing and Materials.
- Bishop, E.D. (1962). Continuity Connection for Precast Prestressed Concrete Bridges. *ACI Journal*, pp. 585–599.
- Caroland, W.B., Depp, D., Janssen, H., and Spaans, L. (1992). Spliced Segmental Prestressed Concrete I-Beams for Shelby Creek Bridge. *PCI Journal*, Vol. 37, No. 5, pp. 22–33.

- Castrodale, R.W. and White, C.D. (2004). Extending Span Ranges of Precast Prestressed Concrete Girders. Transportation Research Board, *National Cooperative Highway Research Program*, Report No. 517, 603 pages.
- CEB-FIP (1993). *CEB-FIP model code 1990*, Thomas Telford, London.
- Endicott, W.A. (1996). Precast Super Bulb Tees Create Innovative Bridge. *Ascent Winter*, PCI publication, pp. 30–32.
- Endicott, W.A. (2005). A Fast Learning Curve: Colorado Flyover Provides Strong Example of the Concept of Curved U-Girders for Use in a Variety of Bridge Projects. *Ascent Winter*, PCI publication, pp. 36–49.
- Ficenc, J.A., Kneip, S.D., Tadros, M.K., and Fischer, L.G. (1993). Prestressed Spliced I-Girders: Tenth Street Viaduct Project, Lincoln, Nebraska. *PCI Journal*, Vol. 38, No. 5, pp. 38–48.
- Fitzgerald, J.B. and Stelmack, T.W. (1996). Spliced Bulb-Tee Girders Bring Strength and Grace to Pueblo's Main Street Viaduct. *PCI Journal*, Vol. 41, No. 6, pp. 40–54.
- Hale, W.M. and Russell, B.W. (2006). Effect of allowable compressive stress at release on prestress losses and on the performance of precast, prestressed concrete bridge girders. *PCI Journal*, Vol. 51, No. 3, pp. 14–25.
- Hueste, M.B., Mander, J.B., Prouty, J.M., Sarremejane, T. and Baie, R. (2014). "Continuous Prestressed Concrete Girder Bridges." TxDOT Report, To be published.
- Hueste, M.B., Mander, J.B., and Parkar, A.S. (2012). "Continuous Prestressed Concrete Girder Bridges Volume 1: Literature Review and Preliminary Designs." TxDOT Report, 176 pages.
- Huo, X.M.S., Al-Omaishi, N. and Tadros, M.K. (2001). Creep, shrinkage, and modulus of elasticity of high-performance concrete. *ACI Materials Journal*, Vol. 98, No. 6, pp.440–449.
- Janssen, H.H. and Spaans, L. (1994). Record Span Spliced Bulb-Tee Girders Used in Highland View Bridge. *PCI Journal*, Vol. 39, No. 1, pp. 12–19.
- Kaar, P.H., Kriz, L.B., and Hognestad, E. (1960), Precast-Prestressed Concrete Bridges, 1. Pilot Tests of Continuous Girders. *Journal of PCA Research and Development Laboratories*, 2(2), pp. 21–37.

- Khayat, K.H., and Mitchell, D. (2009), National Cooperative Highway Research Program (NCHRP) Report 628 Self-Consolidating Concrete for Precast, Prestressed Concrete Bridge Elements. Transportation Research Board, Washington, D.C.
- Lounis, Z., Mirza, M.S., and Cohn, M.Z. (1997). Segmental and Conventional Precast Prestressed Concrete I-Bridge Girders. *Journal of Bridge Engineering*, Vol. 2, pp.73–82.
- Mattock, A.H. and Kaar, P.H. (1960). Precast-prestressed Concrete Bridges III: Further Tests of Continuous Girders. *Journal of PCA Research and Development Laboratories*, 2(3), pp. 51–78.
- Miller, R.A., Castrodale, R.W., Mirmiran, A. and Hastak, M. (2004). Connection of Simple Span Precast Concrete Girders for Continuity. *National Cooperative Highway Research Program*, Report 519, 203 pages.
- Mirmiran, A., Kulkarni, S., Miller, R., Hastak, M., Shahrooz, B. and Castrodale, R. (2001b). Positive Moment Cracking in the Diaphragms of Simple-Span Prestressed Girders Made Continuous. SP 204 Design and Construction Practices to Mitigate Cracking, E. Nawy, Ed., *American Concrete Institute*, Detroit, pp.117–134.
- Newhouse, C.D., Roberts-Wollmann, C.L. and Cousins, T.E. (2005). Development of an Optimized Continuity Diaphragm for New PCBT Girders. *FHWA/VRTC 06-CR3*, Virginia Transportation Research Council, 77 pages.
- Nikzad, K.A., Trochalakis, T., Seguirant, S.J. and Khaleghi, B. (2006). Design and Construction of the Old 99 Bridge – An HPC Spliced Girder Structure. *PCI Journal*, Vol. 23, No. 18, pp. 98–109.
- Oesterle, R.G., Gilkin, J.D., and Larson, S.C. (1989). Design of Precast-Prestressed Bridge Girders Made Continuous. *National Cooperative Highway Research Program*, Report No. 322, Transportation Research Board, Washington, D.C.
- Pan, Z.F., B. Li and Z.T. Lu (2013). Re-evaluation of CEB-FIP 90 prediction models for creep and shrinkage with experimental database. *Construction and Building Materials*, Vol.38, pp.1022-1030.
- Ronald, H.D. (2001). Design and Construction Considerations for Continuous Post-tensioned Bulb Tee Girder Bridges. *PCI Journal*, Vol. 46, No. 3, pp. 44–66.

- Sun, C. (2004), High Performance Concrete Bridge Stringer System. *Ph.D. Dissertation*, The University of Nebraska- Lincoln, 228 pages.
- Tadros, M. K., Al-Omaishi, N., Seguirant, S. J., and Gallt, J. G. (2003). "Prestress losses in pretensioned high-strength concrete bridge girders." *NCHRP Report 496*, Transportation Research Board, Washington, D.C.
- Tadros, M.K. and Sun, C. (2003). Implementation of the Superstructure/Substructure Joint Details. University of Nebraska, Omaha, Department of Civil Engineering, *Nebraska Department of Roads*, Project Number *SPR-PL-1(038)*, 514 pages.
- Tadros, M.K. (2007). Design Aids for Threaded Rod Precast Prestressed Girder Continuity System. *Nebraska Department of Roads Research Report*, 103 pages.
- Trejo, D., Hueste, M.B., Kim, Y.H., and Atahan, H. (2008). "Characterization of self-consolidating concrete for design of precast, prestressed bridge." *Rep. FHWA/TX-09/0-5134-2*.
- Waldron, C.J. (2004). Investigation of long-term prestress losses in prestensioned high performance concrete girders," *Ph.D.Dessertation*, Department of Civil Engineering, Virginia Polytechnic Institute and State University, Blacksburg, 220 pages.
- Webber Company Website, Pictures of Sylvan Avenue Bridge, <http://www.webber.com/wrq-sh-183a-sylvan-avenue-bridge>